| | |
|---|---|
| **Titre:** Title: | Phage-Based Surface Plasmon Resonance Strategies for the Detection of Pathogens |
| **Auteur:** Author: | Nancy Tawil |
| **Date:** | 2013 |
| **Type:** | Mémoire ou thèse / Dissertation or Thesis |
| **Référence:** Citation: | Tawil, N. (2013). Phage-Based Surface Plasmon Resonance Strategies for the Detection of Pathogens [Thèse de doctorat, École Polytechnique de Montréal]. PolyPublie. https://publications.polymtl.ca/1274/ |

UNIVERSITÉ DE MONTRÉAL

# PHAGE-BASED SURFACE PLASMON RESONANCE STRATEGIES FOR THE DETECTION OF PATHOGENS

NANCY TAWIL

INSTITUT DE GÉNIE BIOMÉDICAL

ÉCOLE POLYTECHNIQUE DE MONTRÉAL

THÈSE PRÉSENTÉE EN VUE DE L'OBTENTION

DU DIPLÔME DE PHILOSOPHIAE DOCTOR

(GÉNIE BIOMÉDICAL)

NOVEMBRE 2013

UNIVERSITÉ DE MONTRÉAL

ÉCOLE POLYTECHNIQUE DE MONTRÉAL

Cette thèse intitulée:

PHAGE-BASED SURFACE PLASMON RESONANCE STRATEGIES FOR THE DETECTION OF PATHOGENS

présentée par : TAWIL Nancy

en vue de l'obtention du diplôme de : Philosophiae Doctor

a été dûment acceptée par le jury d'examen constitué de :

Mme HOEMANN Caroline, Ph.D., présidente

M. MEUNIER Michel, Ph. D., membre et directeur de recherche

Mme MANDEVILLE Rosemonde, Ph. D., membre et codirectrice de recherche

M. SACHER Edward, Ph. D., membre et codirecteur de recherche

M. VALLÉE-BÉLISLE Alexis, Ph. D., membre

M. TRIFIRO Mark, M.D., membre

# DEDICATION

*To my mother*

# ACKNOWLEDGEMENTS

I express my deepest appreciation to my thesis supervisor, Prof. Michel Meunier, for his guidance and foresight. He provided me with the opportunity to work on a research project encompassing a plethora of scientific disciplines.

I also wish to thank my co-supervisor and mentor, Dr. Rosemonde Mandeville, for her inspiring attitude and substance of genius. She continually conveyed a spirit of adventure and excitement for new business venutures, novel scientific undertakings, and for life in general.

I acknowledge, with gratitude, my debt of thanks to Dr. Edward Sacher for his guidance and foresight. Dr. Sacher stands at the forefront in providing scientific support for the body of work presented in this thesis.

I thank Professors Hoemann, Vallée-Bélisle, Trifiro and Dorner for taking the time to evaluate this thesis.

I sincerely thank my colleagues and friends at École Polytechnique and Biophage Pharma Inc. for their insight and camaraderie throughout my studies.

I express my deepest gratitude to Professors Merhi, Yahia, Savard, Collins, Mourad, Luong and Egert for providing me with exceptional opportunities to advance my career.

I pay tribute to my parents, whose sacrifices and courage are at the core of all my achievements. Lastly, I thank my husband for his love, patience and encouragements. His dedication, discipline and work ethics have been, and will continue being, and inspiring example.

# RÉSUMÉ

La prévalence croissante des infections bactériennes ayant acquis une résistance aux antibiotiques a créé une crise mondiale en terme de santé publique. Effectivement, l'échec de la médecine traditionnelle pour le traitement efficace de ces infections implique un coût sociétal annuel de 35 milliards de dollars aux États-Unis. Avec les déboires des stratégies conventionnelles de traitement, le diagnostic précoce de pathogènes bactériens résistants aux antibiotiques, tel que le *Staphylococcus aureus* résistant à la méthicilline (SARM), devient primordial pour la prévention et le traitement rapide et efficace des infections. Cependant, les techniques de détection courantes, telles que des tests de culture microbiologiques standards, la réaction en chaîne par polymérase (PCR), les dosages immunologiques, les techniques de fluorescence et la spectrophotométrie, présentent plusieurs inconvénients; notamment, ces techniques requirent des étapes de préenrichissement, un personnel médical hautement qualifié, un temps d'analyse relativement long et des coûts élevés. Il y a donc un besoin pressant pour une méthode de détection rapide, fiable, sensible, spécifique et à coût modique pour la détection de pathogènes.

Cette dernière décennie a vue l'émergence de plusieurs biocapteurs pour fins biomédicales. Cependant, ces capteurs s'appuient majoritairement sur l'utilisation d'anticorps. Ces éléments de reconnaissance présentent plusieurs inconvénients (e.g. coûts de production élevés, instabilité face aux fluctuations environnementales, etc.). Dans ce travail, nous favorisons donc une approche basée sur les bactériophages, des virus qui reconnaissent spécifiquement leurs hôtes bactériens, peuvent distinguer entre les cellules vivantes et les cellules mortes, sont robustes et ont de faibles coûts de production.

Dans ce travail pluridisciplinaire, nous combinons la biologie moléculaire, la virologie, la microbiologie, la chimie des surfaces, la nanotechnologie et le génie physique afin de façonner une méthode innovante, potentiellement miniaturisable, pour la détection clinique d'agents pathogènes à l'aide de bactériophages spécifiques comme éléments de reconnaissance.

Nous commençons par examiner les principes fondamentaux et les progrès récents des technologies utilisant des biocapteurs optiques, électrochimiques et acoustiques pour les diagnostics basés sur les phages. Nous constatons que, malgré un travail notable, une méthode optique, spécifique, sensible pour détecter de faibles concentrations d'agents pathogènes en quelques minutes, à faibles coûts, n'a pas été établie. Nous concluons que l'amélioration des stratégies d'immobilisation des phages ainsi que l'utilisation d'éléments phagiques plus appropriés pour une approche utilisant un biocapteur optique SPR (Surface Plasmon Resonance) permettrait une détection en temps réel plus sensible.

Nous croyons qu'une meilleure compréhension des caractéristiques d'adsorption des monocouches organiques auto-assemblées est nécessaire pour des applications impliquant la modification des surfaces de métaux pour la fixation subséquente d'éléments de reconnaissance. Notre deuxième article porte donc sur l'étude de la cinétique d'auto-assemblage de monocouches de L-cystéine et d'acide 11- mercaptoundécanoïque (MUA) sur l'or en utilisant la SPR [1]. Notre but dans l'accomplissement de ces recherches est d'établir la validité et l'applicabilité de chacune de ces molécules comme élément de liaison pour une utilisation subséquente dans les biocapteurs optiques. Nous constatons que la formation des monocouches de L-cystéine et de MUA n'est décrite par l'isotherme de Langmuir qu'à de faibles concentrations seulement. Nos études démontrent que dans le cas de la formation de la monocouche de L-cystéine, le groupement amine ainsi que le groupement thiol contribuent à la fixation initiale de la molécule, suivie du remplacement des complexes amine-or, formés initialement, par des complexes thiol-or plus stables. La réorganisation de la L-cystéine crée donc plus d'espace à la surface de l'or, entraînant l'adsorption de molécules subséquentes. De plus, la forme zwittérionique de la molécule de L-cystéine permet la physisorption d'une deuxième couche par des interactions électrostatiques. D'autre part, les molécules de MUA s'adsorbent aléatoirement sur la surface de l'or permettant une réorganisation subséquente de la monocouche plusieurs heures après le dépôt initial.

Nous avons ensuite utilisé la résonance plasmonique de surface (SPR) pour effectuer la détection, en temps réel, de l'attachement de bactériophages contre le SARM à l'or, en utilisant plusieurs différentes stratégies d'immobilisation[2]. Nous avons constaté qu'une monocouche auto-

assemblée mixte de L-cystéine et de MUA permet une orientation favorable des phages lorsqu'immobilisés à l'or. Ce positionnement orienté des phages préserve leur biofonctionnalité et leur capacité de lyse bactérienne. Ceci est dû à la formation de cavités uniformes sur les surfaces d'or, permettant une orientation du phage de façon à ce que les protéines caudales, responsables de la reconnaissance des épitopes bactériens, soient exposées vers le milieu externe contenant leurs hôtes bactériens.

Nous avons ensuite utilisé une plateforme SPR pour détecter *E. coli* à l'aide de bactériophages T4 ainsi que des SARMs à l'aide de phages spécifiques BP14[3]. Nous avons constaté que notre technique d'immobilisation, combinée à l'utilisation de la SPR, permet la détection sans marquage préalable, en temps réel, de façon précise, rapide et peu coûteuse d'agents pathogènes, pour des concentrations de $10^3$ colonies/millilitre (CFU/ mL), et ce, en moins de 20 minutes.

Nous avons ensuite porté notre attention sur la détection différentielle de SARM d'origine communautaire (CA-SARM), d'origine nosocomiale (HA-SARM ), des *S. aureus* sensibles à la méthicilline (SASM), et des souches ayant une résistance limite à l'oxacilline (BORSA), en utilisant SPR[4]. Nous avons étudié deux cent cinquante isolats cliniques de *Staphylococcus aureus* pour déterminer leur sensibilité aux antibiotiques β-lactamines. Un biocapteur SPR a été utilisé pour différencier les CA-SARM, des HA-SARM, des BORSA ainsi que des souches de SASM en détectant spécifiquement PBP2a, une protéine liant la pénicilline qui a acquérit une altération conférant ainsi aux souches de *S. aureus* une résistance aux antibiotiques β-lactamines. Nous avons constaté que le système le permet la détection spécifique des agents pathogènes pour des concentrations aussi faibles que 10 CFU/mL, sans avoir recours à la PCR, à un marquage ou à un enrichissement préable. Cette approche présente l'avantage d'être simple et rapide, permettant l'identification de souches résistantes de *Staphylococcus aureus* jusqu'à 48 heures plus rapidement que les techniques microbiologiques classiques. Cette méthode pourrait avoir un impact significatif sur les coûts hospitaliers, le contrôle efficace de l'infection et la mortalité des patients.

Finalement, nous proposons une nouvelle perspective sur la fixation des phages à des nanoparticules d'or[5] pour une meilleure détection SPR. Nous rapportons la synthèse et la caractérisation de nanohybrides or-bactériophages multifonctionnels, ayant un grand potentiel pour des applications nano-biomédicales telles que la SPR localisée. Les nanoparticules d'or (AuNPs) fonctionnalisées au polyéthylène glycol (PEG) et couplées aux phages contre les SARMs ont été étudiées par microscopie électronique à transmission (MET) et par la spectroscopie de photoélectrons à rayons X (XPS). Le rôle de l'interface ainsi que celui de la chimie employée pour fixer les phages aux nanoparticules d'or ont été délimités. L'attachement des phages aux AuNPs a été confirmé par la formation de liens peptidiques entre les amines primaires des phages et le groupement terminal d'acide carboxylique des nanoparticules pegylées, ainsi que par la formation de liens hydrogènes entre les espèces carboxyle et amine. L'utilisation de ces nanoparticules hybrides phagiques peut être étendue à une large gamme d'applications biotechnologiques.

# ABSTRACT

The ever-increasing prevalence of multidrug-resistant infections has created a global public health crisis with the failure for conventional medicine to effectively treat patients, resulting in prolonged hospital occupency, greater risk of death and annual societal cost reaching over $35 billion in the United-States alone. With the failure of conventional treatment strategies, early diagnosis of drug-resistant bacterial pathogens, such as methicillin-resistant *Staphylococcus aureus* (MRSA), becomes primordial in preventing resultant life-threatening illnesses. Conventional detection techniques, such as standard culture-based assays, polymerase chain reaction (PCR), immunological assays, fluorescence and spectrophotometry, suffer from several drawbacks including the requirement for pre-enrichement steps, lengthy assay times, high costs and the necessity for highly-trained medical personnel. There is a need for a rapid, reliable, inexpensive, sensitive and specific method for pathogen detection. The past decade has brought about the increased use of biosensing technologies, relying on the use of antibodies for biomedical purposes. These recognition elements suffer from several drawbacks including high-costs and limited shelve-lives. We thus turn our attention to bacteriophages, viruses that specifically recognize their bacterial hosts, can distinguish between live and death cells, are robust, easy to produce and cost effective.

In this multidisciplinary work, we combine molecular biology, virology, microbiology, surface chemistry, nanotechnology and engineering physics to bring about an innovative, potentially miniaturizable method for the point of care detection of pathogens using specific bacteriophages as a recognition elements.

We start by reviewing the basic principles and recent advances in biosensing technologies using optical, electrochemical and acoustic platforms for phage-based diagnostics. Although much notable work has been done, a low cost, specific, sensitive optical method for detecting low concentrations of pathogens, in a few minutes, has not been established. We conclude from the limited body of work on the subject that improving immobilization strategies and finding more

suitable phage recognition elements would allow for a more sensitive approach. Our aim was to better describe the attachment process of MRSA specific phages on gold surfaces, and the subsequent biodetection of their bacterial hosts by surface plasmon resonance (SPR).

With the knowledge that the adsorption characteristics of thiol-containing molecules are necessary for applications involving the attachment of recognition elements to a functionalized surface, we start by providing comparative details on the kinetics of self-assembly of L-cysteine and 11-mercaptoundecanoic acid (MUA) monolayers on gold using SPR[1]. Our purpose, in carrying out these measurements was to establish each molecule's validity and applicability as a linker element for use in biosensing. We find that monolayer formation, for both L-cysteine and MUA, is described by the Langmuir isotherm at low concentrations only. For L-cysteine, both the amine and thiol groups contribute to the initial attachment of the molecule, followed by the replacement of the amine-gold complexes initially formed with more stable thiol-gold complexes. The reorganization of L-cysteine creates more space on the gold surface, and the zwitterionic form of the molecule permits the physisorption of a second layer through electrostatic interactions. On the other hand, MUA deposits randomly onto the surface of gold as a SAM and slowly reorganizes into a denser, vertical state.

Surface plasmon resonance was then used for the real-time monitoring of the attachment of MRSA bacteriophages to gold, using several immobilization methods[2]. We found that mixed self-assembled monolayers (SAMs) of L-cysteine and MUA permitted oriented positioning of the phages, thus preserving their biofunctionality and their bacterial lysing efficiency. This was due to the formation of uniform cavity islands on the gold surfaces, permitting an oriented positioning of the phages, thus better exposing their recognition proteins towards the medium containing the bacterial hosts.

T4 bacteriophages were then used to detect *E. coli*, while a novel, highly specific phage was isolated, characterized and used to detect MRSA[3]. We found that our technique, combined with the use of SPR permits label-free, real-time, specific, rapid and cost-effective detection of

pathogens, for concentrations of $10^3$ colony forming units/milliliter (CFU/mL), in less than 20 minutes.

We then turned our attention towards the differential detection of community-acquired MRSA (CA-MRSA), hospital-acquired MRSA (HA-MRSA), methicillin susceptible *S. aureus* (MSSA), and borderline resistant oxacillin-resistant *S. aureus* (BORSA), using SPR[4]. We studied two hundred fifty *Staphylococcus aureus* clinical isolates to determine their susceptibilities to β-lactam antibiotics. A surface plasmon resonance (SPR) biosensor was used to differentiate among CA-MRSA, HA-MRSA, BORSA and MSSA strains by specifically detecting PBP2a, an altered penicilling binding proteins that confers resistance to S. aureus strains, on whole bacterial cells, without labeling, without recourse to PCR or enrichment steps. We found that the system permits, specific detection of pathogens for concentrations as low as 10 CFU/mL. This approach has the advantages of being simple and rapid, allowing for identification of resistant strains of *Staphylococcus aureus* up to 48 hours earlier than conventional microbiological techniques. This method could have a significant impact on hospital costs, effective infection control, and patient mortality.

Finally, we offer a new perspective on the attachment of phages to gold nanoparticles[5] for enhanced SPR detection. We report the synthesis and characterization of gold-bacteriophage hybrids multifunctional scaffold with great potential for nanotechnologically-based biomedical applications, such as localized SPR. Gold nanoparticles (AuNPs), stabilized (PEGylated) using heterobifunctional polyethylene glycol (PEG), were coupled to methicillin-resistant S. aureus-specific phagesand studied by transmission electron microscopy (TEM) and X-ray photoelectron spectroscopy (XPS). The role of the interface, and the covalent coupling chemistry employed to attach the phages to the gold nanoparticles, have been delineated and successful attachment of phages to AuNPs was confirmed by the presence of amide between the primary amines of the phage and the carboxylic acid terminal groups of the NPs, and by the formation of strong intermolecular hydrogen bonds between carboxyl and amine species, as shown by N1s and O1s core level shifts. The use of these nanoparticle-phage hybrids can be extended to the targeted separation of specific bacteria from heterogeneous samples, as well as a wide range of

biotechnological applications, such as labels for enhanced fluorescence and dark-field microscopy, and surface-enhanced Raman scattering detection[6].

# CONDENSÉ EN FRANÇAIS

Bien que l'avènement d'antibiotiques se distingue comme l'une des innovations médicales les plus importantes du 20$^{e}$ siècle, la prévalence croissante d'infections microbiennes multirésistantes aux antibiotiques engendre actuellement une crise mondiale en matière de santé publique[7]. Aux États-Unis, l'excès de coûts générés par le milieu hospitalier, attribuables aux infections résistantes aux antibiotiques, atteint 20 milliards de dollars, avec 8 millions de jours supplémentaires d'occupation en hôpital et 35 milliards de dollars en coûts sociaux annuellement [8]. Bien que des efforts considérables soient orientées vers la production de produits antibiotiques dérivés et de produits non-antibiotiques, tels que les vaccins antibactériens, la thérapie phagiques et la formulation d'adjuvants, les méthodes actuellement utilisés en clinique pour l'identification bactérienne demeurent les tests traditionnels de culture microbiennes, qui requièrent de longues périodes d'incubation ainsi que des protocoles laborieux. D'autres techniques conventionnelles, telle que l'amplification en chaîne par polymérase (ACP), les dosages d'immunoabsorption par enzyme liée, les tests de bioluminescence et les méthodes de spectrophotométrie, présentent plusieurs inconvénients. Ils sont lents, coûteux, laborieux et nécessitent des étapes d'enrichissement ainsi qu'un personnel hautement qualifié. Il y a donc une demande croissante pour des méthodes qui éliminent le besoin de culture microbienne, réduisent le temps de diagnostic et augmentent la sensibilité et la spécificité de la détection.

L'avènement de biocapteurs a permis des avancées majeures dans la détection microbienne. Ceux-ci sont habituellement classés en fonction de leurs éléments de transduction et peuvent être optiques, électrochimiques ou acoustiques. En outre, ils peuvent être classés en diverses autres catégories en fonction de leurs éléments de bioreconnaissance. La plupart des biocapteurs reposent sur l'utilisation d'anticorps. Cependant, l'utilisation d'anticorps présente des inconvénients majeurs, telle que leur instabilité relative aux fluctuations environnementales, ce qui peut limiter leur stockage à long terme ainsi que leur applicabilité sur le terrain. De plus, leur production est longue et coûteuse. Par ailleurs, les anticorps polyclonaux ne sont pas extrêmement spécifiques puisqu'ils peuvent reconnaître différents épitopes sur un même organisme, ces épitopes pouvant également être présents dans les organismes connexes non pathogènes[9].

Nous portons donc notre attention sur les bactériophages, qui sont les principaux régulateurs de l'équilibre microbien sur la planète, dépassant en nombre leurs hôtes bactériens par un facteur de dix. Les phages se lient spécifiquement à leur hôte et sont optimisés de façon à être des outils idéaux pour la détection de bactéries pathogènes. En effet, ils sont capables de faire la distinction entre les cellules vivantes et mortes, sont robustes, extrêmement spécifiques, facile à produire et peu coûteux.

Cette thèse a, donc, pour but de décrire une méthode optimale pour l'immobilisation, l'intégration et l'utilisation de bactériophages sur une plateforme de biodétection conçue pour surmonter les nombreuses limites des méthodes analytiques classiques. Par ailleurs, nous venons éliminer les étapes d'enrichissements préalables et la nécessité de personnel hautement qualifié, réduire considérablement les coûts de production et le temps d'analyse requis, tout en permettant une détection sélective, sensible et rapide.

Dans un premier temps, nous faisons une revue de la littérature des techniques de biodétection exploitant la capacité de liaison spécifique des bactériophages. Il s'agit notamment de tests d'amplification, de l'utilisation de phages rapporteurs, de la détection de composantes intracellulaires libérées par la bactérie suite à leur lyse, du marquage des phages par fluorescence, et des biocapteurs utilisant des bactériophages comme éléments de reconnaissance. Nous notons que, bien que ces dernières années ont vu une augmentation considérable du nombre de nouveaux biocapteurs dédiés à la détection de pathogènes, un nombre minime de ces technologies intègrent des éléments phagiques et peu de biocapteurs basés sur l'utilisation de bactériophages sont présents dans les domaines clinique, agro-alimentaire et environnemental. Le manque d'attention porté aux phages pourrait résulter de la fausse notion que les étudier s'avèrerait trop complexe et spécialisé pour la plupart des laboratoires de génie.

Nos recherches nous ont permis de cibler plusieurs lacunes dans les méthodes d'immobilisation des bactériophages sur les diverses plateformes de détection. La fixation des molécules à un

support a trouvé de nombreuses applications dans l'industrie chimique et les dispositifs biocapteurs. En particulier, les monocouches auto-assemblées (SAM), composées d'espèces chimisorbées, jouent un rôle fondamental dans la modification des propriétés interfaciales des métaux, des polymères et des semi-conducteurs. Notamment, les caractéristiques d'adsorption de molécules contenant des thiols sont nécessaires pour les applications impliquant la fixation d'éléments de reconnaissance à une surface fonctionnalisée. Cependant, en dépit des efforts considérables pour étudier la formation des SAM sur l'or, notre connaissance sur leur cinétique d'adsorption en temps réel demeure limitée. Sachant que la fonctionalisation préalable des surfaces d'or par les SAM vient considérablement influencer l'immobilisation subséquente des phages ainsi que la sensibilité de détection de notre plateforme, nous avons étudié, dans un deuxième temps, la formation en temps réel des SAM de L -cystéine et d'acide 11-mercaptoundécanoïque (MUA) sur l'or, à différentes concentrations, en utilisant un biocapteur à résonance plasmonique de surface (SPR). Notre but dans l'accomplissement de ces mesures était de comparer les caractéristiques de liaison de la L-cysteine et de l'MUA afin d'établir la validité et l'applicabilité de chacune de ces molécules comme un élément de liaison pour une utilisation ultérieures dans les biocapteurs SPR. Nous avons démontré que l'auto-assemblage de la L-cystéine diffère de celle de MUA. En effet, le processus de dépôt de la L-cystéine implique non seulement des contributions des atomes de soufre, mais aussi celles d'autres groupes fonctionnels existants. En effet le groupement amine ainsi que les groupes thiol contribuent à la fixation initiale de la L-cystéine, suivie du remplacement graduel des complexes amine-or, préalablement formés, par des complexes thiol-or plus stable. De plus, la réorganisation de la L-cystéine crée plus d'espace sur la surface d'or, permettant le dépôt d'une quantité accrue de L-cysteine, suivie de la physisorption d'une deuxième couche, rendue possible par la forme zwittérionique de la molécule. Contrairement à la L-cysteine, les molécules de MUA se déposent au hasard, de façon désorientée, sur la surface d'or et se réorganisent lentement pour former une SAM dense.

Nous avons donc utilisé ces nouvelles connaissances en matière de SAM afin d'améliorer les stratégies d'immobilisation des phages sur les plateformes d'or en vue de leur utilisation subséquente pour la détection de pathogènes à l'aide d'une plateforme SPR. Le troisième article a pour but d'optimiser les conditions initiales permettant une détection plus sensible et plus spécifique de bactéries *S. aureus* résistants à la méthicilline (SARM) sur l'or. En premier lieu,

nos travaux nous ont permis d'identifier un phage spécifique aux souches de S. aureus ayant une acquis une résistance aux antibiotiques, et permettant une détection SPR accrue des espèces bactériennes. En effet, puisque l'onde évanescente de la SPR ne s'étend que jusqu'à environ 300 nm dans la direction perpendiculaire à la surface de détection, une partie seulement de la bactérie va générer une réponse SPR. Il importe donc de minimiser la grandeur de l'élément de reconnaissance. La première partie de l'article décrit l'isolation et la caractérisation d'un phage podoviridea de 60 nm de diamètre, idéal pour la détection des SARMs par SPR. Dans la deuxième partie de l'article, les méthodes de SPR, de microscopie électronique à balayage (MEB ) et de microscopie à force atomique (AFM) ont été utilisés pour l'étude, en temps réel, de la fixation des phages à la plateforme d'or, en utilisant diverses méthodes d'immobilisation. Nous avons déterminé que l'immobilisation des phages par l'intermédiaire d'une monocouche auto-assemblée mixte de L-cystéine et de MUA conduit à la formation de liaisons covalentes entre les phages et la surface d'or. Les phages immobilisés de cette façon conservent leur pouvoir infectieux, suggérant une liaison de la capside du phage au substrat, permettant l'orientation des fibres de la queue vers le milieu et, par le fait même, l'accessibilité des protéines caudales pour la reconnaissance d'antigènes présents à la surface bactérienne. Les résultats AFM corroborent davantage cette affirmation. En effet, les images topographiques indiquent clairement que les phages se lient préférentiellement dans les cavités uniformes formées par la monocouche auto-assemblée mixte de L-cystéine et de MUA.

Ayant décrit une méthode optimale pour l'immobilisation des phages sur une plateforme d'or, nous avons porté nos efforts vers la détection pathogènes par SPR. Bien que quelques groupes aient récemment été impliqués dans le développement de capteurs à base de bactériophages pour la détection bactérienne, une méthode optique spécifique, sensible, ayant un faible coût pour détecter de faibles concentrations d' agents pathogènes, en quelques minutes n'a pas été établie. Dans le quatrième article présenté dans cette thèse, nous utilisons un capteur impédometrique (PDS , Biophage Pharma) afin de démontrer la spécificité du bactériophage aux SARMs. Afin de surmonter les limitations du détecteur ampérométrique, nous avons utilisé un appareil SPR pour la détection bactérienne. Nous démontrons la possibilité de détecter des concentrations de $10^3$ colonies bactériennes par millilitre, sans marquage préalable ou étapes d'enrichissement, en

moins de 20 minutes. Nous avons démontré l'applicabilité de cette méthode pour la détection de SARM, ainsi que pour *E. coli*.

Ayant raisonnablement atteint notre objectif, nous avons orienté nos chercherches vers le futur. Le cinquième article présenté dans cette thèse porte sur l'applicabilité du système SPR pour la détection clinique de 250 différentes souches cliniques de *S. aureus*. La méthicilline est un membre d'une large classe d'antibiotiques appelée β –lactame, dont l'effet est de perturber la synthèse de la paroi cellulaire bactérienne. Les β–lactames sont les antibiotiques les plus largement prescrits en raison de leur spécificité et de leur effet non-toxique sur les cellules hôtes. Cependant, les SARMs ont développé une résistance à ces antibiotiques en produisant des protéines altérées liants la pénicilline (PLP), codées par le gène MecA, et ayant une faible affinité pour les β –lactames. Les SARMs sont défini comme ayant une concentration inhibitrice minimale de l'oxacilline (CIM) ≥ 4μg/ml. Cependant, l'expression hétérogène de résistance à l'oxacilline dans plusieurs souches de *S. aureus* a compliqué l'identification du SARM via des procédures microbiologiques classiques. Les souches d'un très faible niveau de résistance à la méthicilline sont sensibles à la plupart des antibiotiques non - β -lactames, et les tests de routine peuvent conduire à des résultats faussement positifs. Par exemple, certaines souches de *S. aureus* présentent une résistance limite à l'oxacilline (BORSA) avec un CIM d'environ ≥ 2μg/ml. Par contre, ces souches ne possèdent pas le gène mecA. Les conditions optimales pour l'identification des BORSA et leur différenciation par rapport à SARM n'ont pas été déterminées. Par ailleurs, un nouveau gène codant pour la résistance à la méthicilline a récemment été identifié dans les isolats cliniques de *S. aureus*. Ces souches, qui ont un profil de résistance variable à l'oxacilline, ne peuvent pas être détectées par des techniques moléculaires classiques, telles que la PCR et des tests d'agglutination sur lame, et sont ainsi identifiés à tort comme étant BORSA. Ainsi, notre objectif est de répondre au besoin pressant pour le développement d'une méthode de détection rapide et sensible afin de détecter spécifiquement les SARM et les différencier des souches BORSA ainsi que des souches sensibles à la méthicilline. De plus, nous visons à réduire le temps de diagnostic, qui est crucial un traitement efficace ainsi qu'une réduction de la mortalitité et la prévention de la propagation de la maladie. Nous avons donc utilisé notre biocapteur SPR pour pour différencier les souche SARM des souches BORSA et des souches sensibles à la méthicilline en détectant spécifiquement les protéines altérées liants la pénicilline sur les cellules

bactériennes, sans avoir recours à une technique d'étiquetage, à la PCR ou à des étapes d'enrichissement préliminaires. La limite de détection du biocapeur est de 10 colonies par mL, en moins de 15 minutes. Ainsi, cette approche présente l'avantage d'être simple et rapide, permettant l'identification de souches résistantes de *Staphylococcus aureus* jusqu'à 48 heures plus tôt que les techniques microbiologiques classiques. Cette méthode pourrait avoir un impact significatif sur les coûts hospitaliers, le contrôle efficace de l'infection et la mortalité des patients.

Le sixième et le dernier article rapporte la synthèse et la caractérisation des hybrides or bactériophages en vue de pouvoir utiliser les principes de résonance plasmonique de surface localisée (LSPR) pour permettre une amplification du signal de détection, et donc, une meilleure sensibilité de detection. Dans le cas de LSPR pour la détection des bactéries, des études récentes montrent que la zone de contact entre une cellule bactérienne et une seule NP peut être trop faible pour entraîner un changement détectable. Cela nous a incités à étudier la possibilité de fixer de nombreuses nanoparticules à une seule cellule bactérienne, en exploitant la spécificité des interactions bactériophages des bactéries. Nous avons démontré qu'il est possible de fonctionnaliser des nanoparticules d'or avec un polyéthylène glycol (PEG) hétérobifonctionnel possédant un groupement thiol permettant son attache à l'or et un groupement carboxylique permettant une attache subséquente du bactériophage. Nous avons utilisé la spectroscopie par photoélectrons induits par des rayons X (XPS) pour caractériser chimiquement les surfaces des nanoparticules d'or fonctionalisées avec le PEG hétérobifonctionnel, des bactériophages, et des hybrides NP d'or-phages. Le rôle de l'interface, et la chimie de couplage covalent employées pour fixer les phages à des nanoparticules d'or, ont été délimités. Les nanoparticules d'or, fonctionnalisés avec un PEG hétérobifonctionnel, ont été couplés avec succès aux bactériophages lytiques spécifiques aux SARMs, via une chimie carbodiimide. Ceci fut démontré par la formation de liaisons amide entre les amines primaires du phage et des groupes terminaux d'acide carboxylique des NPs fonctionnalisées, ainsi que par la formation de fortes liaisons hydrogène entre les espèces carboxylique des NPs et amine des phages. Nous concluons que l'utilisation de ces hybrides peut être utilisée pour la LSPR, et peut être étendue ainsi à une large gamme d'applications biotechnologiques, telle que la séparation ciblée des bactéries spécifiques à partir d'échantillons hétérogènes.

# TABLE OF CONTENTS

# LIST OF TABLES

# LIST OF FIGURES

# LIST OF ABBREVIATIONS AND SYMBOLS

| | |
|---|---|
| AIDS | Acquired immunodeficiency syndrome |
| AFM | Microscopie à force atomique |
| | Atomic force microscopy |
| ADP | Adenosisne diphosphate |
| AK | Adenylate kinase |
| ATCC | American Type Culure Collection |
| ATP | Adenosisne triphosphate |
| ATR | Attenuated total relection |
| AuNP | Nanoparticule d'or |
| | Gold nanoparticle |
| ACP | Amplification en chaîne par polymérase |
| BCCP | Biotin carboxyl carrier protein |
| BE | Binding energy |
| BORSA | Staphylococcus aureus présentatnt une résistance limite à l'oxacilline |
| | Borderline oxacillin-resistant Staphylococcus aureus |
| bp | Base pair |
| BSA | Bovine serum albumin |
| CA-MRSA | Community-acquired methicillin-resistant Staphylococcus aureus |
| CA-SARM | Staphylococcus aureus resistant à la méthicilline d'orige communautaire |
| CBM | cellulose binding module |
| CCD | Charge-coupled device |
| CDC | Centers for Disease Control and Prevention |
| CIM | Concentration inhibitrice minimale |

| | |
|---|---|
| CFU/mL | Colonies par millilitre<br>Colony forming units per milliliter |
| DC | Dendritic cell |
| DNA | Deoxyribonucleic acid |
| *E. coli* | *Escherichia coli* |
| EDC | 1,(3-dimethylaminopropyl)ethylcarbodiimide hydrochloride |
| ECIS | Electric cell-substrate impedance sensing |
| EIS | Electrical impedance spectroscopy |
| ELISA | Enzyme-linked immunosorbent assay |
| FESEM | Field emission scanning electron microscopy |
| FDA | United States Food and Drug Administration |
| FITC | Fluorescein isothiocyanate |
| GFP | Green fluorescent protein |
| HA-MRSA | Hospital-acquired methicillin-resistant Staphylococcus aureus |
| HA-SARM | Staphylococcus aureus résistant à la méthicilline d'origine nosocomiale |
| HPLC | High-performance liquid chromatography |
| IMS | Immunomagnetic separation |
| LB | Luria-Bertani |
| LPS | Lipopolysaccharide |
| LSPQ | Laboratoire de Santé Publique du Québec |
| LSPR | Résonance plasmonique de surface localisée<br>Localized surface plasmon resonance |
| MEB | Microscopie électronique à balayage |
| MET | Microscopie électronique à transmission |

| | |
|---|---|
| MIC | Minimum inhibitory concentration |
| MLST | Multi-locus sequence typing |
| MRSA | Methicillin-resistant Staphylococcus aureus |
| MUA | Acide 11-mercaptoundécanoïque |
| | 11-Mercaptoundecanoic acid |
| NHS | N-hydroxysuccinimide |
| NP | Nanoparticule |
| | Nanoparticle |
| OD | Optical density |
| ORF | Open reading frame |
| PBP | Penicillin-binding protein |
| PBP2a | Altered penicillin binding protein 2a |
| PBS | Phosphate buffered saline |
| PBST | Phosphate buffered saline + Tween |
| PCR | Réaction en chaîne par polymérase |
| | Polymerase chain reaction |
| PEG | Polyéthylène glycol |
| | Polyethylene glycol |
| PFGE | Pulse-field gel electrophoresis |
| PFU/mL | Plaque forming units per milliliter |
| PLP2a | Protéines altérées liant à la pénicilline |
| PTA | Phosphotungstic acid |
| PVL | Penton-Valentine leukocidin |
| QCM | Quartz crystal microbalance |

| | |
|---|---|
| RIU | Refractive index units |
| RNA | Ribonucleic acid |
| rpm | Revolutions per minute |
| RT-PCR | Reverse transcriptase PCR |
| SAM | monocouche auto-assemblée |
| | Self-assembled monolayer |
| SARM | Staphylococcus aureus résistant à la méthicilline |
| SASM | Staphylococcus aureus sensible à la méthicilline |
| SCC*mec* | Staphylococcal cassette chromosome *mec* |
| SDS | Sodium dodecyl sulphate |
| PAGE | Polyacrylamide gel electrophoresis |
| SEB | Staphylococcal enterotoxin type-B |
| SEM | Scanning electron microscopy |
| SLED | Superluminescent light-emitting diode |
| S/N | Signal to noise ratio |
| SP | Surface plasmon |
| SPR | Résonance plasmonique de surface |
| | Surface plasmon resonance |
| STEC | Shiga toxin-producing Escherichia coli |
| TB | Tuberculosis |
| TEM | Transmission electon microscopy |
| TNF-α | Tumor necrosis factor α |
| tRNA | Transfer ribonucleic acid |
| UA | Uranyl Acetate |

| | |
|---|---|
| WHO | World Health Organization |
| XPS | Spectroscopie de photoelectrons à rayons X<br>X-ray photoelectron spectroscopy |

**Amino acids**

| | |
|---|---|
| A | Alanine |
| E | Glutamic acid |
| F | Phenylalanine |
| H | Histidine |
| I | Isoleucine |
| K | Lysine |
| L | Leucine |
| M | Methionine |
| N | Asparagine |
| Q | Glutamine |
| S | Serine |
| T | Threonine |
| V | Valine |
| Y | Thyrosine |

**Nucleotides**

| | |
|---|---|
| A | Adenine |
| C | Cytosine |
| G | Guanine |

| | |
|---|---|
| T | Thymine |
| U | Uracil |

**Chemical elements**

| | |
|---|---|
| Au | Gold |
| C | Carbon |
| F | Fluorine |
| H | Hydrogen |
| N | Nitrogen |
| Na | Sodium |
| O | Oxygen |
| S | Sulfur |

**Latin Letters**

| | |
|---|---|
| [A] | Analyte concentration |
| °C | Degree Celsius |
| *c* | Concentration of the thiol solution |
| $C_{s0}$ | Initial surface concentration of binding sites |
| *D* | Diffusivity of the analyte |
| *Da* | Damköler number |
| *d(h)* | Tickness of the diffusive boundary layer as a function of channel hight |
| eV | Electron Volt |

| | |
|---|---|
| $\Delta G_{ads}$ | Change in Gibbs free energy of the adsorption |
| $h$ | Channel hight |
| K | Kelvin |
| $k_a$ | Association constant |
| $K_{ai}$ | Normalized association constant where $i$ = 1,2,3 |
| $k_d$ | Dissociation constant |
| $K_{di}$ | Normalized dissociation constant where $i$ = 1,2,3 |
| $K_{eq}$ | Equilibrium constant |
| $K_r$ | Normalized reorientation constant |
| [L] | Concentration of surface ligands |
| $L$ | Length of the reactive zone |
| $[LA_1]$ | Surface density of adsorbed analyte molecules via thiol group in the case of L-cysteine **or** |
| | Surface density of MUA chains deposited in a random manner in the case of MUA |
| $[LA_2]$ | Surface density of adsorbed analyte molecules via amine group in the case of L-cysteine **or** |
| | Surface density of MUA chains deposited in an aligned manner in the case of MUA |
| $[LA_2A]$ | Surface density of the second layer in the case of L-cysteine |
| $Q$ | Flow rate |
| $t$ | Time |
| *v/v* | volume-volume |
| $W$ | Channel width |

**Greek Letters**

| | |
|---|---|
| $\varepsilon$ | Dielectric constant |
| $\zeta$ | Connective/diffusive length |
| $\Theta$ | Covered fraction of the gold surface |
| (1- $\Theta$) | Uncovered fraction of the gold surface |
| $\Phi$ | Unreacted fraction of the gold surface after ligand reorientation |
| (1-$\Phi$) | Reacted fraction of the gold surface after ligand reorientation |

# INTRODUCTION

Antibiotic treatment has been at the forefront of therapeutic intervention since the discovery of penicillin by Alexander Flemming in 1928. However, the over- and misuse of antibiotics has had adverse consequences, such as the evolution and spread of bacterial resistance, becoming an alarming threat to public health. The increasing prevalence of antibiotic resistance in many bacterial species, combined with the failures of antibiotic therapy, causes hundreds of thousands of deaths annually. The development of novel antibiotics to combat this crisis has come to a standstill, with the US Food and Drug Administration (FDA) approving only seven new drugs in the last decade [10]. Moreover, pathogens continuously evolve resistance to novel antibiotics, further hindering pharmaceutical efforts to address this problem. Knowing that the use of antibiotics will inevitably promote resistance, it becomes important to develop novel diagnostic and treatment strategies to prevent the inadequate use of these drugs. To address this problem, researchers are turning their attention to the bacterium's natural enemies: bacteriophages. These viruses were discovered a century ago, in 1915, by Frederick Twort, and almost simultaneously, in 1917, by Félix d'Hérelle. D'Hérelle termed these viruses bacteria-eaters, and tested phage therapy in livestock and humans. The reason for the newfound interest is that phages and bacteria are both locked in a constant evolutionary battle, where bacteria constantly produce new defense mechanisms to proliferate in adverse environments (e.g. antibiotic-rich environments), and phages develop counter-strategies to respond to their ever-evolving hosts. Thus, it is not surprising that the idea of using phages as a weapon against multidrug-resistant infections has made a comeback: there is plenty of market opportunity, with phage-products having the potential to become a billion-plus dollar industry[10]. Although phage therapy is a very exciting prospect, one cannot offer effective treatment without a proper diagnosis. Because of this, we posed the following question: ''Is it possible to use these ultra-specific viruses, combined with a biodetection platform, to recognize their bacterial host in a rapid, reliable and inexpensive fashion?'' In the following chapters, we will offer guidance through our thought processes, describing the chemical functionalization of gold sensing platforms, phage immobilization strategies, the screening process for a phage candidate suitable for SPR sensing, and the phage-based detection of *E. coli* and multiple strains of *S. aureus*. We will then compare the use of phages against antibodies, before turning our attention to the future, where phage-detection is combined with nanotechnology for potential new ways of detecting pathogens.

# CHAPTER 1 GOING VIRAL : THESIS OBJECTIVES AND ORGANISATION

## 1.1 Objectives

This work aims at developing a phage-based biosensing SPR system, suited to the specific and sensitive detection of bacterial pathogens in a rapid and inexpensive fashion. Our aim is to better describe the attachment process of MRSA-specific phages on gold surfaces, and the subsequent biodetection of their bacterial hosts by SPR. The objectives of the present work can be summarized as follows :

### 1.1.1 1st objective: Understand the surface characteristics of the functionalized gold sensing platform and its effects on bacteriophage immobilization

The attachment of molecules to a support, resulting in reduced mobility of the target molecule, has found multiple applications in industrial chemistry and in biosensing devices. However, this immobilization can result in the partial or total loss of activity of the recognition element. This is due to the fact that phages that are randomly oriented when immobilized on a surface can have an altered structural conformation, as well as the inability to recognize their target hosts due to the unavailability of their caudal proteins to the external environment. It is, thus, important to understand and characterize the functional surface, to derive better strategies for the oriented immobilization of the phages to the gold sensing platform.

### 1.1.2 2nd objective: Detect bacterial pathogens using an phage-based SPR biosensor

The second objective concerns the development and optimization of the SPR methodology for the detection of large biological objects, such as living cells and bacteria. While providing excellent sensitivity to thin surface biofilms, SPR shows certain limitations to thicknesses larger than the evanescent wave penetration depth. Because the evanescent wave of the SPR is limited to 300 nm in the direction perpendicular to the surface of detection (for visible light), only a

portion of the bacterium will generate a response by interfering with it. We hypothesize that it is possible to detect low concentrations of bacteria in real time, if surface immobilization chemistries and bacteriophage candidates are optimized for SPR detection. Our initial objective was to detect bacterial concentrations of less than $10^4$ CFU/mL in 20 minutes, without prior labeling or enrichment steps.

### 1.1.3 3rd objective: Compare phage-based detection with antibody-strategies for the SPR detection of clinical strains of S. aureus

Despite rapid progress in biosensor development for pathogen detection, applications of biosensors in a clinical setup are still rare, with the exception of glucose monitoring. In order to achieve point-of-care testing, it is necessary to meet the sensitivity and selectivity requirements for nosocomial pathogens. The latter is a major barrier for technology transfer to a clinical setup, as clinical samples differ greatly from homogeneous laboratory ones. As a result, it is essential to develop a biosensing tool that can effectively differentiate between strains of bacteria displaying a large spectrum of resistance. Because phages specific to different resistant strains of *S. aureus* are not yet isolated, we effectively modified the SPR sensing plateform to differentiate between 250 clinical strains of *S. aureus* displaying different antibiotic resistance patterns.

### 1.1.4 4th objective: Develop methodologies for nanoparticle-phage hybrids for enhanced biodetection applications such as LSPR.

Combining phages to nanoparticles can improve the sensitivity of biodectection as well as extend their use to a wide range of biotechnological applications, such as the targeted separation of specific bacteria from heterogeneous samples, labels for enhanced fluorescence and dark-field microscopy, and surface-enhanced Raman scattering.

## 1.2 Thesis organization

This thesis consists of one introductory chapter, six articles and one final chapter. While the first chapter outlines our objectives, the second, comprising the first article, is a review describing the

various antimicrobial approaches to treat bacterial infections, and why these conventional treatments are failing. We describe the leading emerging pathogens that are problematic in today's society. We then focus on bacteriophages and their mechanisms of action, and review the techniques that have been developed to exploit the specific binding ability of phages, including phage-based assays and biosensors. Finally, we outline the basic principles and recent advances in optical, electrochemical and mass sensitive biodetection technologies.

The second article, comprising the third chapter, concerns the real-time adsorption kinetics of SAMs at the gold interface, as monitored by SPR. Thiolated SAMs play a central role in biosensing technologies, as these molecules permit the generation of well-defined surfaces with chemical functionalities that permit further immobilization of recognition elements. Our goal was to compare the binding characteristics of L-cysteine and MUA, in order to establish the validity and applicability of each molecule as a linker element for biosensing purposes. Our findings allowed for a better understanding of the binding characteristics of SAMs and amino acids, permitting the elaboration of better strategies for the attachment of bacteriophages on gold.

In the fourth chapter, the third article discusses the use of SPR to monitor the real time attachment of MRSA bacteriophages to gold, using different immobilization approaches, including physisorption, the use of gluteraldehyde, L-cysteine, MUA, EDC/NHS or their combination. Our aim was to delineate the best strategy for the immobilization of the phages on the gold surface, while preserving their biofunctionalities and lytic efficiencies. We found that a mixed self-assembled monolayer of L-cysteine and MUA (in article 2) encouraged the oriented positioning of the phages with their caudal recognition proteins being exposed to the bacteria-containing medium.

The fourth article, in Chapter 5, integrates the findings of the previous articles and focuses on the phage-based detection of two pathogens by SPR, *E. coli* and MRSA. Furthermore, we report on the isolation and characterization of a novel phage that is highly specific for MRSA, and whose morphological characteristics make it more suitable for SPR detection. We find that our technique permits a label-free, real time, specific and cost-effective detection of pathogens, for concentrations lower than $10^3$ CFU/mL, in less than 20 minutes. This detection scheme is of

particular interest for public health, and its applicability can be extended to the military, agro-food and water industries.

With the goal of proving the validity and transferability of our biodetection system to the clinic, we partnered with the Laboratory of Public Health of Québec (Laboratoire de Santé Publique du Québec), who provided us with 250 clinical isolates of *S. aureus*. We first determined the susceptibility of these isolates to antibiotics, and found that the strains differed largely in their resistance patterns. The fifth article, Chapter 6, reports on the differential detection of community-acquired MRSA (CA-MRSA), hospital-acquired MRSA (HA-MRSA), methicillin susceptible *S. aureus* (MSSA), and borderline resistant oxacillin-resistant *S. aureus* (BORSA), using SPR, by specifically detecting PBP2a on whole bacterial cells, but without labeling, PCR or enrichment steps. We find that this method significantly impacts hospital costs, treatment, and infection control.

The sixth article, in Chapter 7, concerns the attachment and characterization of phages to heterobifonctional gold nanoparticles for nanotechnologically-based biomedical applications, such as enhanced SPR detection. We delineate the role of the interface, and the covalent coupling chemistry employed for the successful attachment of MRSA-specific phages to the gold nanoparticles. The applicability of those nano-bio hybrids can be extended to the targeted separation of specific bacteria from heterogeneous samples, labels for enhanced fluorescence and dark-field microscopy, and surface-enhanced Raman scattering detection.

The final chapter is devoted to critical discussions of the previous results, and presents our final recommendations.

## 1.3 Publications and presentations by the candidate

### 1.3.1 Publications included in the present work:

[1] **Tawil N**, Sacher E, Mandeville R, Meunier M. Bacteriophages: Powerful tools for microbial biosensing. Analyst. 2013 (Submitted, manuscript ID: AN-MRV-10-2013-001989).

[2] **Tawil N**, Hatef A, Sacher E, Maisonneuve M, Gervais T, Mandeville R, et al. Surface Plasmon Resonance Determination of the Binding Mechanisms of L-Cysteine and Mercaptoundecanoic Acid on Gold. Journal of Physical Chemistry C. 2013;117:6712-6718.

[3] **Tawil N**, Sacher E, Mandeville R, Meunier M. Strategies for the Immobilization of Bacteriophages on Gold Surfaces, Monitored by Surface Plasmon Resonance and Surface Morphology. Journal of Physical Chemistry C. 2013;117:6686-6691.

[4] **Tawil N**, Sacher E, Mandeville R, Meunier M. Surface plasmon resonance detection of *E. coli* and methicillin-resistant *S. aureus* using bacteriophages. Biosensors & Bioelectronics. 2012;37:24-9.

[5] **Tawil N**, Mouawad F, Levesque S, Sacher E, Mandeville R, Meunier M. The Differential Detection of Methicillin-Resistant, Methicillin-Susceptible and Borderline Oxacillin-Resistant Staphylococcus aureus by Surface Plasmon Resonance. Biosens Bioelectron. 2013;49:334-340.

[6] **Tawil N**, Sacher E, Mandeville R, Meunier M. X-Ray Photoelectron Spectroscopic and Transmission Electron Microscopic Characterization of Bacteriophage-Nanoparticle Complexes for Pathogen Detection. Journal of Physical Chemistry C. 2013; 117(40), 20656-20665

## 1.3.2 Other publications

### 1.3.2.1. Journal articles :

[1] Yao L, Lamarche P, **Tawil N**, Khan R, Aliakbar AM, Hassan MH, et al., CMOS Conductometric System for Growth Monitoring and Sensing of Bacteria. IEEE Transactions on Biomedical Circuits and Systems. 2011;5:223-30.

### 1.3.2.2. Book :

[1] Rahman M, Laurent S, **Tawil N**, Yahia LH, editors, Protein-Nanoparticle Interactions - The Bio-Nano Interface. Springer; 2013. ISBN 978-3-642-37554-5

### 1.3.2.3.Book chapters :

[1] Rahman M, Laurent S, **Tawil N**, Yahia LH, Mahmoudi M. The biological significance of nano-interactions. In: Rahman M, Laurent S, Tawil N, Yahia LH, editors, Protein-Nanoparticle Interactions - The Bio-Nano Interface. Springer; 2013. ISBN 978-3-642-37554-5

[2] Rahman M, Laurent S, **Tawil N**, Yahia LH, Mahmoudi M. Nanoparticle and protein corona. In: Rahman M, Laurent S, Tawil N, Yahia LH editors, Protein-Nanoparticle Interactions - The Bio-Nano Interface. Springer; 2013. ISBN 978-3-642-37554-5

[3] Rahman M, Laurent S, **Tawil N**, Yahia LH, Mahmoudi M. Protein Corona : Applications and challenges. In: Rahman M, Laurent S, Tawil N, Yahia LH editors, Protein-Nanoparticle Interactions - The Bio-Nano Interface. Springer; 2013. ISBN 978-3-642-37554-5

[4] Rahman M, Laurent S, **Tawil N**, Yahia LH, Mahmoudi M. Analytical methods for corona evaluations. In: Rahman M, Laurent S, Tawil N, Yahia LH editors, Protein-Nanoparticle Interactions - The Bio-Nano Interface. Springer; 2013. ISBN 978-3-642-37554-5

### 1.3.3. International internships

[1] Henkel KGaA, Research and Development, Düsseldorf, Germany (July 2009-October 2009)

### 1.3.4. Presentations :

[1] Developing a highly sensitive, highly specific biosensor for nosocomial bacterial detection. **N. Tawil**, E. Sacher, R. Mandeville, M. Meunier. Biomedical Science and Technology Research Group (GRSTB). Montreal, May 2009. (1st Prize for poster presentation)

[2] Phage-Based biosensor for the detection of methicillin-resistant *Staphylococcus aureus*. **N. Tawil** , E. Sacher, R. Mandeville, M. Meunier. 9th Workshop on Biosensors and Bioanalytical microtechnique in environmental and clinical analysis. Montreal, June 2009. (1st prize for poster presentation in ‘’Pathogen’’ section)

[3] Biocompatibility of nanoparticles and potential for biomedical applications. **N. Tawil**, E. Sacher, R. Mandeville, LH. Yahia, M. Meunier. Regroupement Québécois en Matériaux de Pointe. Sherbrooke, Octobre 2009.

[4] Surface plasmon resonance for the specific and real time detection of *E. coli* and MRSA. **N. Tawil**, E. Sacher, R. Mandeville, M. Meunier. Biophotonics in infectious disease. Quebec, September 2010.

[5] Surface Plasmon resonance for real time monitoring of thiolate-molecules and phage adsorption kinetics. **N. Tawil**, E. Sacher, R. Mandeville, M. Meunier. Regroupement Québécois en Matériaux de Pointe. Montreal, May 2010.

[6] Phage-based SPR biosensor for nosocomial bacterial detection. **N. Tawil**, E. Sacher, R. Mandeville, M. Meunier. IEEE Engineering in Medicine and Biology Society. Boston, September 2011.

[7] Bacteriophage-nanoparticle complexes for pathogen detection. **N. Tawil**, D. Rioux, E. Sacher, W. Chan, R. Mandeville, M. Meunier. NanoQuébec. Montreal, January 2012.

# CHAPTER 2 ARTICLE 1: BACTERIOPHAGES : POWERFUL TOOLS FOR MICROBIAL BIOSENSING

This chapter is a comprehensive literature review, concerning phage-based analytical and biosensing methods. We begin this review by concisely informing the reader of bacterial-host evasion mechanisms, as well as different types of antibiotics presently available on the market to combat bacterial infections. We discuss the problem of resistance and its societal costs, and delineate the clinically relevant bacterial pathogens, of worldwide concern, that are targeted by today's biodection research and development efforts. We then describe bacteriophages, their mechanism of action, and their relevance in theranostics. We discuss and review phage-based assays, notably phage amplification, reporter phage, phage lysis, and bioluminescence assays for the detection of bacterial species. We finally thoroughly review phage-based biosensors, including optical (comprising SPR sensors and fiber optic assays), electrochemical (comprising amperometric, potentiometric, and impedimetric sensors), acoustic wave and magnetoelastic sensors.

This chapter will pave the way for a better comprehension of the articles to follow, devoted to phage-based biosensing strategies for the detection of bacterial pathogens, and more specifically, *Staphylococcus aureus*.

# Bacteriophages: Powerful tools for microbial biosensing.

*Nancy Tawil*[1, 2,3], *Edward Sacher*[1], *Rosemonde Mandeville*[2], *Michel Meunier*[1,3]

[1] Regroupement Québécois de Matériaux de Pointe, Department of Engineering Physics, École Polytechnique de Montréal, Case Postale 6079, succursale Centre-ville, Montréal, Québec H3C 3A7, Canada

[2] Biophage Pharma, 6100 Royalmount, Montréal, Québec H4P 2R2, Canada

[3] Laser Processing and Plasmonics Laboratory, Department of Engineering Physics, École Polytechnique de Montréal, Case Postale 6079, succursale Centre-ville, Montréal, Québec H3C 3A7, Canada

## 2.1. Abstract

Pathogen detection is of utmost importance in many sectors, such as in the food industry, environmental quality control, clinical diagnostics, bio-defence and counter-terrorism. Failure to appropriately, and specifically, detect pathogenic bacteria can lead to serious consequences, and may ultimately be lethal. Public safety, new legislation, recent outbreaks in food contamination, and the ever-increasing prevalence of multidrug-resistant infections have fostered a worldwide research effort targeting novel biosensing strategies. This review concerns phage-based analytical and biosensing methods targeted towards theranostic applications. We discuss and review phage-based assays, notably phage amplification, reporter phage, phage lysis, and bioluminescence assays for the detection of bacterial species, as well as phage-based biosensors, including optical (comprising SPR sensors and fiber optic assays), electrochemical (comprising amperometric, potentiometric, and impedimetric sensors), acoustic wave and magnetoelastic sensors.

## 2.2. Introduction to virulent pathogenic bacteria

Bacterial pathogens have developed several mechanisms that aid in circumventing the host defences. The pathogenicity and virulence of a microorganism are highly complex and are governed by the bacterium-host interactions. Classical bacterial virulence factors include toxins and molecules essential for adhering and invading the host, as well as evading the host's detection mechanisms and immune response.

Classically, these virulent bacteria have been treated with antibiotics since the discovery of penicillin in 1928 [11]. Major mechanisms of antibiotic action include the inhibition of the synthesis of DNA (quinolones), RNA (rifamycins), and cell walls (β-lactams and glycopeptides) or proteins (macrolides, lincosamides, streptogramins, amphenicols, oxazolidinones, tetracyclines, aminocyclitols and aminoglycosides) [12]. Quinolones interfere with DNA replication by introducing DNA breaks and trapping topoisomerase II (for Gram-negative bacteria) and topoisomerase IV (primarily in Gram-positive bacteria) at the cleavage stage, thus compromising strand rejoining[12]. Similarly, rifamycins inhibit DNA transcription by binding to the β-subunit of an active RNA polymerase. Additionally, bactericidal activity can be achieved by inhibition of cell wall synthesis.

Bacterial cell walls are composed of peptidoglycan layers that are extended by transglycosylases and cross-linked by penicillin-binding proteins (PBPs) [13]. β-lactams bind to the active site of PBP and inhibit the formation of the peptide bond that cross-links peptidoglycan subunits, inducing changes in cell-wall morphology and subsequent bacterial death. Moreover, a broad-range of drugs inhibits protein synthesis by affecting either the 50S or the 30S ribonucleoprotein subunits. Drugs that inhibit the 50S ribosome subunit either block the initiation of protein transcription or the elongation of the nascent peptide chain. Furthermore, 30S inhibitors either prevent aminoacyl tRNA from binding to the ribosome or induce tRNA mismatching, either of which result in protein mistranslation[12].

Although the development of antibiotics stands as one of the most substantial medical innovations, the ever-increasing prevalence of multidrug-resistant infections has created a global public health crisis [7]. In the United States, excess health costs attributable to antibiotic-resistant infections annually reach $20 billion, with 8 million days of additional hospital occupancy, and $35 billion in societal costs [8].

Antibiotic resistance can be acquired through several mechanisms including mutations due to selective pressure and horizontal transfer of genetic material through transformation, conjugation and transduction. These genes include a variety of enzymes and efflux pumps that are detrimental to the antibacterial agent. Moreover, these genes can alter the metabolic pathway resulting in the production of altered cell-wall proteins that evade antibiotic targeting.

Although substantial efforts are directed toward producing antibiotic and non-antibiotic derivatives, such as antibacterial vaccines, phage therapy, immunostimulants, adjuvants, probiotics, and antivirulence therapies, the *gold standard* for bacterial detection persists to be traditional culture-based assays, which are cumbersome and time-consuming. Other conventional techniques, such as the polymerase chain reaction (PCR), immunological assays, fluorescence and spectrophotometry, suffer from several drawbacks: they are time-consuming, expensive, laborious, and require enrichment steps and highly trained personnel. There is, therefore, a increasing need for methods that eliminate the necessity for microbial cultures, reduce the time of diagnosis, and increase the sensitivity and specificity of detection.

The advent of biosensors has permitted major advancements in microbial detection. Depending on their transduction elements, these can be classified as optical, electrochemical or acoustic. Moreover, they can be classified according to their biorecognition elements. Most biosensors rely on the use of antibodies. However, polyclonal antibodies suffer from high costs of production and environmental instability, thus limiting their shelf-life, storage and applicability in non-regulated environments such as humid and high temperature climates. Moreover,

polyclonal antibodies have the ability to recognize different epitopes present on the same pathogen or on related non-pathogenic organisms, thus hindering their selectivity [9]. On the other hand, monoclonal antibodies can be produced more rapidly, and are selective, but their production is still costly and they are fragile to environmental fluctuations, such as temperature, pH, ionic strength, and cross-reactivity.

We now turn our attention to bacteriophages, which are a key factor in microbial homeostasis on Earth, outnumbering their bacterial hosts tenfold. Throughout history, bacterial pathogens have developed multiple strategies to combat viruses, which were circumvented by phages' ability to evolve and survive in adverse environments. Bacteriophages' specificity to their bacterial hosts, robustness, low-cost and ease of production make them ideal recognition elements for bacterial biodetection purposes.

Here we delineate the clinically relevant bacterial pathogens, of worldwide concern, that are targeted by today's biodetection research and development efforts. We then describe bacteriophages, their mechanisms of action, and relevance in therapeutics and diagnostics. We finally review phage-based analytical and biosensing methods, notably phage-amplification, reporter phage, phage lysis, bioluminescence assays, as well as the novel optical, electrochemical and mass-sensitive biosensor technologies using bacteriophages as a recognition element.

## 2.2. Clinically relevant bacterial pathogens

Microorganisms are an intrinsic part of our environment, and play a fundamental role in human hemostasis. Problems arise when immunocompromised patients come into contact with certain pathogens that have developed resistance to antimicrobial agent in our health care system. The most predominant nosocomial agents are *Enterococcus faecium, Staphylococcus aureus, Klebsiella pneumoniae, Acinetobacter baumanni, Pseudomonas aeruginosa,* and *Enterobacter*

species, commonly known as “the ESKAPE bugs”[14]. In the following section, we briefly describe some of these bacteria, as well as other virulent bacteria that cause major problems in hospitals in the developed and developing countries. Most of these bacteria have been targeted in biosensing technologies depicted in this review.

### 2.2.1. *Staphylococcus aureus*: the case of the golden killer bacterium

*S. aureus* is a ubiquitous Gram-positive microorganism that colonizes the nasal passages and skin of approximately 50% of healthy individuals [15]. *S. aureus* can cause a broad spectrum of infections, ranging from common skin infections to sepsis. It is the leading cause of nosocomial pneumonia, bloodstream infection, and infections caused by surgical wounds and prosthetic implants [16, 17]. *S. aureus* has quickly acquired resistance against β-lactam antibiotics by producing a specific penicillinase enzyme [18] encoded by a plasmid. This prompted the introduction, in 1959, of methicillin, a modified penicillin that was unaffected by the staphylococcal penicillinase [17]. Its success was, unfortunately, short-lived. β-lactams, are substrate analogs of a penicillin-binding protein, which, as previously mentioned, catalyzes the formation of peptide crosslinks between glycan chains of the bacterial cell wall. This time, *S. aureus* acquired a mecA gene that encodes PBP2a , that confers a broad spectrum of resistance against methicillin, as well as all other β-lactams (i.e. synthetic penicillins, cephalosporins and carbapenems) [18]. Recently, strains resistant to glycopeptides, such as vancomycin, have immerged and acquired a *vanA* gene cluster [19]. These strains are very hard to detect and are often associated with therapeutic failure. MRSA has become an increasingly alarming problem, as it is no longer contained in hospital settings, but has emerged into the community, and is now pandemic. According the Centers for Disease Control and Prevention (CDC), more patients died from MRSA-related infections in the United States, in 2005 [20], than did from acquired immunodeficiency syndrome (AIDS) complications [21].

### 2.2.2. *Y. Pestis*: from ‘‘black death’’ to biological warfare

*Yersinia pestis* is the causative organism of plague, which is often thought about as an ancient disease, but which is, to this day, endemic in parts of Asia, Africa, and America, causing a reported three thousand deaths annually [22]. *Y. pestis* is a Gram-negative bacterium of the *Enterobacteriaceae* family. It infects human macrophages, which are transported to draining lymph nodes. It becomes extracellular upon apoptosis of the infected host macrophage, colonizing major organs and causing systemic failure, leading to death [23]. The lack of proper diagnostic tools that can effectively and rapidly detect this pathogen has contributed to underreporting of cases and major shortcomings in case-management and surveillance [22].

### 2.2.3. *E. coli* O157:H7: an emerging lethal food-borne pathogen

Enterohemorrhagic *E. coli* is a zoonotic life-threatening bacterium that was first described in 1982, and leads to diarrhea, hemorrhagic colitis and hemolytic-uremic syndrome in humans. O157:H7 is a pathogenic subset of the Shiga toxin-producing *E. coli* (STEC) that is mainly transmitted by consumption of undercooked meat, unpasteurized dairy products, and produce contaminated with bovine faeces. Detection and control of these pathogens represent a challenging problem, with regard to their high virulence and the extremely low infectious dose required to induce disease [24].

### 2.2.4. *Salmonella*: a non-negligible threat

*Salmonella* bacterium colonize a broad spectrum of host organisms, efficiently infecting both animals and plants. Among the *Salmonella* species, *Salmonella enterica* is the primary cause of food-borne poisoning in humans, contaminating a wide range of produce, such as pre-cut meats, poultry, eggs, vine vegetables, fruits, nuts, sprouts, leafy greens, roots and beans [25]. The CDC

reports that approximately 15% of United States citizens will become infected with food-borne pathogens, with salmonellosis ultimately responsible for the largest number of hospitalizations and related deaths [26].

### 2.2.5. *Listeria monocytogenes*: an emerging pathogen

*L. monocytogenes* is a Gram-positive rod responsible for listeriosis, a flu-like disease, gastroenteritis and fever in healthy individuals. However, listeriosis can be deadly, with symptoms ranging from septicemia, meningitis or spontaneous abortion, in immune-compromised patients, children, the elderly, and pregnant women [27]. *Listeria* is one of the leading emerging pathogens associated with food-borne diseases, with an estimated 1600 cases yearly in the United States[28].

### 2.2.6. *M. tuberculosis*: the modern ‘‘white plague’’

Tuberculosis (TB) is a disease caused by *Mycobacterium tuberculosis*, and is one of the most destructive bacterial diseases to afflict humans. The World Health Organization reports that approximately 33% of mankind is latently infected with TB, with 1.8 million annual deaths and 9.8 new infections every year.

Following the inhalation of the bacilli, the bacteria deposit in the lung alveolar space, and multiply in the alveolar macrophages. They are then carried to the lymph nodes by dendritic cells (DCs), which undergo programmed cell death and release mycobacterial antigenic peptides. These antigens activate T-cells that will proliferate and become effector T cells, which go back to the lungs to fight the infection. This is followed by the generation of granuloma, that can ultimately contain the infection. Many factors, such as a poor diet, immunosuppression, steroid

use, and HIV therapy, can reactivate the latent state of the infection and cause bacteria to become metabolically active and reactivate the disease.

Drug-susceptible TB can be successfully treated by daily administrating a regimen of drugs to the patient, for an initial treatment phase of two months, followed by a continuation phase ranging from four to seven months [29]. However, major complications arose following the emergence of multidrug-resistant and extensively drug-resistant strains, around the world. As with MRSA, there are very few compounds in clinical development for anti-TB drugs; thus, fast detection becomes paramount for a better management of the disease.

## 2.3. The potent bacteriophage

Bacteriophages serve as the natural counterbalance to bacteria, and have become the most ubiquitous source of life on earth ($10^{30}$ - $10^{32}$ phage species). They are commonly found in human intestines, having been consumed by humans via foods (e.g., ground beef, pork sausage, chicken, farmed freshwater fish, oil sardines, raw skim milk, cheese, and drinking water) [30], and are vastly distributed in our ecosystem.

Modern phage research was initiated by Frederick W. Twort 1915 [30, 31] and carried on by Félix d'Herelle, in 1917 [32] who uncovered the phages' natural ability to combat bacterial pathogens and prevent infections [33],[34],[35]. Bacteriophages are viruses that infect both Gram-negative and -positive bacteria by using their pili as receptors. Phages are parasites that use their bacterial host machinery to direct their replication. Each phage particle is constituted of genomic material enclosed in a protein or lipoprotein coat, called a capsid [30]. Phages are subdivided in multiple genera, based on their morphology, nucleic acid homology, and serology, and two groups, based on their life cycles, replication, and propagation [36]. Lytic bacteriophages are virulent phages that specifically recognize and infect their host bacterium, use the bacterial

machinery to replicate its genome, produce and assemble their structural components, and ultimately lyse and kill the bacterium to release the newly assembled virions.

Temperate phages differ from lytic phages as they are capable of of both lytic and lysogenic propagation. These phages have the capacity of incorporating their genomic material into bacterial chromosomes and assuming a quiescent state (prophage), which will allow both the bacterium and the prophage to co-exist for a period of time without lysis [36], shielding the host bacterium from further phagic infection, and introducing novel genetic material such as reistance genes and restriction systems [30].

Curently, phages are grouped in nineteen families, of which two possess an RNA genome and five are enveloped. Tailed phages of the order of the Caudovirales accounts for approximately 95% of present-day isolated bacteriophages. The virions are constituted of an isocahedral head composed of repeating units of one or two proteins, which enclose the phage's genomic double-stranded DNA [30]. Tailed phages are grouped according to their morphology: phages possessing a long flexible tail belong to the *Siphoviridae*, while the *Myoviridae* comprise phages with contractile tails, and the *Podovidrea* being phages with very small non-contractile tail [30].

Ten more families account for a vast variety of tailless phages which are polymorphic in shape, may have a lipid coat, differ in their genomic material with the nucleocapsid containing either ssDNA, dsDNA or RNA. Moreover, these phages can differ on the basis of their means of propagation, and by whether they are segmented or not [30]. The difference between tailed and tailless phages is of major importance for host recognition and adsorption. The interaction between the phage and the receptor of the bacteria is an on-and-off process, ultimately followed by the irreversible binding of the phage to its host [37]. Tailed-phages specifically recognize their bacterial hosts through the interaction of a single central fibre called adhesin, or a cluster of 3,6 or 12 fibers found on their caudal extremity. These caudal proteins will recognise and adhere to specific epitopes on their host membrane and achieve irreversible binding through the interaction of a secondary tail protein to another bacterial membrane receptor.

Some types of bacteriophages, such as P22, have short tail fibers, called tail spike proteins, which recognize and bind the host bacteria. Furthermore, the phage tail often exhibits enzymatic activity capable of locally breaking down the cell wall. Filamentous phages, on the other hand, consist of a long structure made of repeating pVIII proteins. The length of the phage is proportional to the number of nucleotides in its genome (there are 0.435 pVIII proteins per nucleotide, which corresponds to 0.1435 nm per nucleotide) [38]. Figure 2-1 shows a transmission electron microscope (TEM) photomicrograph of bacteriophages specifically interacting with a MRSA bacterium.

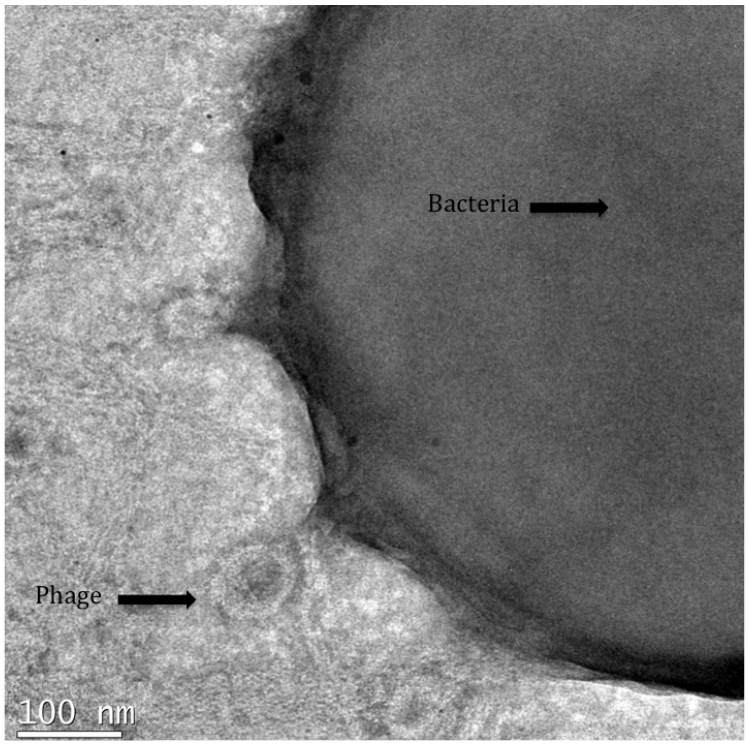


Figure 2-1: TEM photomicrograph of bacteriophages adhering specifically to the MRSA bacterium

Bacteriophages' specificity, ability to persist in a vast range of environmental conditions, and their ease of production in suitable hosts, make them a critical vehicle for the coevolution and horizontal gene transfer between different bacterial species[30]. Moreover, the many advantageous properties of bacteriophages make them an important tool for the diagnosis and the control (prevention and therapy) of bacterial diseases.

The therapeutic potential of bacteriophages for the treatment of bacterial infections in humans was recognized in the early 1920s with the pioneering work of d'Herelle who successfully treated patients infected with the bubonic plague while stationed in Egypt, and patients suffering from cholera in India[30]. However, phage research came to a standstill with the advent of antibiotics and their mass-production during World War II. Recent interest in bacteriophages was brought about by the alarming incidence of multi-drug resistant pathogens. Today, the commercial and medical opportunities of phage-based products are vast owing to their beneficial properties. Characterization of novel phages targeting specific bacterial pathogens is achieved much faster and at a lesser cost than antibiotics. Moreover, bacteriophages' specificity allow for a targeted action against host whit minimal effects on the otherwise desirable microbial flora, and target problematic bacterial states such as biofilms and persister cells[39, 40]. Phage's ability of to distinguish between live and death cells aid in overcoming major limitations of routinely used techniques for microbial diagnostics such as PCR and hybridization-based assays. Finally, bioengineered phages with novel functionalities [41, 42] and phage-functionalized nanoparticles [43] can be used for sensing as well as other relevant techniques, such as molecular imaging.

## 2.4. Phage-based assays

Since their discovery by Twort and d'Hérelle, bacteriophages have been extensively exploited to specifically target and identify bacteria. To this day, phage typing is used to differentiate between diverse strains of particular species of bacteria. Phage typing exploits phages' ability to specifically recognize, infect, and ultimately lyse their host. However, characterization and epidemiological identification of bacteria, using this method, requires the maintenance of a large phage library, thus restricting its use to a limited number of reference laboratories. Therefore,

there is a paramount need for phage-based technologies that can be used for the detection of pathogenic bacteria in a clinical setting. Three main methods exploiting bacteriophages are used to detect clinically relevant bacterial pathogens: (1) bacterial amplification of phages followed by the detection of progeny phages, (2) detection of light produced by reporter phages or fluorescent reporter phages following infection of bacteria, and (3) detection of intracellular components following infection and lysis of the bacterial host.

### 2.4.1. Phage amplification assays

Lytic phage propagation consists of adhesion to the bacterial host, transfection and replication of the phage genome, followed by the assembly of the virion structural components. This culminates in the release of the progeny phages as a result of bacterial cell lysis. The increased number of phages in the solution can be used as a marker of the specific infection and and phage lytic propagation in a target bacterium. In the past, this technique has been hampered by the necessity of a large bacterial titer, as well as the cost and complexity of identifying the progeny phages with high-performance liquid chromatography (HPLC). Novel advances in phage amplification assays have obviated the need for complicated instruments and require a low abundance of initial target pathogens. Phages are incubated with their target bacteria, and phagicidal reagent is added before lysis can occur to inactivate free phages. The virucide is then neutralized and helper cells, susceptible to be infected by the progeny phages, are added to the solution and plated onto a soft agar overlay. The phages are allowed to replicate within the previously infected bactrerial pathogens and can, in turn, infect the helper cells, resulting in the formation of lysis plaques. This technique has the advantages of being able to detect initially low concentrations of bacteria, as well as target bacteria in a heterogeneous bacterial sample. Diagnostic kits and novel assays based on phage amplification are available for *M. tuberculosis* [44-49], *Staphylococcus aureus* [50-52], and *Yersinia Pestis* [45, 53]. Table 2.1 lists phage-based amplification assays for the detection of a large number of bacterial species. Phage amplification assays, combined with the addition of antibiotics, can help distinguish between resistant and susceptible strains, such as antibiotic resistant *M. tuberculosis* [54-57] and MRSA [58]. Moreover, phage typing is often combined with other techniques, such as PCR [59, 60], mass spectrometry [51, 53] and competitive ELISA [61].

Table 2.1:Phage-based amplification assays for the detection of bacterial species

| **Bacterial Species** | **Phage** | **Time of detection** | **Sensitivity** | **References** |
|---|---|---|---|---|
| *E. coli O157:H7* | LG1 | 23 h | 2 CFU/25 g | [62, 63] |
| *E. coli O157:H7* | AR1 | 3.5 h | 1 CFU/mL | [63, 64] |
| *E. coli* | MS2 | 2 h | $10^4$ CFU/mL | [65] |
| *Salmonella* | P22 | 4 h | $10^4$ CFU/g | [66] |
| *Salmonella* | SJ2 | 20 h | 3 CFU/25 g | [62] |
| *Salmonella enterica* | SJ2 | 5 h | $10^4$ CFU/mL | [67] |
| *Mycobacterium avium paratuberculosis* | D29 | 48 h | 10 CFU/mL | [68] |
| *M. tuberculosis* | D29 | 48 h | $10^2$ CFU/mL | [68] |
| *Y. pestis* | ΦA1122 | 5 h | $10^6$ CFU/mL | [69] |
| *Y. pestis* | ΦA1122 | 4 h | $10^3$ CFU/mL | [69] |
| Y. pestis | L-413 C | 4 h | $10^5$ CFU/mL | [45] |
| *Pseudomonas aeruginosa* | NCIMB 10116 | 4 h | 10 CFU/mL | [50] |
| *Salmonella* | Felix-01 | 4 h | $10^2$ CFU/mL | [50] |
| *S. aureus* | N-15 | 5 h | $10^5$ CFU/mL | [51] |

### 2.4.2. Reporter phage assays

It is possible to engineer recombinant phages for pathogen detection. This can be done by inserting the reporter gene into the target cell and monitoring the production of the protein encoded by the inserted genomic material. The method of gene insertion into the phage varies considerably. Cloning can only be used with somewhat small phage genomes and is made difficult by the need of customized genetic manipulation, systems and nucleic acid packaging. An easier, more efficient and cost-effective method is the insertion of the reporter gene into the intergenic parts of the phage genome, resulting in multiple and diverse particles that can later be selected, depending on the desired properties. Cloning of the reporter phage into a plasmid is another method of insertion. The introduction of a plasmid into a phage host will result into double-crossover homologous recombination between the plasmid and the phage DNA, and the introduction of the plasmid into the phage genome. Again, the expression of the reporter gene in the host cell will result in a measurable signal. The use of a reporter phage provides an economic and timesaving method of detection of pathogenic bacteria. A variety of reporter genes, such as firefly luciferase (Lux), green fluorescent protein (GFP), and yellow fluorescent protein (ZsYellow), have been incserted into non-coding regions of a phage and were subsequently used for bacterial detection (Table 2.2).

Table 2.2:Reporter phage assays for the detection of bacterial species

| **Reporter gene** | **Bacterial specie** | **Phage** | **Time of detection** | **Sensitivity** | **Refs** |
|---|---|---|---|---|---|
| *luxI* and *luxR* | *E. coli* | λ | 10 h | 1 CFU/mL | [70] |
| *luxI* and *luxR* | *E. coli O157:H7* | PP01 | 22 h | 1 CFU/mL | [71] |
| *luxI* and *luxR* | *E. coli O157:H7* | PP01 | 6 h | 1 CFU/mL | [71] |
| *luxI* and *luxR* | *E. coli O157:H7* | PP01 | 12.5 h | 1 CFU/mL | [71] |
| *luxAB* | *E. coli O157:H7* | AR1 | 3 h | 10 CFU/mL | [64] |
| *luxAB* | *Y. Pestis* | ΦA1122 | 30 min. | $10^6$ CFU/mL | [72] |
| *luxAB* | *Salmonella enteritidis* | P22 | 24 h | 63 CFU/mL | [73] |
| *luxAB* | *Salmonella Typhimurium* | P22 | 16 h | $10^6$ CFU/mL | [74] |
| *luxAB* | *Salmonella enterica* | P22 | 6 h | 10 CFU/mL | [73] |
| *luxAB* | *L. monocytogenes* | A511 | 20 h | 1 CFU/g | [75] |
| *luxAB* | *Enteric bacteria* | Cocktail | 5 h | 10 cells/g | [76] |
| *luxAB* | *B. anthracis* | Wβ | 1 h | $10^3$ CFU/mL | [72] |
| *lacZ* | *E. coli* | T4 | 8 h | 10 CFU/mL | [77] |
| *inaW* | *Salmonella* | P22 | 2 h | 10 CFU/mL | [78] |

| | | | | | |
|---|---|---|---|---|---|
| *luc* | *M. tuberculosis* | phAE142 | 1-2 weeks | $10^3$ CFU/mL | [79] |
| *luc* | *M. tuberculosis* | Che/phAETRC16 | 24 h | $10^8$ CFU/mL | [80] |
| GFP | *E. coli* | IP008e-/2xGFP | 6 h | Not reported | [81] |
| GFP | *E. coli* | λ | 6 h | $10^2$ CFU/mL | [82] |
| GFP | *M. tuberculosis* | TM4 | 4 h | 100 cells | [83] |

### 2.4.3. Phage lysis assays

The lytic propagation of bacteriophages results in the lysis and the release of bacterial intracellular components, as well as the liberation of progeny virions into the extracellular environment. Phages' lytic properties are attributed to two phagic proteins implicated in the break-down of the bacterial cell wall. The first functions as a holing protein, forming small pores in the bacterial cytoplasmic membrane, while the second protein, an endolysin, degrades peptidoglycans, resulting in the release of a multiple intracellular markers that can be easily detected [84]. Table 2.3 lists phage-mediated cell lysis assays. The most popular method is the measurement of bacterial intracellular adenosine triphosphate (ATP). The amount of ATP metabolized by a bacterium declines quickly following cell death. The firefly luciferase/luciferin enzyme system allow for the detection and enumeriation of viable bacterial cells by sensing intracellular ATP [85]. The enzyme system allows for the production of light that can be measured by a small hand-held luminometers and is directly proportional to the quantity of ATP in the assay. However, this system is limited by the fact that detection of specific pathogens is not possible. The specificity can only be achieved by specific cell lysis, which can be accomplished by phages [84]. Therefore, pathogen-specific phages and ADP are added to the sample, where the phage will only infect the target bacteria and not interact with other microorganisms that may be

present in the sample. The sensitivity of this assay can be improved by measuring the amount of released adenylate kinase (AK). Similarly, intracellular AK will be released after phage lysis. When ADP is present in excess, the equilibrium of the reaction shifts toward the creation of ATP, and the overall quantity of fluorescent light emitted from a firefly luciferase will be proportional to the number of viable cells in the sample. Table 2.4 lists bioluminescence assays, including those utilizing AK. So as to further improve the sensitivity of the assay, AK is combined with an immunomagnetic separation (IMS) step, where the pathogens of interest can be captured on antibody-coated magnetic beads [84]. Another method for the identification and quantification of bacterial pathogens relies on the amperometric detection of enzymatic activity induced by intracellular bacterial enzymes liberated following phage-induced lysis. Betagalactosidase and endolysins can also be monitored.

Table 2.3: Phage-mediated cell lysis assays for the detection of bacterial species

| **Bacterial Specie** | **Phage** | **Time of detection** | **Sensitivity** | **Refs** |
|---|---|---|---|---|
| *E. coli O157:H7* | CSLO157 | 10 h | 10 cells/25 g | [86] |
| *E. coli* | PhiX174 | 2 h | $10^5$ cfu/mL | [87] |
| *E. coli* | NCIMB 10359 | 1 h | $10^4$ cfu/mL | [88] |
| *E. coli* | AT-20 | 2 h | $10^3$ cfu/mL | [89] |
| *E. coli* | T4 | 2 h | $10^3$ cfu/mL | [90] |
| *E. coli* | λ | 6 h | $10^2$ cfu/mL | [91] |
| *B. cereus* | B1-7064 | 8 h | 10 CFU/mL | [92] |
| *Salmonella* | SJ2 | 2 h | $10^3$ cfu/mL | [89] |
| *Salmonella newport* | Felix-01 and Newport | 2 h | $10^4$ cfu/mL | [88] |

Table 2.4:Bioluminescence assays for the detection of bacterial species

| **Assay type** | **Bacterial specie** | **Phage** | **Time of detection** | **Sensitivity** | **Refs** |
|---|---|---|---|---|---|
| Adenylate kinase assay | *E. coli* | E. coli phage | 1h | $10^3$ cfu/mL | [88] |
| YOYO-1 fluorescent dye | *E. coli O157:H7* | LG1 | 6 h | 2 CFU/g | [63] |
| DAPI fluorescent dye | *E. coli* | T4 | 6 h | Not reported | [93] |
| Adenylate kinase assay | *Salmonella Newport* | Newport phage | 2h | $10^3$ cfu/mL | [88] |
| Adenylate kinase assay | *Salmonella enteritidis* | SJ2 | 2h | $10^3$ cfu/mL | [89] |
| Adenylate kinase assay | *E. coli G2-2* | AT20 | 2h | $10^3$ cfu/mL | [89] |
| Bioluminescent phage | *Bacillus anthracis* | Wβ:*luxAB* | 60 min | $10^3$ cfu/mL | [72] |

## 2.5. Phage-based biosensors

Recent years have seen the increased use of biosensors as a novel method for pathogen detection. These new systems are designed to overcome the many limitations of conventional detection platforms, such as reverse transcriptase PCR (RT-PCR) and enzyme-linked immunosorbent assays (ELISA). Although RT-PCR and ELISA are popular, and prove effective in detecting the presence of pathogens, they still require an enrichment step prior to analysis, as well as highly trained personnel. On the other hand, biosensors are selective, sensitive, cost-effective, rapid and portable alternatives to conventional analytical methods. Various recognition elements, such as nucleic acids and antibodies, can be used in pathogen detection. There are, however, very few biosensing technologies using bacteriophages in the clinical, agro-food or environmental fields. The lack of attention paid to phages may result from the misconception that their study is too specialized an undertaking for most engineering laboratories. However, viral diversity and novelty are astounding, and including them in sensing platforms has several benefits. Here we outline the basic principles and recent advances in biosensing technologies using optical, electrochemical and mass monitoring for phage-based diagnostics.

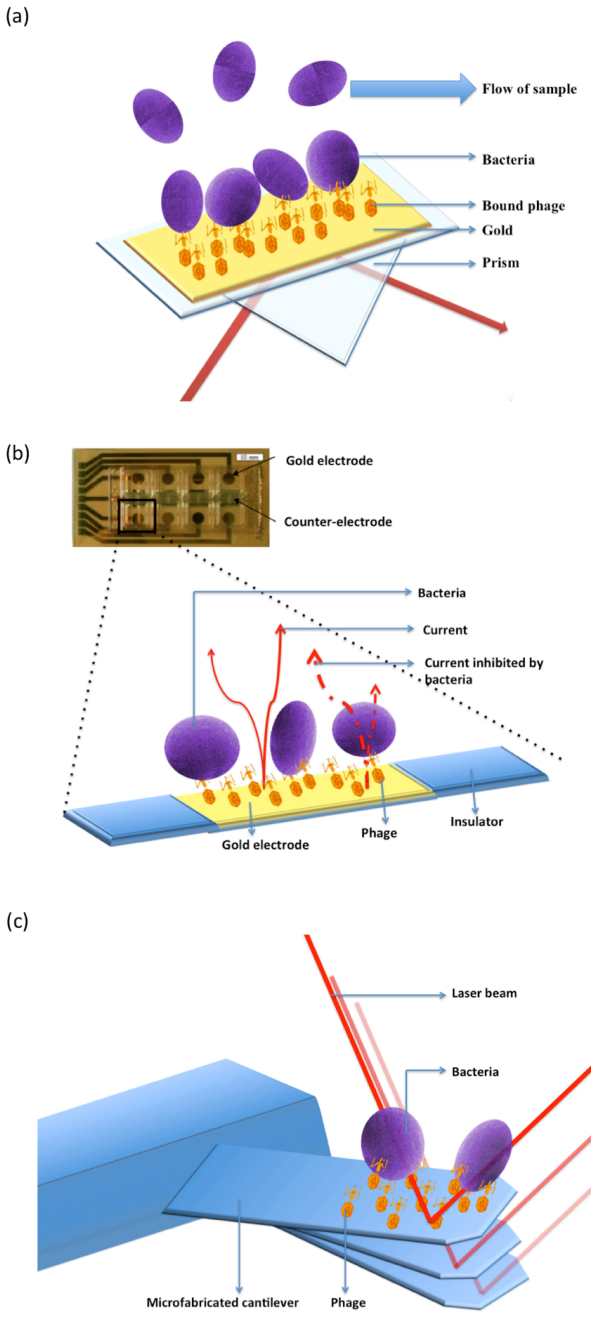


Figure 2-2: Schematic representation of phage-based biosensing techniques for the detection of bacterial pathogens using (a) optical, (b) electrochemical, and (c) mass monitoring techniques.

### 2.5.1. Optical biosensors

Optical biosensors have been extensively investigated as a means of detecting pathogens, due to their well-known selectivity and sensitivity. Of the various optical techniques used for the detection of pathogens, surface plasmon resonance and evanescent field optical fiber systems dominate the industry (e.g. Biacore, Biosensing Instruments, Inc. and Research International).

#### 2.5.1.1. Surface plasmon resonance biosensors

Surface plasmon resonance (SPR) is a method that can be suitably modified for bacterial detection, as it is designed for the real-time monitoring of all dynamic processes, without labeling and complex sample preparation. Therefore, adsorption rate, association and dissociation kinetics, as well as affinity constants and ligand interactions, can be easily and rapidly examined [94].

In 1902, Wood observed slender, dark bands when illuminating a metallic diffraction grating with polychromatic light, which he called anomalies [95]. Later, Fano came to the conclusion that the excitation of electromagnetic surface waves on the diffraction grating caused these anomalies [96]. Moreover, while illuminating thin metal films on a substrate in 1958, Turbadar noticed a decrease in reflectivity [97]. A decade later, Otto explained these results and demonstrated that this drop in reflectivity is due to the excitation of surface plasmons observed in attenuated total reflection (ATR) [98]. This phenomena was also reported the same year by Kretschmann and Raether, while using another ATR configuration[99].

A surface plasmon is a specific mode of the electromagnetic field (i.e. a longitudinal charge density wave) that propagates at the interface between a metal and a dielectric [100]. Surface

plasmons are characterized by a field distribution and a complex propagating constant which is highly sensitive to changes in the refractive index distribution [100]. It is important to use the right kind of metal, as this metal must fulfill certain requirements. The metal of choice must exhibit free electron behavior: the metal must follow the free electron model and its permittivity component, in the visible and near infrared regions of the spectrum, must be negative [100]. This is due to the fact that a surface plasmon exists at the metal-dielectric interface only at wavelengths longer than a certain critical wavelength. This critical wavelength is contingent on the plasma frequency, and is specific to the metal. Metals, such as gold, silver and aluminum, are all suited for surface plasmon resonance because their critical wavelengths lie in the UV or visible region of the spectrum. Gold is one metal of choice because of its stability, and silver, because it provides a sharp SPR resonance peak.

Surface plasmons are excited by light waves, using 1) prism coupling and attenuated total reflection, 2) diffraction on a metal diffraction grating, and 3) coupling among parallel optical waveguides [100].

An SPR optical sensor generally comprises an optical system, a transducing medium and an electronic system permitting data processing. Analysis is performed by capturing a recognition element on the sensor surface, and by injecting the analyte over the sensor surface. A measurable signal will be generated in the event of analyte binding to the immobilized ligand on the sensor surface, resulting from a refractive index change in the evanescent field, shifting the SPR angle. Figure 2-2 is a schematic representation of the SPR direct detection of captured bacteria, via immobilized bacteriophages, on a gold sensing platform.

Current instruments have a detection limit of $10^{-7}$ refractive index units (RIU), corresponding to 0.1 pg $mm^{-2}$ of molecules gathering on the sensor surface [101]. When applied to pathogen detection, the current detection limit is about $10^5$ CFU/mL for *Listeria monocytogenes* [102], *E. coli* O157:H7[103], *Campylobacter jejuni* [103], *S. typhimirium* [103], and *S. aureus* [104], using different recognition elements. Balasubramanian et al. showed that it was possible to specifically detect *Staphylococcus aureus*, using a Spreeta biosensor, by physically adsorbing bacteriophages

on the gold surface. However, the surface coverage of the platform by bacteriophages did not have a significant effect on the sensitivity of detection [105]. The authors assumed that the non-favorable orientation of the phages resulted in blocking the bacterial adhesion sites. Moreover, their results showed that it was difficult to detect bacteria in solution, due to the size of the bacterium cell (0.5-1μm). Because the evanescent wave of the SPR is limited to 300 nm in the z-direction, only a portion of the bacterium will generate a response by interfering with the evanescent wave. Improving immobilization strategies and phage recognition elements allowed for a more sensitive approach (i.e. detection limit ranging from $10^2$-$10^3$ CFU/mL) for the detection of *S. aureus* [3, 106, 107] and *E. coli* [3]. Table 2.5 compiles recent advances in phage-based SPR detection of pathogens.

Table 2.5:Phage-based SPR assays for the detection of bacterial species

| **Species** | **Phage** | **Time of detection** | **Sensitivity** | **Refs.** |
|---|---|---|---|---|
| *E. coli* K12 | T4 | 20 min. | 7 x $10^2$ cfu/mL | [108] |
| *E. coli* K12 | T4 | 15 min. | $10^3$ cfu/mL | [3] |
| *MRSA* | BP14 | 15min. | $10^3$ cfu/mL | [3] |
| *Salmonella* | P22 phage TSP | 30 min. | $10^3$ cfu/mL | [109] |
| *C. jejuni* | Phage NTC 12673 TSP | 25 min. | $10^2$ cfu/mL | [110] |
| *S. aureus* | Phage 12600 | 40 min. | $10^4$ cfu/mL | [111] |
| *S. aureus* | Phage 12600 | 10 min. | $10^6$ cfu/mL | [112] |
| *L. monocytogenes* | Phage Lm P4:A8 | 2 h | $10^6$ cfu/mL | [113] |

#### 2.5.1.2. Fiber optic biosensors

As with SPR biosensors, fiber optic sensors react to changes in the evanescent field due to modifications of the refractive index at the sensor surface following analyte binding. [114]. In general, fiber-optic sensors utilize lasers to generate evanescent waves that excite fluorescently labeled pathogens present on the surface of the waveguide [115]. This generates fluorescent signals that can be detected in real time. Fluorescein isothiocyanate (FITC) is the most consistently used fluorescent marker. Fiber optic sensors can be couple to PCR and ELISA assays for the detection of multiple pathogens, such as staphylococcal enterotoxin type-B (SEB), *Francisella tularensis* LVS, *Bacillus anthracis* Sterne, ricin, *Yersinia pestis* F1 antigen, MS2 bacteriophage, cholera toxin, and *Salmonella typhimurium* [116]. Phage-based fiber optic sensors have been reported in the literature [117-119] (Table 2.6).

Table 2.6:Fiber optic assays for the detection of bacterial species

| **Species** | **Phage** | **Time of detection** | **Sensitivity** | **Refs.** |
|---|---|---|---|---|
| *E. coli* | T4 | 25 min. | $10^4$ CFU/mL | [117] |
| *E. coli* | T4 | 20 min. | $10^8$ CFU/mL | [118] |
| *E. coli* | T4 | 20 min. | $10^3$ CFU/mL | [119] |

### 2.5.2. Electrochemical biosensors

Electrochemical sensors measure the changes in current or in potential due to interactions occurring at the electrode/matrix interface. Significant advantages of these types of sensors, such as their potential for miniaturization, their compatibility with turbid media and their simplicity, have rendered them very popular in research laboratories. Electrochemical sensors are classified with regard to the transducer used, and can thus be amperometric, potentiometric, or impedimetric. Phage-based electrochemical biosensing of bacterial pathogens are found in Table 2.7.

#### 2.5.2.1. Amperometric sensors

Amperometric biosensors are composed of a reference electrode, and a working electrode that measure changes in current generated by either enzyme-catalyzed redox reactions or bioaffinity reactions between the analyte and the recognition element. This current change will dependent on the ionic concentration of the surrounding medium. Moreover, signal amplification can be achieved by an enzyme complex that catalyzes an electoactive product that will, in turn, enhance the detected current. Applications, for amperometric sensors used for the detection of various pathogens, have been reported in the literature [120]. Amperometric sensors integrating phages have been reported to successfully detect bacterial species [91, 121, 122], based on the principle that bacterial lysis, induced by phage infection, leads to the release of bacterial cell contents, such as enzymes, intracellular adenosine triphosphate (ATP), or β-D-galactosidase, into the surrounding medium, which can then be measured, using a specific substrate. ATP is the most common marker, and can be measured with a firefly luciferase-based bioluminescent assay[73, 74].

Table 2.7:Phage-based electrochemical biosensing for the detection of bacterial species

| Transducer | Species | Phage | Time of detection | Sensitivity | Refs. |
|---|---|---|---|---|---|
| Amperometric | *E. coli* EK12 | λ | 6 h | $10^3$ CFU/mL | [91] |
| | *E. coli* | T4 | 5 h | $10^4$ CFU/mL | [121] |
| | *E. coli* | M13K07 | 3h | 1 CFU/mL | [122] |
| | *B. cereus* | B1-7064 | 8 h | 10 CFU/mL | [92] |
| | *L. monocytogenes* | Listeria scFvs | 5 min. | 500 CFU/mL | [123] |
| | *M. smegmatis* | D29 | 8 h | 10 CFU/mL | [92] |
| Impedimetric | *E. coli* EK12 | T4 | 20 min | $10^4$ CFU/mL | [124] |
| | *E. coli* | T4 | 6 h | $10^4$ CFU/mL | [125] |
| | *E. coli* | T4 | 30 min. | $10^4$ CFU/mL | [126] |
| | *S.* Newport | GIII | 2 h | $10^3$ CFU/mL | [127] |

#### 2.5.2.2.Potentiometric sensors

Phage-based potentiometric sensors have found limited use in applications concerning pathogen detection [128]. These sensors usually consist of a selective outer layer and a bioactive element that will catalyze reactions to either generate or consume chemical species [114]. Pathogen detection is possible through the detection of pH or ionic fluctuations.

#### 2.5.2.3. Impedimetric sensors

Impedimetric sensors are based on electrical impedence spectroscopy (EIS), where low voltage is applied to an electrochemical cell at various frequencies. The resulting impedance is determined by measuring the current. The rationality behind phage-based EIS is that bacterial growth will result in a change of the composition of the medium, i.e., the transformation of uncharged metabolites, such as carbohydrates, into charged products, mainly acids, causing an increase in medium conductivity. The lysis of host bacteria by phages reduces microbial growth. The conductances of phage-treated and untreated samples are then compared. Limitations of direct impedimetric detection include the necessity of optimizing the medium for electrical measurements, as well as selecting microorganisms that produce sufficient amounts of ionized metabolites to permit their detection [129]. Successful phage-base impedimetric detections of *E. coli*, *MRSA* and *Salmonella* have been reported in the literature [124, 126, 130-132].

### 2.5.3. Phage-based mass biosensors

#### 2.5.3.1.Acoustic wave biosensors

Acoustic wave biosensors are mass-sensitive detectors, using quartz-crystal resonators. These oscillating crystals resonate at a frequency that depends on their geometry. There is a direct relationship between the mass adsorbed on the surface of the crystal and its resonant frequency in air. Most acoustic biosensors use piezoelectric transducers that generate and transmit acoustic waves with a vibrating crystal, which resonates in a frequency-dependent manner. Of the acoustic wave sensors using a piezoelectric transducer, the quartz crystal microbalance (QCM) is largely used for pathogen detection. Applying an electrical field to electrodes situated on each side of the crystal creates a potential difference across the two sides. This produces a mechanical oscillation with a characteristic vibrational frequency, and is sensitive to mass. Olsen et al. reported the detection of *Salmonella typhimurium,* using specific bacteriophage, with a detection limit of $10^2$ CFU/mL[133].

#### 2.5.3.2.Magnetoelastic sensors

Magnetoelastic sensors are composed of a magneto-restrictive material that contracts or lengthens when exposed to an external magnetic field. The resonant frequency is dependent on the mass bound to the surface of the resonator. The phage-based detection of *Salmonella typhimurium* and *Bacillus anthracis* has been reported with a detection limit in the range of $10^3$ CFU/mL[134-144] (Table 2.8).

Table 2.8:Phage-based magnetoelastic biosensing for the detection of bacterial species

| **Species** | **Phage** | **Time of detection** | **Sensitivity** | **Refs.** |
|---|---|---|---|---|
| *B. anthracis* | JRB-7 | 30 min. | $10^3$ CFU/mL | [144] |
| *B. anthracis* | Filamentous landscape phage | 1 h | 1 cell per spore | [138] |
| *B. anthracis* | JRB-7 | 2 h | $10^4$ CFU/mL | [134] |
| *S. typhimurium* | Filamentous phage | 20 min. | $10^3$ CFU/mL | [139] |
| *S. typhimurium* | JRB-7 | 30 min. | $10^3$ CFU/mL | [145] |

## 2.6. Concluding remarks

Novel diagnostic technologies are of primordial importance for the control of drug-resistant pathogens. Rapid, specific, and sensitive sensors should aim at facilitating the diagnosis and enabling an accurate and efficient decision-making in individual point-of-care settings. The selectivity, specificity, robustness, and low production cost of phages make them ideal recognition elements for bacterial detection. However, despite efforts in commercializing phage-based diagnostic devices, traditional microbiological methods remain the gold standard for diagnosis in a clinical setting. Although vast efforts have reduced identification times from days to hours when using modern molecular techniques, such as PCR, most assays still require an amplification period to increase the bacterial load of the specimen to be tested. There is, therefore, a requirement for biosensing technologies with sensitivities allowing for the detection of concentrations below $10^2$ CFU/mL. Moreover, future research efforts should be aimed at detecting bacteria within complex matrices, in order to effectively move phage diagnostics from the laboratory to the clinic.

## 2.7. Acknowledgments

We thank the Natural Sciences and Engineering Research Council of Canada and Biophage Pharma for funding this work.

# CHAPTER 3 .ARTICLE 2: SURFACE PLASMON RESONANCE DETERMINATION OF THE BINDING MECHANISMS OF L-CYSTEINE AND MERCAPTOUNDECANOIC ACID ON GOLD

The high selectivity of biological sensing elements, such as antibodies or bacteriophages is exploited in biosensors by capturing the biomolecule on the surface of the transducer. As a consequence, immobilization strategies are of paramount importance for the preservation of the biomolecule's biological activity. The strategies used typically involve the adhesion of SAMs of thiolated molecules to a gold surface. Although the physical and structural characterizations of alkanethiol SAMs have been extensively reviewed, little is known about their real time adsorption kinetics. Moreover, insufficient information exists about the assembly of amino acids, such as L-cysteine, on gold.

In this article, SPR was used to study the formation of SAMS of L-cysteine and MUA on gold. Comparative details of the kinetics of assembly of both molecules are provided, and numerical models are introduced to describe their adhesion at lower and higher concentrations. Understanding the differences in the adlayer formation of L-cysteine and MUA on gold is an important issue for biosensing purposes, and paves the way for a more effective immobilization strategy for bacteriophages on gold. Figure 3-1 depicts L-cysteine and 11-MUA structures

a) b)

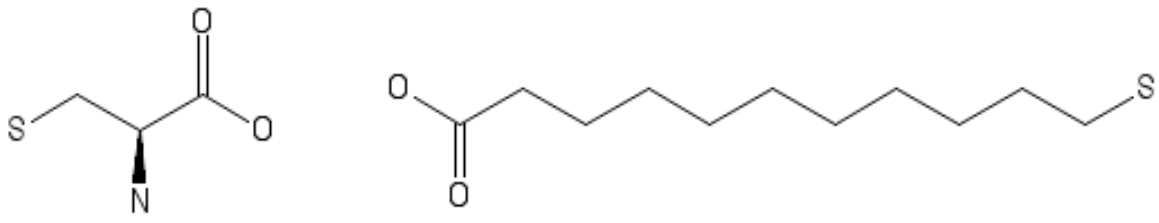


Figure 3-1: Schematic representation of (a) L-cysteine, and (b) 11-MUA

# Surface Plasmon Resonance Determination of the Binding Mechanisms of L-Cysteine and Mercaptoundecanoic Acid on Gold

*Nancy Tawil*[1,2,4], *Ali Hatef*[1], *Edward Sacher*[2], *Mathieu Maisonneuve*[1], *Thomas Gervais*[3], *Rosemonde Mandeville*[4], *Michel Meunier*[1,2]

[1] Laser Processing and Plasmonics Laboratory; Department of Engineering Physics, École Polytechnique de Montréal, Case Postale 6079, succursale Centre-Ville, Montréal, Québec, H3C 3A7 Canada

[2] Laboratory for the Analysis of the Surfaces of Materials, Department of Engineering Physics, École Polytechnique de Montréal, Case Postale 6079, succursale Centre-Ville, Montréal, QC H3C 3A7, Canada

[3] Department of Engineering Physics, École Polytechnique de Montréal, Case Postale 6079, succursale Centre-Ville, Montréal, QC H3C 3A7, Canada

[4] Biophage Pharma, 6100 Royalmount, Montreal, QC H4P 2R2, Canada

**Keywords:** L-cysteine, kinetics, 11-mercaptoundecanoic acid, numerical model, surface plasmon resonance

Received : January 25, 2013 Published : March 14, 2013

dx.doi.org/10.1021/jp400873t J. Phys. Chem. C 2013, 117, 6712-6718

## 3.1 Abstract

Surface plasmon resonance was used for the real-time monitoring of the formation of self-assembled monolayers of L-cysteine and 11-mercaptoundecanoic acid (MUA) on gold surfaces. We provide comparative details on the kinetics of the assembly of short thiols with multiple functional groups, as opposed to longer alkanethiols with fewer functional groups. Our results indicate that the adsorption of L-cysteine is a rapid process, involving both amino- and thiol-Au interactions, followed by the exchange of amino-Au to thiol-Au species and the physisorption of a second cysteine layer. The formation of MUA is also rapid, followed by a slower structural rearrangement of the monolayer. We find that monolayer formation, for both L-cysteine and MUA, is described by the Langmuir isotherm at low concentrations only. Numerical models are introduced to describe the assembly of both higher and lower concentrations of thiolated molecules on gold.

## 3.2 Introduction

The attachment of molecules to a support, resulting in their immobilization, has found multiple applications in industrial chemistry and biosensing devices. Self-assembled monolayers (SAMs), composed of chemisorbed species, play a fundamental role in altering the interfacial properties of metals, polymers and semiconductors. Notably, the affinity of thiols for gold permits the generation of well-defined surfaces with various desirable chemical functionalities and optical properties. Currently, thiols are the most utilized form of organic thin-film material.

The physical and structural characterizations of SAMs have been extensively reviewed in the literature[146, 147]. However, despite considerable efforts to study their formation on gold, little is known about their real-time adsorption kinetics[148]. Although the chemistry appears to be straightforward, the details of the assembly at the interface are still approximated qualitatively by a Langmuir absorption model[149]. Originally, SAM formation was thought to occur by the activation of the S-H bond at the surface[146]. Alternative interpretations, such as a two-stage adsorption process for longer chains, have been reported, where the surface coverage reaches 60%-90% of its maximum in the first few minutes, followed by a slower period of several hours, before which maximum coverage is attained[150, 151]. Some authors have shown that the dynamics of this adsorption follows a simple Langmuir rate model[152], whereas others have shown that a diffusion-controlled Langmuir model is a better fit at low concentrations[153]. Such contradictory results could, in part, be attributed to one or more of several sources, such as the presence of contaminants on the gold surface, the effects of the concentrations of solvent and thiol, and the sensitivity of the method used[152]. Previous studies, using atomic force microscopy[154], ellipsometry[155, 156] and contact angle measurements[157], were limited in time resolution, which is why we chose to use surface plasmon resonance (SPR), making real-time adsorption analysis possible. This article describes the real-time formation of SAMs of L-cysteine and 11-mercaptoundecanoic acid (MUA) at different concentrations, on a gold sensor platform using SPR and evaluation by numerical methods. Our purpose, in carrying out these measurements with both L-cysteine and MUA, was to compare the binding characteristics of both molecules and establish each molecule's validity and applicability as a linker element for use in biosensing.

## 3.3 Experimental Section

### 3.3.1 Preparation of Au surfaces

Biacore Platypus biosensor chips, to be described below, were used as the gold surface. Prior to modification, they were placed in freshly prepared "Piranha" solution, a 7:3 mixture of concentrated $H_2SO_4$ and 30% $H_2O_2$ (Caution: piranha solution reacts vigorously with organics and can splatter), at room temperature for 30 min, then rinsed thoroughly with MilliQ water (Millipore, Mississauga, Ont.), ultrasonicated in water for 15 min, and dried in a nitrogen flow.

### 3.3.2 Chemicals

L-cysteine, MUA, sodium chloride, magnesium sulfate and phosphate buffered saline (PBS) were purchased from Sigma-Aldrich.

### 3.3.3 Surface plasmon resonance apparatus

Superluminescent light-emitting diode (SLED), emitting at 650 nm, was used as the light source. An achromatic lens produced a collimated beam, which passed through a polarizer. The linearly *p*-polarized light was focused by a lens and then used to excite surface plasmons on the sensing surface, situated on top of a coupling prism. A commercial sensing surface (Platypus Technologies), consisting of a glass microscope slide (BK7) covered by an adhesion layer of 5 nm of titanium and a sensing layer of 50 nm of gold, was placed in oil immersion contact (Cargille Laboratories) on the top of the coupling prism. For the real-time tests, a flow injection double channel-measuring cell, with a 12 $\mu$L volume, was developed. The entire system was placed on a goniometer stage, with 2-D linear translation for exact beam angle and position, permitting surface plasmon excitation at the gold/adjacent medium interface. The spatial distribution of the reflected light intensity was recorded by a CCD camera (Hamamatsu C4742-95), and examined by an appropriate software image treatment. A more detailed description of the system can be found in reference [3].

### 3.3.4 SPR detection L-cysteine and MUA adsorption to gold

The cleaned gold slides were placed on the SPR coupling prism, using a refractive index-matching immersion liquid (Cargille Laboratories). Prior to L-cysteine injection, MilliQ water was injected at a flow rate of 111 μL/min, controlled by a peristaltic pump, to obtain a baseline. Solutions of different concentrations of L-cysteine in MilliQ water were subsequently pumped into the SPR apparatus at the same flow rate. This was followed by a washing step with MilliQ water.

In the case of water-insoluble MUA, ethanol was first injected onto the chip, followed by injection of different concentrations of freshly prepared solutions of MUA in ethanol, and ethanol was used for the washing step.

## 3.4 Results and Discussion

### 3.4.1 L-Cysteine

Planar gold was used to characterize the attachment of L-cysteine and MUA, because of the ease of preparation of such substrates and their compatibility with surface plasmon resonance spectroscopy.

L-Cysteine is a neutral amino acid with hydrophilic properties. It is reported to bind to gold via its thiol group. However, it has two other terminal groups that are chemically active, $-NH_2$ and -COOH, which, depending on the pH, may play a role in the formation and organization of the monolayer.

The Langmuir adsorption isotherm is based on the fraction of available sites that have already reacted. Thus, the rate of adsorption is expected to follow Langmuir adsorption kinetics

$$\frac{d\Theta}{dt} = k_a(1-\Theta)c - k_d\Theta \qquad (1)$$

where Θ is the fraction of the gold surface that is covered, (1-Θ) is the uncovered fraction, $k_a$ is the association constant, $k_d$ is the dissociation constant, and c is the concentration of the thiol solution.

We have examined L-cysteine adsorption kinetics at several concentrations. The raw data are a direct result of the refractive index change induced by L-cysteine adsorption onto the gold surface.

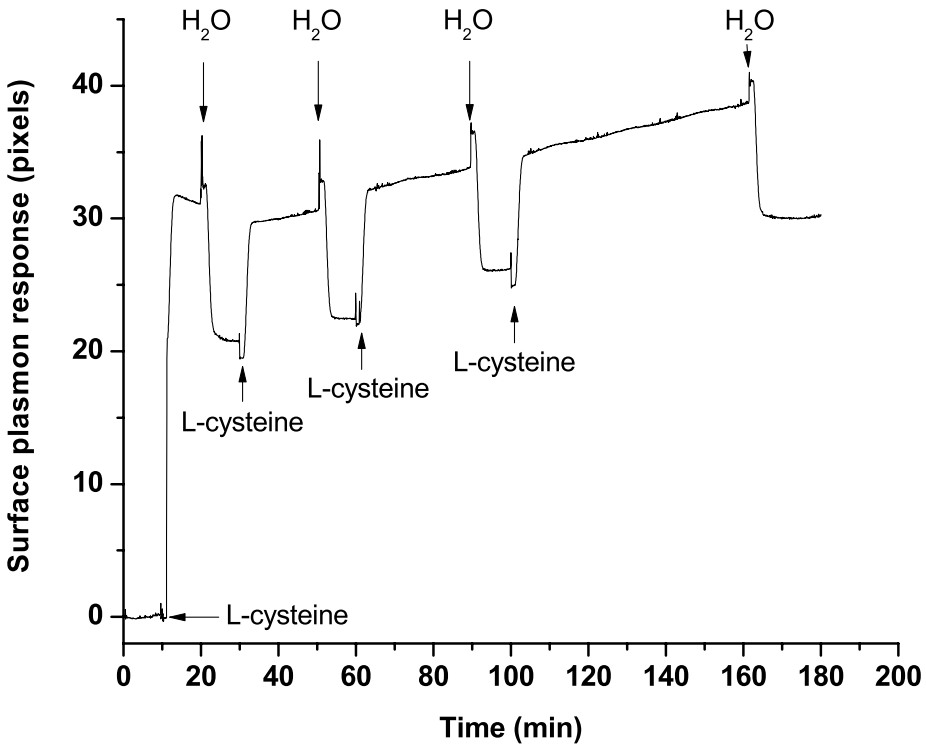


Figure 3-2: Relationship between physisorption and chemisorption of L-cysteine on gold. A baseline was created by flowing MilliQ water for 10 min over the sensor surface. Following this, a solution of 1 mg of L-cysteine per mL of MilliQ water was injected for varying periods of time (10, 20, 30 and 60 min), each followed by a washing step of 10 min duration. The first 30 min shows a negative slope, whereas there is a positive shift of the plasmon response within 30 min after the initial injection of L-cysteine. The physisorption and chemisorption components responsible for the plasmon shift reach equilibrium 30 min after L-cysteine injection.

Figure 3-2 provides insight into the relationship among physisorption, chemisorption, concentration and time. In this experiment, MilliQ water was first injected for 10 min, to create a baseline, after which 1 mg/mL of L-cysteine was injected for a period of 10 min, followed by a 10 min washing step. The same solution of L-cysteine was further injected for longer periods of time (20, 30 and 60 min), each separated by a washing step of 10 min to remove the loosely bound, physisorbed L-cysteine molecules. Our results show that the slope is negative for the first 30 min, but goes from negative to positive over a longer time period (between 30 and 180 min). The equilibrium between chemisorption (SPR signal following washing) and physisorption (SPR signal after further injection of 1mg/mL of L-cysteine) is attained in > 30 minutes after initial injection, as is shown by the identical slopes of both signals. Moreover, it can be seen that the rearrangement of the adsorbed thiol is a very slow process, taking hours. Because the strength of the -SH chemisorption bond is large (125-167 kJ/mol)[158, 159], any desorption of the adsorbed thiol is assumed to be negligible. This leads us to believe that the loss of plasmon response units, on washing, is due to the removal of a second, loosely bound layer. This is corroborated by other studies, showing the prevalence of a double layer configuration of L-cysteine[160]. Moreover, in an XPS study on self-assembled films, Cavaleleri et al. reported that for L-cysteine a physisorbed layer forms on top of the chemisorbed monolayer and that the analysis of the N1s spectrum indicated the prevalence of a zwitterionic state[161]. It has also been reported that molecules tend to adopt conformations that allow high degrees of van der Walls interactions and hydrogen bonding to minimize the free energy of the organic layer[162, 163]. The washing away of physisorbed L-cysteine molecules, electrostatically attached to the chemisorbed monolayer, appears to explain the loss of surface plasmon response after the washing step. This is supported by Abraham et al., where solid-state NMR spectroscopy showed that cysteine adsorbs to gold via the formation of a two-layer boundary, in which a second layer of L-cysteine molecules interact with the cysteine molecules chemisorbed on gold through hydrogen bonding between the charged groups of the zwitterions[164].

Moreover, because physi- and chemisorption quickly reach equilibrium, we conclude that reaching a steady state condition is a consequence of the ordering and rearrangement of the monolayer chains alone.

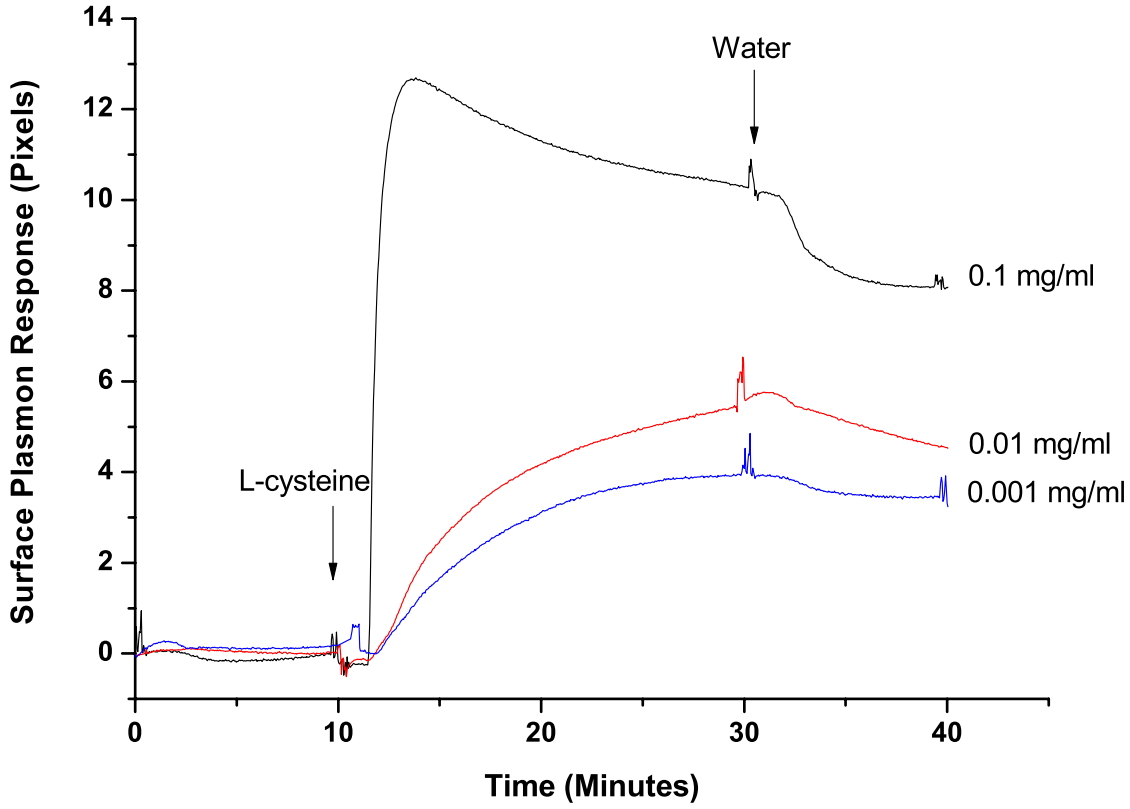


Figure 3-3: SPR sensogram of the adsorption of different concentrations of L-cysteine on gold. A baseline was created by injecting MilliQ water on the sensor surface for a period of 10 min. This was followed by the injection of different concentrations of L-cysteine (0.001, 0.01 and 0.1 mg/mL). Subsequently, a washing step was performed, in which MilliQ water was injected on the sensor surface for another 10 min.

Figure 3-3 shows the real-time adsorption of several concentrations of L-cysteine on gold at 295K. Lower concentrations of L-cysteine (0.001 and 0.01 mg/mL) appear to follow simple Langmuir adsorption kinetics while the higher concentration (0.1 mg/mL) does not. From the SPR data for lower concentrations, we determine the kinetic parameters using equation 1, $k_a$ = 3.87 L $mol^{-1}$ $s^{-1}$ and $k_d$ = 0.00266 $s^{-1}$, making $K_{eq}$ = 1.455 x $10^3$ L $mol^{-1}$ and $\Delta G_{ads}$ = -17.9 kJ $mol^{-1}$ . Thus, desorption does not play an important role in the formation of the chemisorbed layer and

that most of the adsorption sites on the surface are occupied. Because mass transfer is central to exploring biochemical reactions in a surface-based detection system, we wish to ensure that the SPR signal is indeed reaction-limited; that is, the diffusion time of the analyte to the surface is much smaller than the binding time. To verify this property, we use the expressions for the convective/diffusive length, $\zeta=LWD/Qh$, and the Damköler number, $Da=k_aC_{s0}d(h)/D$, for a first-order surface reaction; $L$ is the length of the reactive zone, $W$ is the channel width, $D$ is the diffusivity of the analyte, $Q$ is the flow rate, and $d(h) = h*\zeta^{1/3}$ is the characteristic thickness of the diffusive boundary layer as a function of channel height. $C_{s0}$, the initial surface concentration of binding sites, was found to be of a typical densely packed thiol monolayer (~7.47 x $10^{-6}$ mol/$m^2$)[163]. We find that for both L-cysteine and MUA $\zeta<<1$ (~$10^{-5}$), suggesting that mass transfer occurs through a thin boundary layer of characteristic thickness $d \approx 1$ μm, greatly speeding up diffusion. Furthermore, the Damköler number is of the order of $10^{-3}$, indicating that the transport is limited by the process on the surface and that a constant concentration profile can be expected across the channel[165]. Therefore, the diffusive effects are negligible.

Figure 3-4 models the adsorption of L-cysteine on gold. The rapid response in the first few minutes is attributed to the chemisorption of the L-cysteine via both amine and thiol groups. The subsequent negative slope is attributed to the reorientation of that fraction of the L-cysteine, initially adsorbed via its amine end, to a more stable Au-S bound species. This is in agreement with Kuhnle et al. [166], where L-cysteine is shown to be bound by both sulphur-gold and amino-gold bonds. L-Cysteine molecules can exist in either neutral or zwitterionic forms, depending on the pH of the solution. It is believed that at low coverage, the neutral form of L-cysteine is present simultaneously with zwitterionic form, whereas the zwitterionic form is dominant at monolayer coverage and beyond[161, 167, 168] . Furthermore, because the L-cysteine solution has a pH of 4.7, its amine is protonated ($NH_3^+$)[169], enabling an additional layer[170], physisorbed by electrostatic interactions to the chemisorbed layer. We present a simulation in Figure 3-4b,c that qualitatively shows the interaction. The binding kinetics of a surface-immobilized ligand to capture an analyte in solution, including the second layer formation, is modeled as a four-step

reaction. For L-cysteine, the net reaction rates of the different concentrations follow Langmuir adsorption kinetics, as indicated by the set of equations:

$$\frac{d[L]}{d\tau} = -K_{a1}[A][L] - K_{a2}[A][L] + K_{d1}[LA_1] + K_{d2}[LA_2] + \Phi K_r[LA_2] \quad (2\text{-a})$$

$$\frac{d[LA_1]}{d\tau} = K_{a1}[A][L] - K_{d1}[LA_1] + (1-\Phi)K_r[LA_2] \quad (2\text{-b})$$

$$\frac{d[LA_2]}{d\tau} = K_{a2}[A][L] - K_{d2}[LA_2] - K_r[LA_2] \quad (2\text{-c})$$

$$\frac{d[LA_2A]}{d\tau} = K_{a3}[A][LA_2] - K_{d3}[LA_2A] \quad (2\text{-d})$$

For simplicity, we have normalized all terms by a constant, having units of $min^{-1}$; that is, $\tau = K_0 t$. [L] and [A] represent, respectively, the concentrations of surface ligands and analytes in bulk solution. [$LA_1$], [$LA_2$], and [$LA_2A$] represent, respectively, the surface densities of adsorbed analyte molecules via thiol group, amine group and second-layer. [A] is assumed to be constant with time, whereas [L] is depleted, due to the binding reaction. Φ is the unreacted fraction of the gold surface after the reorientation of L-cysteine molecules, (1-Φ) is the reacted fraction, $K_{ai}$ (i=1, 2, 3) is the normalized association constant, $K_{di}$ (i=1, 2, 3) is the normalized dissociation constant, and $K_r$ is the normalized reorientation constant. The initial conditions at time t = 0 are [L] = 10 and [$LA_1$] = [$LA_2$] = [$LA_2A$] = 0. In these equations, the positive and negative terms show the formation and breaking, respectively, of the ligands and complexes in the system. For example, in eq 2-a, the first and second terms represent the breaking of the ligands for a constant value of analyte concentration, which leads to the formation of the [$LA_1$] and [$LA_2$] complexes. The third and the forth terms represent the formation of ligands by dissociation of the [$LA_1$] and [$LA_2$] complexes. Finally, the fifth term represents the formation of ligand by reorientation of the [$LA_2$] complex. We used a numerical solver, available in the Maple software package (Maplesoft, a division of Waterloo Maple, 2012) to solve the coupled differential equation system.

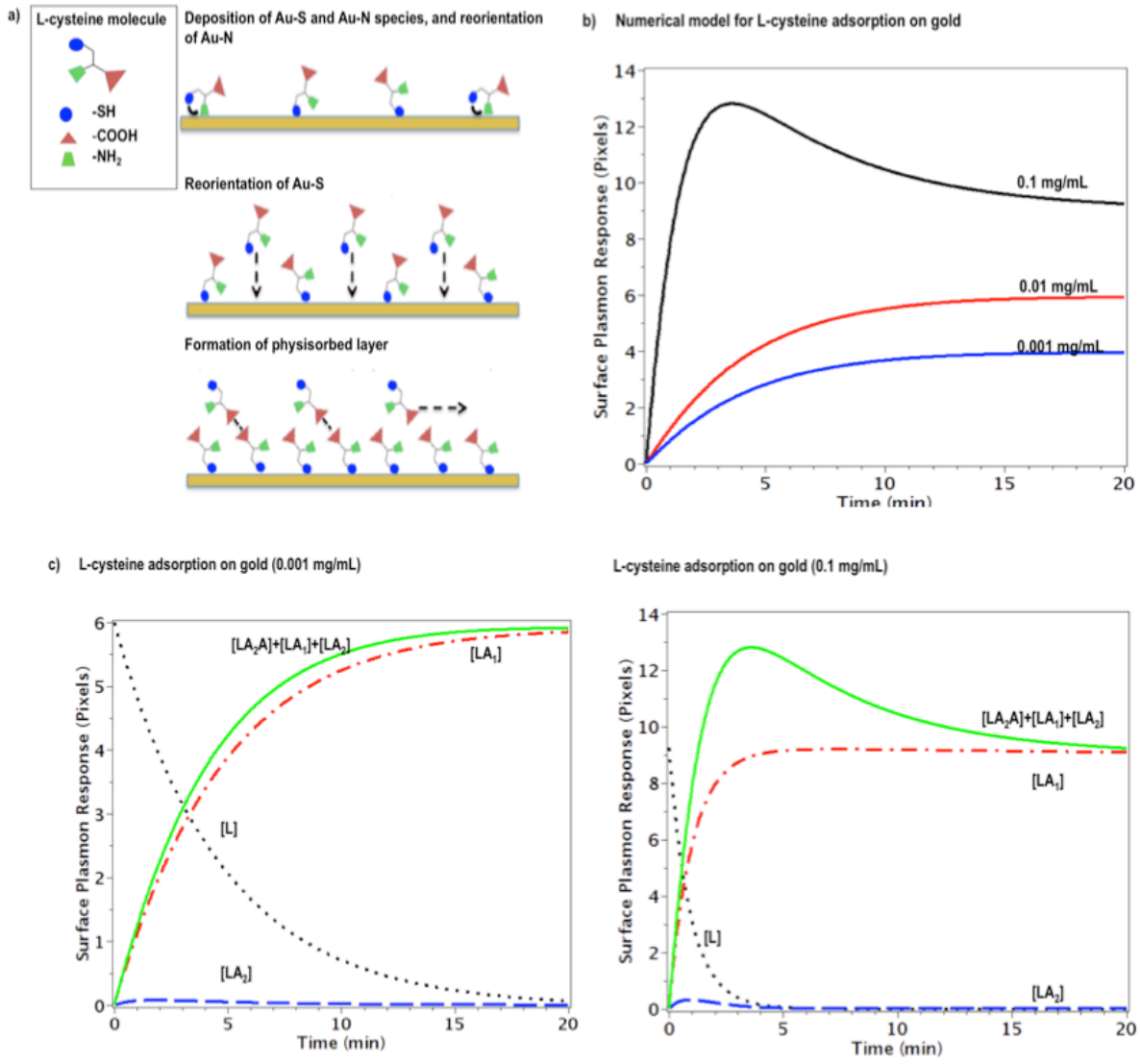


Figure 3-4: Adsorption kinetics of L-cysteine on gold. a) L-Cysteine may attach to gold via its thiol or amine groups. The amine-gold interaction is short-lived, and the L-cysteine reorients to attach via its thiol group. This is followed by an ordering of the chemisorbed layer and the subsequent formation of a second, physisorbed, layer atop the chemisorbed L-cysteine species. b) Numerical model for different concentrations of L-cysteine. c) Surface plasmon resonance of 0.001 mg L-cysteine/mL $H_2O$ profile versus time. The dotted, dash-dotted, dashed, and solid curves represent [L], [$LA_1$], [$LA_2$] and [$LA_2A$]+[$LA_1$]+[$LA_2$], respectively. d) Surface plasmon resonance of the 0.1 mg L-cysteine/mL $H_2O$ profile versus time. The dotted, dash-dotted, dashed and solid curves represent [L], [$LA_1$], [$LA_2$], and [$LA_2A$]+[$LA_1$]+[$LA_2$], respectively.

The model applies at both lower (Figure 3-4c) and higher concentrations (Figure 3-4d). It can be seen that our model can be simplified to the Langmuir model at low concentrations (Figure 3-4b). In the Langmuir model, θ represents the surface occupied by the analyte, which is equivalent to [LA] in the previously described model, and the unbound surface (1- θ) is equivalent to (L). Thus, although all the terms in the model are necessary at higher concentrations, reactions with lower adsorption rates (i.e. $[LA_2]$**),** become negligible at lower concentrations and the model is simplified to the Langmuir isotherm, using eq 2-b. This is also observed experimentally.

### 3.4.2 11-MUA

The common protocol for the generation of alkanethiol SAMs involves the immersion of cleaned substrates in dilute ethanolic solutions of thiols for several hours at room temperature. Ethanol is used because alkanethiols, such as MUA, are not soluble in water. Although the dielectric constant of ethanol (24.3) is lower than that of water (78.5), it is still much higher than that of non-polar solvents (e.g. $\varepsilon_{hexane} = 1.9$) [171]. Figure 3-4 follows the real-time attachment of MUA to a gold surface. Ethanol was first injected for 10 min, to create a baseline, following which several concentrations ($10^{-4}$, $10^{-3}$ and $10^{-2}$ mol $L^{-1}$) of MUA in ethanol were injected for 20 min. Finally, ethanol was re-injected for the washing step. Exposure of the gold surface to MUA resulted in a rapid increase in the SPR response in the first 30 min, followed by a slow increase over the next 2 h (data not shown).

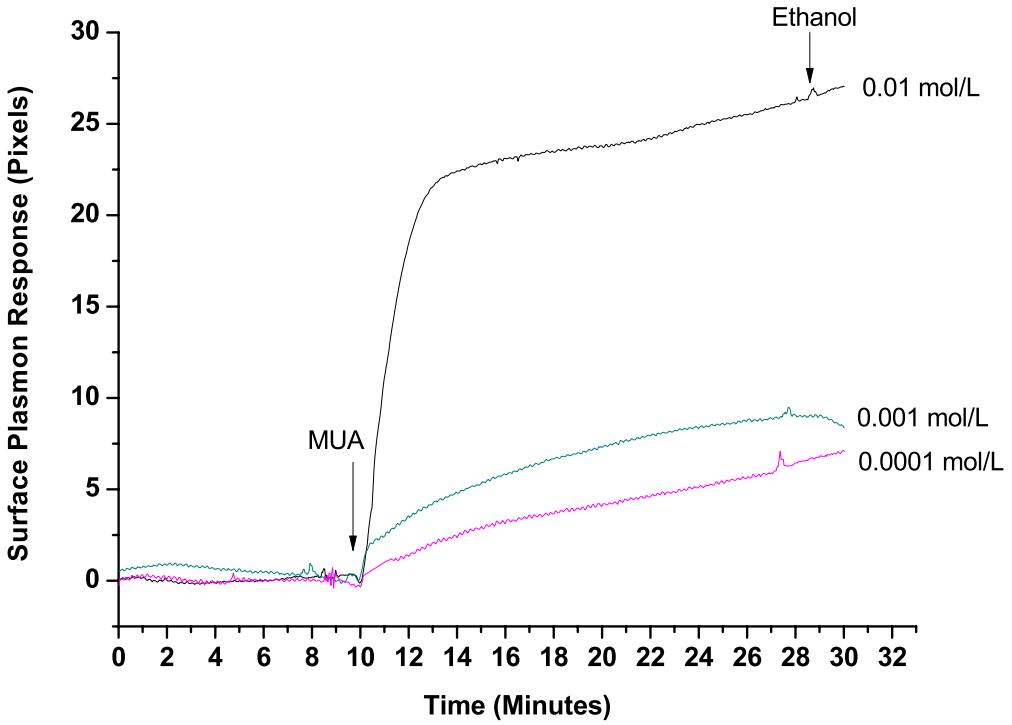


Figure 3-5: Various concentrations of MUA adsorbed onto gold. An ethanol baseline was first obtained; after 10 min, a solution of MUA was injected for another 20 min, followed by a short ethanol washing step.

A rapid coverage of the gold is achieved within the first few minutes, followed by a slower increase of the SPR response. The attachment of MUA to the gold surface also follows a two-step process but is different than that of L-cysteine (Figure 3-6a). We hypothesize that the chains deposit in a random manner, followed by their restructuring into a SAM. The gradual increase in plasmon response, over the next few hours, indicates that as expected sites on the gold surface slowly become available because this reorientation makes new sites available, permitting further adsorption. Differences in models for low and high concentrations are attributed to a loose, horizontal configuration for low-coverage adsorption, whereas a compact, vertical phase is observed for higher coverage [172]. Our results are in agreement with recent studies, showing that solutions with lower concentrations of SAMs do not have the same physical properties as those created from more concentrated solutions[173]. From lower concentrations of MUA, we

determine $k_a$ = 1.233 L $mol^{-1}$ $s^{-1}$ and $k_d$ = 8.86 x $10^{-4}$ $s^{-1}$. A value of $\Delta G_{ads}$= -17.8 kJ $mol^{-1}$ was obtained, which is similar to the value estimated in the literature [174, 175] .The low value of $k_d$ tells us that desorption does not play an important role in the formation of the monolayer.

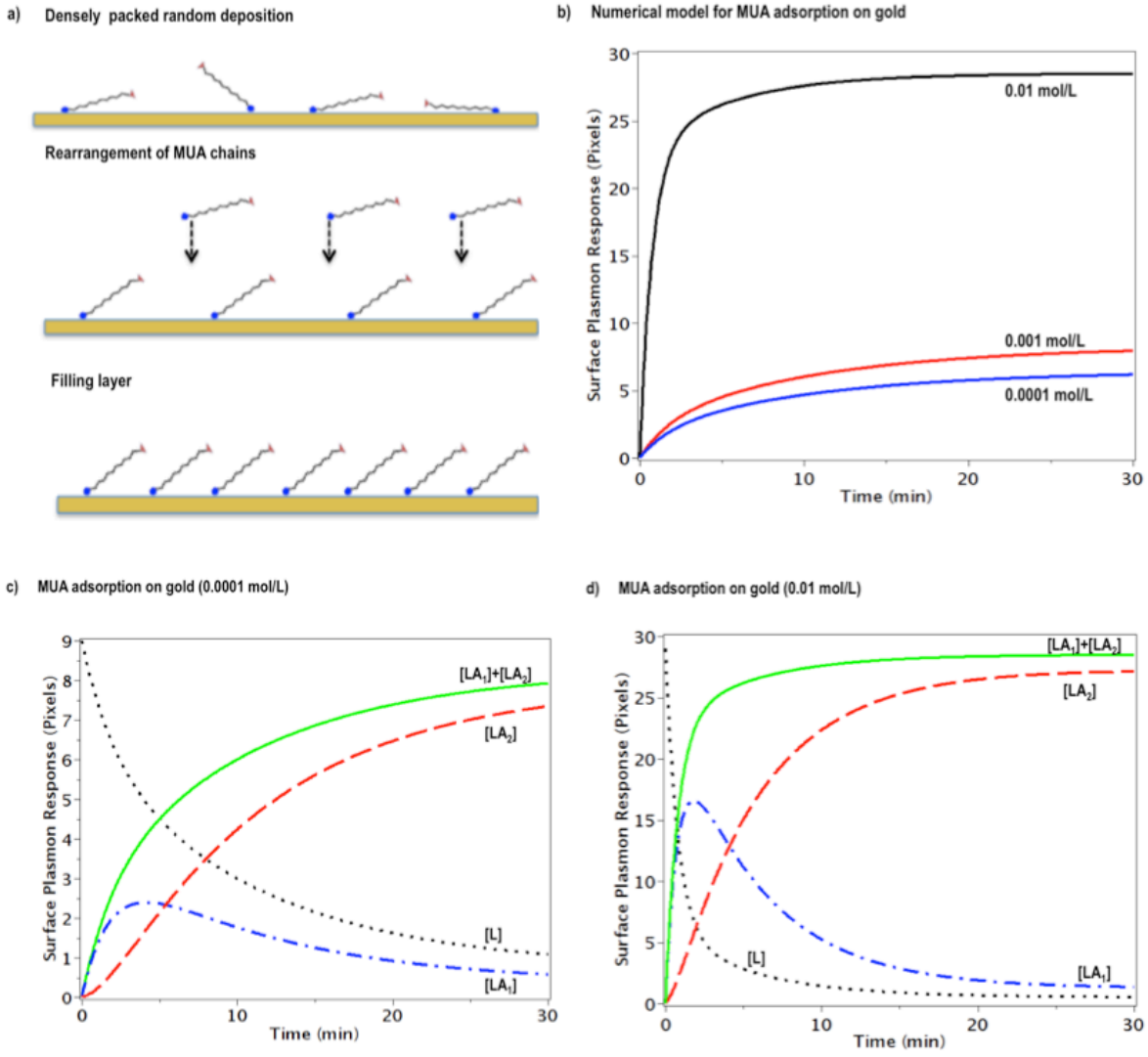

Figure 3-6: Model for the attachment of MUA on gold. a) MUA chains first deposit on the surface of the gold in a random manner, followed by their rearrangement, which provides more sites for further chain attachment to gold. b) Numerical model for different concentrations of L-cysteine. c) Surface plasmon resonance profile of 0.01 mol MUA/L of ethanol versus time. The dotted, dash-dotted, dashed and solid curves represent [L], [$LA_1$], [$LA_2$] and [$LA_1$]+[$LA_2$], respectively. d) Surface plasmon resonance profile of 0.001 mol MUA/L of ethanol versus time. As in panel b, the dotted, dash-dotted, dashed and solid curves represent [L], [$LA_1$], [$LA_2$] and [$LA_1$]+[$LA_2$], respectively.

For MUA, the net reaction rates of the different concentrations are written as:

$$\frac{d[L]}{d\tau} = -K_{a1}[A][L] - K_{a2}[A]\Phi[L] + K_{d1}[LA_1] + K_{d2}[LA_2] + \Phi K_r[LA_1] \quad (3\text{-a})$$

$$\frac{d[LA_1]}{d\tau} = K_{a1}[A][L] - K_{d1}[LA_1] - K_r[LA_1] \quad (3\text{-b})$$

$$\frac{d[LA_2]}{d\tau} = K_{a2}[A]\Phi[L] - K_{d2}[LA_2] + (1-\Phi)K_r[LA_1] \quad (3\text{-c})$$

In eqs 3-a to 3-c, [$LA_1$] and [$LA_2$] represent the surface densities of MUA chains on the surface of the gold in a random (dense random deposition) and aligned manner (filling layer), respectively (Figure 3-6a). This is in agreement with multiple studies reporting an intermediate low coverage phase arising prior to the nucleation and growth of the upright higher coverage phase[176]. Using these equations, we numerically modeled the adsorption of MUA on gold (Figure 3-6b). In this process, MUA first deposits on gold in a random fashion ([$LA_1$]), it then reorients with a rate of $K_r$, providing more space ($\Phi$ [L]) for further MUA attachment to gold ([$LA_2$]). As with L-cysteine, the model applies to both lower (Figure 3-6c) and higher concentrations (Figure 3-6d) of MUA. The initial conditions for 0.01 mol/L at time t = 0 are [L] = 29, and [$LA_1$] = [$LA_2$] = 0.

### 3.4.3 Comparison of kinetic profiles of L-cysteine and MUA

Although there is an extensive literature on alkanethiol SAMs, those of amino acids, such as L-cysteine, have been overlooked in comparison. In the case of L-cysteine, the presence of both the carboxy and the amino groups confers broader possibilities for metal-molecule and molecule-molecule interactions through electrostatic, hydrogen, and peptide bonding. Understanding the differences in the adlayer structure of L-cysteine and MUA on gold surfaces is an important issue for biosensing purposes. L-Cysteine is a much smaller molecule and its zwitterionic state results in various intermolecular forces that govern its interaction with the metal surface. Thus, even though it is believed that the chemical reaction that binds cysteine to gold is similar to that that permits the formation of MUA SAMs, we have found that the thiol and amino groups of L-cysteine first compete for the adsorption on the metal. Our results are in agreement with those of various groups whose findings show that cysteine most likely employs multiple functional groups in its bonding to gold surfaces[166, 172]. Over a period of time, the thermodynamically more stable SH groups replace NH groups on gold, giving additional space on the surface, resulting in increased bonding and, ultimately, packing the surface. This primary rearrangement of the groups is not seen with MUA because the primary covalent interaction is due to the thiol group. That group is thus more readily attached in the case of MUA, explaining why very little desorption is seen when washing the surface compared to L-cysteine. Moreover, L-cysteine is found in a zwitterionic form, and electrostatic interactions expose the amine group, permitting possible molecular coordination. Furthermore, the zwitterionic form facilitates the coupling of unbound molecules, provoking the formation of a second, physisorbed, layer, a phenomenon not seen with MUA. We believe that the zwitterionic character of cysteine is directly linked to its ability to form H-bonded molecular networks. This hydrogen-bonded network will affect the conformation and the overall packing of the SAM[162]. Moreover, the geometrical structure of the H-bonded network was found to be dependent on both layer coverage and temperature[177]. To that effect, Renzi et al. found that, at room temperature, L-cysteine first-layer deposition was quite heterogeneous, and that both weakly and strongly bound molecules coexist. This could partially explain the negative slope observed in the first adsorption cycle of L-cysteine. Finally, MUA SAMs were found to be more stable than those of L-cysteine because long-chain adsorbates are more robust than their shorter counterparts due to contributions of attractive lateral

interactions[147] . It should be noted that studies on the molecular diffusion mechanisms of cysteine on gold show that the substrate is central to the formation of the monolayers, a factor not accounted for in the model described[178]. New structures not previously reported, such as cysteine trimers, molecular rows, or ordered networks, can form due to surface defects. In the case of L-cysteine, it has been postulated that the amount of zwitterionic fraction, when compared to the acidic fraction, is dependent on the lattice symmetry of the metal surface[168]. Gonella et al. believe that the neutral acidic fraction, relevant only at low coverage, is likely related to isolated molecules or to the formation of dimers and is possibly related to the surface morphology of the substrate. Additional studies clarifying the substrate impact on SAM formation are desirable.

## 3.5 Conclusion

The adsorption characteristics of thiol-containing molecules are necessary for applications involving the attachment of recognition elements to a functionalized surface. We have considered their attachment to gold surfaces for plasmon resonance biosensing applications. We have shown that the self-assembly of L-cysteine differs from that of MUA. It is evident that the deposition process involves not only contributions of the sulfur bonds but also those of other existant functional groups as well as those of subsequent noncovalent adsorbed molecules. Both the amine and thiol groups of L-cysteine contribute to its initial attachment, followed by replacement of the amine-gold complex initially formed with the more stable thiol-gold complex. The reorganization of L-cysteine creates more space on the gold surface, and the zwitterionic form of the molecule permits the physisorption of a second layer through electrostatic interactions. Such a structure has high potential for further biofunctionalization. MUA deposits randomly onto the surface of gold as a SAM and slowly reorganizes into a denser, vertical state.

## 3.6 Acknowledgments

We thank NanoQuébec for its financial support, and Dr. Paul. Boyer and Etienne Boulais for their insight and assistance.

# CHAPTER 4 ARTICLE 3: STRATEGIES FOR THE IMMOBILIZATION OF BACTERIOPHAGES ON GOLD SURFACES, MONITORED BY SURFACE PLASMON RESONANCE AND SURFACE MORPHOLOGY

The immobilization of bacteriophages on an SPR sensing platform requires sophisticated approaches to avoid random orientation, as the bacteriophage's bacterial recognition proteins are situated on the phage tail. In the past, researchers have labored to find ways to improve phage capture efficiency by immobilizing the phage via its capsid. These methods span from introducing affinity tags to specifically biotinylating fusion proteins. Although these methods were proven to be reasonably successful, they are labour-intensive, cumbersome and cannot be introduced to all lytic bacteriophages.

In this article, we use SPR, standard microbiological methods, SEM and AFM to investigate several phage immobilization strategies, including physisorption, and chemisorptions by L-cysteine, gluteraldehyde, and MUA. These studies are an important preliminary step for the actual phage-based SPR biodetection of live pathogens.

# Strategies for the Immobilization of Bacteriophages on Gold Surfaces Monitored by Surface Plasmon Resonance and Surface Morphology

*Nancy Tawil*[1,2,3], *Edward Sacher*[2], *Rosemonde Mandeville*[3], *Michel Meunier*[1,2]

[1] Laser Processing and Plasmonics Laboratory; Department of Engineering Physics, École Polytechnique de Montréal, Case Postale 6079, succursale Centre-Ville, Montréal, Québec, H3C 3A7 Canada

[2] Regroupement Québecois de Matériaux de Pointe, Department of Engineering Physics, École Polytechnique de Montréal, Case Postale 6079, succursale Centre-Ville, Montréal, QC H3C 3A7, Canada

[3] Biophage Pharma, 6100 Royalmount, Montreal, QC H4P 2R2, Canada

Received : January 17, 2013 Published : March 12, 2013

dx.doi.org/10.1021/jp400565m J. Phys. Chem. C 2013, 117, 6686-6691

**Keywords:** Bacteriophage, self-assembled monolayers, Methicillin-resistant *Staphylococcus aureus,* Surface plasmon resonance, biosensor

## 4.1 Abstract

The use of bacteriophages as recognition elements for biosensing techniques has recently provoked much interest. Surface plasmon resonance, scanning electron microscopy, and atomic force microscopy were used for the real-time monitoring of the attachment of methicillin-resistant *Staphylococcus aureus* (MRSA) bacteriophages to gold using several immobilization methods. The MRSA bacterial capture efficiency of phage-functionalized surfaces was studied. We found that whereas the physisorption of phages to gold surfaces affects their biofunctionality, as expressed by their lysing efficiency of bacteria, phages bound via mixed self-assembled monolayers of L-cysteine and 11-mercaptoundecanoic acid permitted both the recognition and disruption of bacterial membranes. This is due to the formation of uniform islands on the gold surfaces, permitting an oriented positioning of the phages, thus better exposing their recognition proteins.

# 4.2 Introduction

The attachment of molecules to a support, for use in the immobilization of a target molecule, has found multiple applications in industrial chemistry and biosensing devices. Bacteriophages, a group of viruses that attack and lyse specific bacteria, have recently gained much attention as recognition elements for biosensing purposes[3, 105, 121, 179, 180]. The many advantages of bacteriophages make them an important component for the detection and identification of bacterial pathogens as well as potentially excellent vehicles for the diagnostics and therapeutics of bacterial disease. Particular advantages include the specificity of the interaction of this type of viruses with their target host cell, their lytic ability, and their capacity to multiply during the infection process. This work has been directed toward investigating the chemical attachment of bacteriophages onto gold surfaces using several immobilization methods.

Self-assembled monolayers (SAMs), composed of chemisorbed species, play a fundamental role in immobilizing phages on gold. It was reported that modifying surfaces with cysteine, followed by treatment with 2% gluteraldehyde, resulted in a 37-fold improvement of bacteriophage

attachment compared with physisorption [180]. Other groups tried to specifically immobilize phages by exploiting the high affinity of biotin to streptavidin [101] ; this strategy involves the genetic biotinylation of the capsid heads of the bacteriophages and the natural affinity of the biotin/streptavidin system [121]. Gervais and his collaborators reported a 15-fold increase of the attachment densities of bacteriophages over physisorption [121]. However, chemical biotinylation of amino groups on the phage had the additional effect of modifying the phage groups involved in the recognition and binding to their host cell, resulting in their partial inactivation [181]. Sun et al. showed that biotinylated bacteriophages, immobilized on magnetic beads coated with streptavidin, captured up to 30% of host cells, which was below the capture efficiency reported for antibodies [182]. Tolba et al. used phage display methods to introduce affinity tags (biotin carboxyl carrier protein, BCCP, and cellulose binding module, CBM), in the head of T4 bacteriophages, to provide a uniform oriented immobilization of the latter on solid surfaces [179]. Although the immobilized phages retained infectivity, the authors reported a considerably reduced burst size and a longer latent period for both methods of attachment. Furthermore, the capture efficiencies of the immobilized phages were significantly different for both constructs, as the capture of bacteria by the immobilized CBM-T4 construct was not detectable by plate counting [179]. Moreover, these methods are costly, time-consuming, require the genetic modification of a given bacteriophage, and cannot be applied to all bacteriophages. Arya et al. used dithiobis(succinimidyl propionate) self-assembled monolayer to covalently bind T4 phages via their $NH_2$ groups[108]. Although this method of attachment shows great promise, the authors report a large decrease in SPR signal after washing the substrate with ethanolamine to remove non-specifically adhered T4 phages. This was attributed to the removal of a large number of physically adsorbed T4 phages, which created empty areas on the sensor surface. Moreover, there is a lack of systematic investigations of the relationship between the immobilization conditions, and the resulting orientation of these adsorbed phages, and their bioreactivity. A better understanding of the immobilization process will improve the potential to design better bio-sensing platforms.

This article describes the real-time formation of bacteriophage-modified gold surfaces via several chemical linkers, using SPR measurements. In addition, the activity, specificity and infectivity of

phages towards MRSA were evaluated by standardized microbiological methods and scanning electron microscopy (SEM). Finally, a method for immobilizing phages in an oriented manner is described and validated by atomic force microscopy (AFM).

## 4.3 Experimental Section

### 4.3.1 Preparation of Au surfaces

Biacore Platypus biosensor chips, to be described below, were used as the gold surface. Prior to modification, they were placed in freshly prepared "Piranha" solution (caution: a 7:3 mixture of concentrated $H_2SO_4$ and 30% $H_2O_2$) at room temperature for 30 min, then rinsed thoroughly with MilliQ water (Millipore, Mississauga, Ont.), ultrasonicated in water for 15 min, and dried in a nitrogen flow.

### 4.3.2 Chemicals

L-cysteine, 1-(3-dimethylaminopropyl)ethylcarbodiimide hydrochloride (EDC), N-hydroxysuccinimide (NHS), 11-mercaptoundecanoic acid (MUA), bovine serum albumin, gelatin, sodium chloride, magnesium sulfate and phosphate buffer saline (PBS) were purchased from Sigma-Aldrich. Luria-Bertani (LB) medium was purchased from Quelabs (Montreal, Quebec, Canada). We dissolved 25 g of LB powder were dissolved in 1 L of distilled water and autoclaved. LB-agar plates were prepared by adding granulated agar (6 g) to LB medium (400 mL). LB-agar was also autoclaved, melted, and placed in Petri dishes. SaA4 bacteria, a MRSA strain, and BP14, a MRSA-specific bacteriophage, were isolated by Biophage Pharma.

### 4.3.3 Bacterial culture

SaA4 bacteria were grown in an incubator-shaker at 37°C in LB (4mL) broth for 3 h. The bacteria were then centrifuged at 2500 g (Sorvall RT7, 3500 rpm) for 20 min. The supernatant was discarded, and the bacteria were resuspended in PBS. This was repeated twice. The concentration of bacteria was determined by plate count and expressed in colony forming units per mL (CFU/mL).

### 4.3.4 Bacteriophage preparation

Bacteriophages were amplified by pipetting 100 μL of a suspension of $10^6$ plaque forming units/mL (PFU/mL) of bacteriophages in a solution containing 1 mL of $10^6$ CFU/mL of freshly prepared bacteria. After 15 min of room temperature incubation, the infection mix was added to 250 ml of LB medium and incubated for 6 hours at 37°C in an incubator-shaker. The infected culture was then centrifuged at 2500 *g* for 20 min, filtered (0.22 μm) and titrated on LB-agar Petri dishes to determine the bulk bacteriophage concentration. For the SPR measurements, the bacteriophages were further centrifuged for 60 min, following which the supernatant was removed and the phages were resuspended in PBS.

### 4.3.5 Surface plasmon resonance apparatus

A superluminescent light-emitting diode (SLED), operating at 650 nm, was used as the light source. An achromatic lens produced a collimated beam, which passed through a polarizer. The linearly *p*-polarized light was focused by a lens and then used to excite surface plasmons on the sensing surface, situated on top of a coupling prism. A commercial sensing surface (Platypus Technologies), consisting of a glass microscope slide (BK7) covered by an adhesion layer of 5 nm of titanium and a sensing layer of 50 nm of gold, was placed in oil immersion contact (Cargille Labs) on the top of the coupling prism. For the real-time tests, a flow injection, double channel measuring cell with a 12 μL volume was developed. The entire system was placed on a goniometer stage with 2-D linear translation for exact beam angle and position location, permitting surface plasmon excitation at the gold/adjacent medium interface. The spatial distribution of the reflected light intensity was recorded by a CCD camera (Hamamatsu C4742-95) and examined by appropriate software image treatment.

### 4.3.6 SPR detection of bacteriophage adsorption to gold

The cleaned gold slides were placed on the SPR coupling prism using a refractive index-matching immersion liquid (Cargille Labs). Prior to bacteriophage injection, PBS was flowed on top of a previously functionalized gold surface at a flow rate of 111 μL/min, controlled by a peristaltic pump, to obtain a baseline. A solution of $2.2 \times 10^9$ PFU/mL of MRSA-specific phages was flowed into the SPR chamber. All experiments were carried out at room temperature.

### 4.3.7 SEM

Phage activity and bacterial adhesion were monitored by field emission scanning electron microscopy (FESEM, Hitachi S-4700, operating at 30 kV). Au substrates were cleaned with Piranha solution and ultrasonicated for 15 min. BP14 bacteriophages were immobilized with L-cysteine, MUA, or their mixture. We washed gold surfaces three times with MilliQ $H_2O$ and exposed them to $10^9$ CFU/mL MRSA bacteria for 20 min. Gold surfaces were again washed 3 times and fixed with a drop of 2% gluteraldehyde for 5 min.

### 4.3.8 AFM

Tapping-mode AFM measurements were performed with a NanoScope III Dimension 3100 AFM (Digital Instruments, Santa Barbara, CA, USA). Etched silicon probes (Digital Instruments), with cantilever lengths of 125 μm and resonance frequencies of 200–400 kHz, were used. Images were recorded with a scan rate of <1 Hz.

## 4.4 Results and Discussion

### 4.4.1 Bacteriophage immobilization

Bacteriophages bind to bacteria via their tail-proteins, which must be free and oriented perpendicular to the surface. Figure 4-1 shows the SPR response of bacteriophage attachment onto gold, using various chemistries, including physisorption, gluteraldehyde fixation, and L-cysteine combined with MUA and EDC/NHS. PBS was first injected into the sensor to create a baseline. After 5 min, a solution of 2.2 x $10^6$ PFU/mL of MRSA-specific phages was injected. The bacteriophages were allowed to attach to the functionalized surface. Phage-treated surfaces were not allowed to dry, as drying greatly affects phage binding affinity and lytic properties[183]. For all methods except direct gold adsorption, we saw no measurable desorption of the attached bacteriophages during the washing step. Physical adsorption results in a low surface coverage and dramatically diminishes the sensitivity of the platform. This can lead to a heterogeneous surface distribution of adsorbed phages [184]. More importantly, a change in the structural configuration of the phage epitopes and orientation is possible, which can lead to a reduction of its activity and unavailability of the active site [184]. A higher density of immobilized phages is usually

attributed to an increased bacterial capture. However, the literature reports that a high density of phages can result in the aggregation of the phages immobilized on the surface and reduce bacterial capture due to the steric hindrance and interaction of neighboring phage tails[108, 109]. In our previously characterized SPR biosensor[3], one pixel corresponds to a change of 0.00015 refractive index units (RIU), and a change of 0.001 RIU corresponds to 1 ng/mm$^2$ of binding protein. Our results show that employing a surface functionalized with mixed self-assembled monolayer consisting of L-cysteine and MUA, we obtain a surface density of 19 ng mm$^{-2}$ for an initial bacteriophage solution of 2.2 x 10$^6$ PFU/ml. Densities of immobilized phages are all reduced when employing L-cysteine (12 ng mm$^{-2}$), gluteraldehyde (8 ng mm$^{-2}$) or physisorption (8 ng mm$^{-2}$).

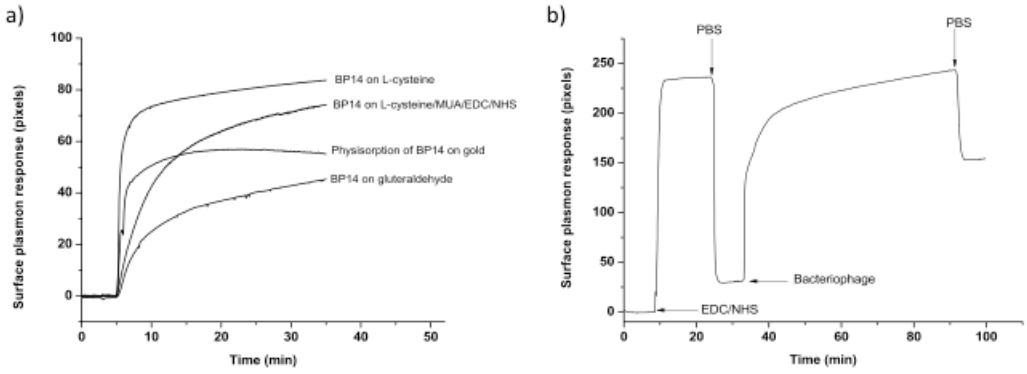


Figure 4-1: Immobilization and activity of bacteriophages on gold surfaces using various attachment strategies. (a) MRSA-specific bacteriophages were immobilized on gold surfaces via physical adsorption, L-cysteine and glutaraldehyde, L-cysteine, MUA, MUA/EDC/NHS and L-cysteine/MUA/EDC/NHS. SPR response shifts due to the attachment of phages onto gold surfaces using the various methods were monitored. (b) PBS was injected for 10 min atop a gold slide previously functionalized with L-cysteine and MUA to create a baseline. Phages were then injected, and the SPR response was monitored for 60 min. Loosely bound phages were removed by a 10 min washing step with PBS.

Covalent attachment of the phages to the gold support is rendered possible by the use of the catalysts, EDC and NHS, which can couple carboxylic acid to amine groups to form amide bonds [184, 185]. Figure 4-1b shows the EDC/NHS–catalyzed adsorption of bacteriophages onto a gold surface previously functionalized with L-cysteine and MUA. MilliQ water was injected for the first 10 min, to create a baseline. Following this, a solution of 1 mol $L^{-1}$ EDC was instantly mixed with a solution of 0.1 mol $L^{-1}$ NHS. The mixture was injected into the biosensor and held there for 15 min, followed by a 10 min MilliQ water washing step. Following this, a $10^9$ PFU/mL solution of bacteriophages was injected, and held for 60 min, before a final washing step.

To determine whether the activity of phages was affected by the method of immobilization, we immobilized rMRSA-specific phages either via physisorption or on gold slides previously coated with the following species: (a) L-cysteine, (b) L-cysteine and gluteraldehyde, (c) MUA, (d) MUA combined with EDC/NHS, or (e) L-cysteine combined with MUA and EDC/NHS on a gold-coated microscope slides (Figure 4-2a). These gold slides were then deposited in vials containing 40 mL of LB medium to which were added 500 μL of $10^6$ CFU/mL freshly prepared MRSA bacteria. If the immobilized bacteriophage was to retain its activity, then it would attach to the bacterium and lyse it. If the immobilization process rendered the immobilized bacteriophages inactive, then the bacteria would replicate. As negative and positive controls, we observed both the growth of MRSA without bacteriophage and the growth of MRSA with 100 μL of 2.2 x $10^9$ PFU/mL of phages. After the experiment was terminated (200 min, five lytic cycles), a sample was taken from each mixture and titrated on LB-Agar Petri dishes to calculate the final bacterial load of the sample (Figure 4-2a). Thus, the generation of progeny phages and ability to freely interact with bacteria will have an impact on the final titer, only if the immobilized phages remain active on the gold surface. Physisorbed bacteriophages showed the lowest activity with a final bacterial load of 7.1 ± 0.9 x $10^{10}$ CFU/mL, compared to the control value of 7.9 ± 0.4 x $10^{10}$ CFU/mL, as the bacteriophages are thought to adsorb preferably via their positively charged tails, rendering them inactive [186].

In a recent study [1], the use of sugars improved the binding capacity of bacteriophages to the surface by two- to three-fold, whereas modifying the surface with amino acids showed a seven-

fold improvement compared with physisoption. Nevertheless, the stability and uniformity of the coverage was poor. Our results suggest that modifying the gold surface with L-cysteine improved the attachment of phages on the surface compared to physisorption; however, the activity of the attached phages showed only a two-fold improvement with $4.4 \pm 0.1 \times 10^{10}$ CFU/mL. Furthermore, Singh et al. report a 37-fold improvement of bacteriophage adhesion when surfaces were treated with cysteine and gluteraldehyde when compared with physisorption[180]. However, our results show that combining gluteraldehyde and L-cysteine did not significantly improve the phage activity ($5.2 \pm 0.6 \times 10^{10}$ CFU/mL) nor did attaching phages with MUA alone ($3.5 \pm 0.1 \times 10^{10}$ CFU/mL). However, a 10-fold improvement, compared to physisorption, can be seen when combining MUA and EDC/NHS ($4.1 \pm 1.1 \times 10^{9}$ CFU/mL). Moreover, the L-cysteine/MUA/EDC/NHS strategy improved the lysis of bacteria by a factor of $10^3$ ($4.3 \pm 1.2 \times 10^{7}$ CFU/mL) when compared to physisorption. SEM images of bacterial adherence to physisorbed phages on gold (Figure 4-2b), phages adsorbed with L-cysteine (Figure 4-2c), phages adsorbed to MUA (Figure 4-2d), and phages adsorbed to a mixed layer of L-cysteine and MUA (Figure 4-2e) all corroborate these results.

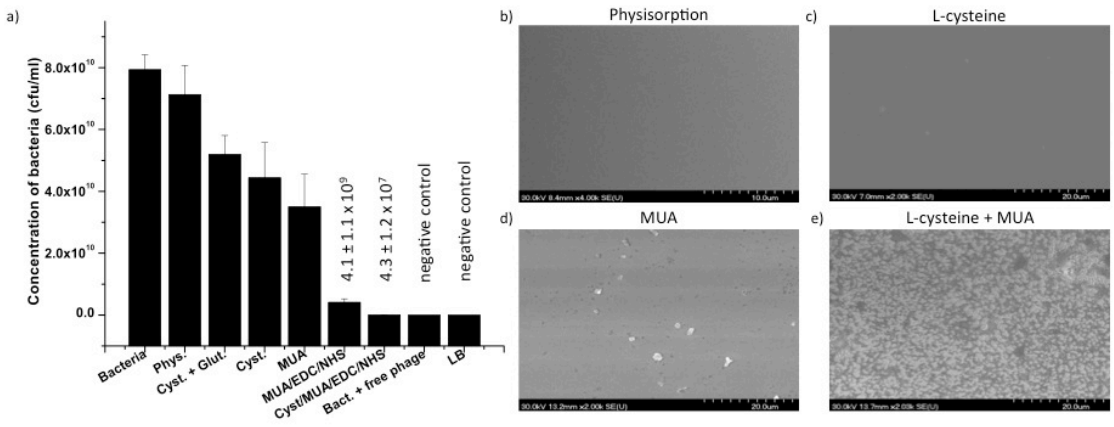


Figure 4-2: Immobilization and activity of bacteriophages on gold surfaces using various attachment strategies. MRSA-specific bacteriophages were immobilized on gold surfaces via physical adsorption, L-cysteine and glutaraldehyde, L-cysteine, MUA, MUA/EDC/NHS and L-cysteine/MUA/EDC/NHS. (a) Gold slides were then put in contact with MRSA bacteria, and solutions were titrated after 200 min. SEM images show the attachment of bacteria on bacteriophages immobilized on gold surfaces through (b) physisorption, (c) L-cysteine, (d) MUA and (e) L-cysteine and MUA.

On the basis of these results, the density of immobilized phages cannot solely account for increased binding of host bacteria and, ultimately, a better sensitivity of the detection platform. This can be demonstrated by the fact that although the surface density of the phages immobilized with L-cysteine is higher than those immobilized with gluteraldehyde no significant difference can be observed in the bacterial lysis experiments. This implies that although the phages are successfully immobilized on the gold surface their activity can still significantly be hindered no matter what the surface density. This activity is directly related to their orientation if we assume that the treatment itself does not damage the phage tail proteins.

AFM analysis is used to complement SPR by providing further information on the relationships between surface topologies and biological interactions. Figure 4-3 shows representative topographic images obtained by tapping-mode AFM. L-Cysteine-modified gold shows atomically flat Au grains with ill-defined step edges that are in good agreement with typical AFM images of

thiol-modified Au substrates. The exposure of L-cysteine-modified surfaces to MUA produced a noticeably different topological image: compact linear bodies are finely distributed, covering the substrate surface almost completely. Our findings reveal that roughness of the surface did not play an important part in the attachment of the phages to the surfaces (unmodified gold Au (1.10 nm); L-cysteine (0.998 nm) ; MUA (0.799 nm) and L-cysteine + MUA (0.934 nm)). However, modification of the surfaces with structurally different thiols did create vacancy cavities of different depths, as shown by the AFM profiles (insets of Figure 4-3). The average length of the cavities formed on the surface of bare gold (38 ± 16 nm), L-cysteine modified Au (39 ± 19nm), and MUA modified Au (45± 21 nm) varies greatly over the surface. However, the presence of both L-cysteine and MUA allow for a more uniform coverage, with vacancy islands of 37 ± 6 nm of width, corresponding to the width of the bacteriophage head (36 ± 2 nm), as measured by AFM. We hypothesize that the presence of both L-cysteine and MUA on gold creates cavities that fit the heads of the phages, which can explain their increased chemical stabilities and activities on gold. The inset to Figure 4-3d clearly shows that the combination of L-cysteine and MUA produces a surface having regularly separated depressions. The inset to Figure 4-3e shows that many of these depressions are filled with phages projecting above the depressions. The phages have been attached through the use of EDC/NHS, which causes binding through the $-NH_2$ groups available on both the tail and the body of the phages. We expect some differences in the orientations of the deposited phages, ranging from tail-up, through horizontal, to tail-down. Because lysis can only occur when the phage is in the tail-up position, and our results show increased lysis in this case, it appears that there is a preference for tail-up deposition.

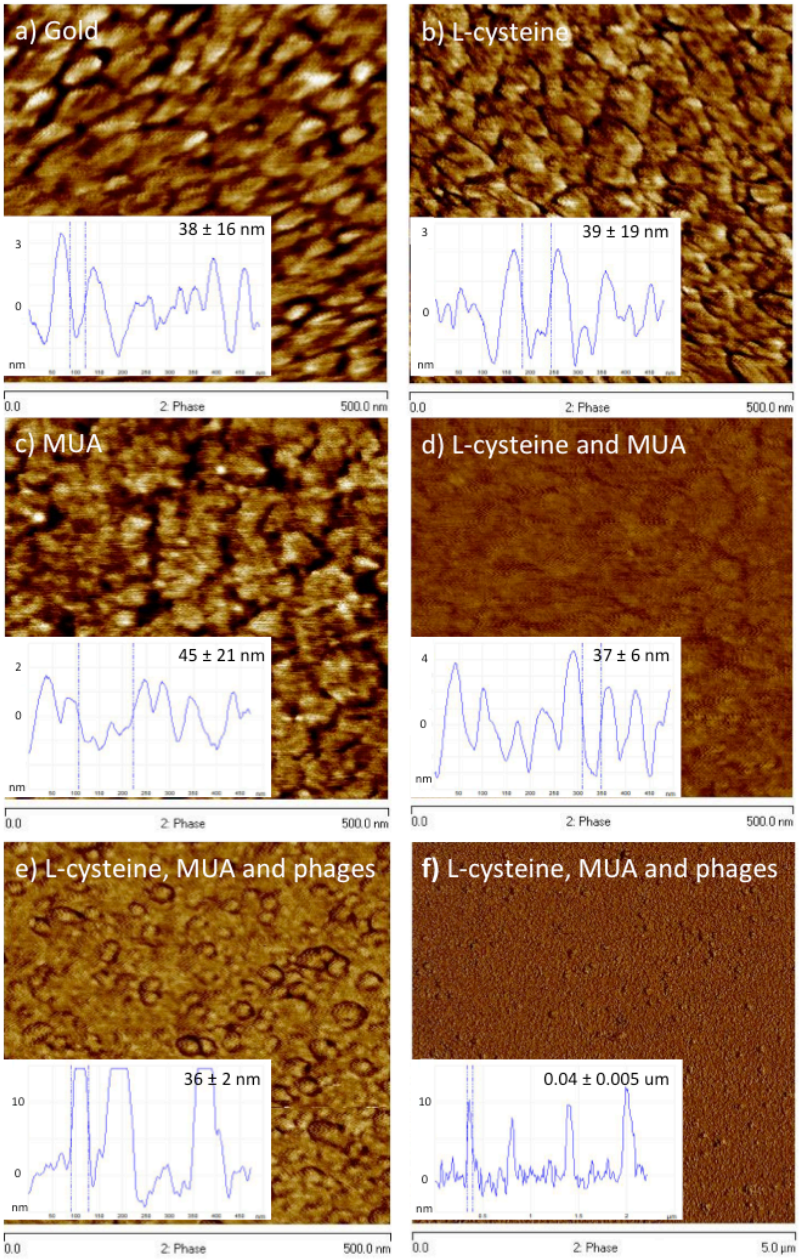


Figure 4-3: Atomic force micrographs of thiol and phage immobilization on gold. AFM tapping mode was used to probe (a) unfunctionalized gold (b) L-cysteine-functionalized gold, (c) MUA-functionalized gold, (d) L-cysteine- and MUA-functionalized gold, (e) immobilized bacteriophages on L-cysteine- and MUA-functionalized gold (500 nm resolution) (f) immobilized bacteriophages on L-cysteine- and MUA-functionalized gold (5 µm resolution).

The multivalent binding capabilities and high affinities of bacteriophages to host cells make them suitable recognition elements for bacterial biosensing. To permit more efficient binding, the tail fibers of the phage should face the medium, and thus the phage must be bound to the substrate by its head capsid. Alternatively, phages partially oriented with their tail fibers facing the sensor surface will not be accessible to bacterial surface antigens. Therefore, the sensitivity of this type of biosensor will be strongly dependent on the orientation of the immobilized phages. The immobilization of phages via a mixed SAM of L-cysteine and MUA resulted in the formation of covalent binding between the phages and the gold surface. L-Cysteine and MUA attached to gold through their SH- end group and formed amide bonds between their carboxy-end groups and the amines on the phages capsid via EDC-NHS chemistry. Immobilized phages retained their infectivity, suggesting that the phages were immobilized, with their tail proteins oriented upwards. AFM results further corroborate this claim. The topographic images clearly indicate that the phages preferentially bind in the cavities formed by the mixed SAM of L-cysteine and MUA. This implies that steric hindrance between adjacent molecules plays an important role in the immobilization of phages. We believe that this method of immobilization improves phage stability and increases their intrinsic reactivity toward their targeted bacteria by orienting the tail fibers toward the incoming medium. Moreover, the use of the mixed SAM provided a more uniform surface for the attachment of phages in a more ordered similarly uniform fashion, thus improving the detection of bacteria.

## 4.5 Conclusions

We have considered the attachment of bacteriophages to gold surfaces for plasmon resonance biosensing applications. It was found that compared to physisorption the covalent chemisorption of phages preserves their activity. In particular, the L-cysteine/MUA/EDC/NHS chemisorption combination provides a $10^3$-fold improvement in phage activity compared with physisorption due to the creation of uniform cavities on the gold surface, whose size is that of the phage head, permitting a more uniform distribution and oriented attachment of the phages. The characterization of the physical processes of bacteriophage interaction with functionalized Au surfaces and the stability of the resulting complexes are of critical importance to biosensor applications.

## 4.6 Acknowledgments

We thank NanoQuébec for their financial support, S. Patskovsky for SPR assistance, and P. Moraille for AFM support.

# CHAPTER 5 ARTICLE 4: SURFACE PLASMON RESONANCE DETECTION OF *E. COLI* AND METHICILLIN-RESISTANT *S. AUREUS* USING BACTERIOPHAGES

The rapid and specific detection of pathogenic bacteria is important in many areas pertaining to human health, such as food safety, air quality, nosocomial and community infection outbreaks, and homeland security. Conventional microbiological methods and emerging technologies, such as PCR, ELISA, and flow cytometry, require cumbersome sample preparation, highly trained personnel, and are costly and time-consuming. Therefore, although these methods are relevant in a laboratory setting, they cannot adequately serve the needs of health care practitioners in a clinical setting. Phage-based SPR biosensors present a viable solution to these problems, as they are specific, sensitive, inexpensive, well adapted to miniaturization, and can, therefore, provide disposable chips for field applications.

The present work pertains to the development of a sensitive phage-based SPR biosensor for the real time, label-free, rapid detection of whole bacteria in less than 20 minutes. We first describe our experimental SPR setup, as well as a novel bacteriophage specific for *MRSA*, whose morphological characteristics are suitable for SPR detection. The specificity of the phage was tested via spectrophotometry and impedance sensing. We then present the successful detection of *E. coli* and *MRSA* for concentrations lower than $10^3$ CFU/mL, without prior labelling or enrichment steps in less than 20 minutes.

# Surface Plasmon Resonance Detection of *E. coli* and Methicillin-Resistant *S. aureus* using Bacteriophages

*Nancy Tawil[1,2,31], Edward Sacher[1], Rosemonde Mandeville[2], Michel Meunier[3]*

[1] Regroupement Québecois de Matériaux de Pointe, Département de Génie Physique, École Polytechnique de Montreal, Case Postale 6079, succursale. Centre-Ville, Montreal, Québec, H3C 3A7 Canada

[2] Biophage Pharma Inc, 6100 Royalmount, Montreal, Québec, Canada H4P 2R2

[3] Laser Processing and Plasmonics Laboratory, Département de Génie Physique, École Polytechnique de Montreal, Case Postale 6079, succursale. Centre-Ville, Montreal, Québec, H3C 3A7 Canada

Received : March 2, 2012 Published : April 13, 2012

dx.doi.org/10.1016/j.bios.2012.04.048 Biosensors Bioelectronics 2012, 37, 24-29

KEYWORDS: bacteriophage, biosensor, methicillin-resistant *Staphylococcus aureus* (MRSA), surface plasmon resonance (SPR)

## 5.1 Abstract

Early diagnosis and appropriate treatment of *Escherichia coli* (*E. coli*) O157:H7 and methicillin-resistant *Staphylococcus aureus* (MRSA) are key elements in preventing resultant life-threatening illnesses, such as hemorrhagic colitis, hemolytic uremic syndrome, and septicemia. In this report, we describe the use of surface plasmon resonance (SPR) for the biodetection of pathogenic bacteria, using bacteriophages as

[1] Address correspondence to nancy.tawil@polymtl.ca

the recognition elements. T4 bacteriophages were used to detect *E. coli*, while a novel, highly specific phage was used to detect MRSA. We found that the system permits label-free, real-time, specific, rapid and cost-effective detection of pathogens, for concentrations of $10^3$ colony forming units/milliliter, in less than 20 min. This system promises to become a diagnostic tool for bacteria that cause major public concern for food safety, bioterrorism, and nosocomial infections.

## 5.2 Introduction

Nosocomial infection is the leading cause of death for hospitalized patients, affecting more than 2 million such patients per year, and leading to approximately 90,000 deaths annually [187]. The average treatment cost varies between $14,000 and $38,000 per patient, for a total reported cost of $4.5 billion annually [188]. Methicillin-resistant staphylococcus aureus (MRSA) is the leading cause of nosocomial and community-acquired infections. Reducing the time of diagnosis is directly related to reducing morbidity and mortality rates [189]. A non-pathogenic form of *Escherichia coli* was used as a detection model for other harmful bacteria, such as E. coli O157:H7, a microorganism that causes severe gastrointestinal diseases in humans, such as bloody diarrhea, hemorrhagic colitis, and hemolytic uremic syndrome, reaching a mortality rate of over 50% in children and seniors [190].

Conventional culture methods that are predominantly used for bacterial detection are time-consuming and require enrichment steps in order to visualize colonies on agar plates. Over the years, mass spectrometry and biochemical detection systems have been developed to ameliorate and increase the speed and sensitivity of culture methods. However, these methods retain negative aspects such as high cost and difficulty in handling. PCR and immunoassays are other approaches aimed at ameliorating the sensitivity of detection. Nevertheless, routine PCR detects the presence of nucleic acid and cannot differentiate between live and dead cells. More importantly, PCR techniques still require DNA extractions, which are time-consuming and suffer from fidelity of DNA replication. In contrast, immunoassays, such as ELISA, are simple and

rapid to use, but they lack suitable sensitivity for pathogen detection. Moreover, assay times vary from 24-52 hours for bacteria [191], which can be a decisive factor when treating a patient.

Other major shortcomings of the available biosensors are the use of ligands that cannot differentiate between pathogenic and non-pathogenic organisms with sufficiently high sensitivity and accuracy. Polyclonal antibodies recognize different epitopes on the same pathogens, which can also be present in related non-pathogenic organisms [9]. Major disadvantages of monoclonal antibodies are their relative instability to environmental fluctuations, which can limit their long term storage and their field applicability. Furthermore, their production remains time-consuming and costly.

Bacteriophages are the main regulators of microbial balance on earth, as they total an estimated $10^{32}$ entities [30]. The many advantages of bacteriophages make them an excellent method for the detection and identification of bacterial pathogens. Among these advantages are the specificity of the interaction of this type of virus with its target host cell, its lytic ability, and its capacity to multiply during the infection process. They are able to distinguish between live and dead cells, and they are robust, easy to produce, and cost-effective.

Requirements for pathogenic bacterial detection are rapidity, sensitivity, specificity and cost. Recently, many groups have been involved in developing bacteriophage-based sensors for bacterial detection [105, 121, 133, 192, 193]. Balasubramanian et al. were able to identify Staphylococcus aureus with a detection limit of $10^4$ colony forming units/milliliter (CFU/mL); however, detection suffered from the physical adsorption of phages onto the sensor surface [105]. Moreover, the phages were not directed against methicillin-resistant strains of *S. aureus*. Oh et al. used self-assembled G protein to immobilize antibodies [193], a strategy that cannot be used to detect *S. aureus*. Our group has employed biotinylated T4 bacteriophages to detect E. coli [121], but the genetic modification of all phages is not possible. Although much work has been done, a low cost, specific, sensitive optical method for detecting low concentrations of pathogens, in a few minutes, has not been established.

Our work consists, in part, of creating an accurate and sensitive biosensor for bacterial detection, with the potential for miniaturization. We use an already characterized impedometric sensor (PDS, Biophage Pharma) [194] to screen for the specificity of the bacteriophage to its target bacterium. Direct impedometric detection is limited by the facts that the medium utilized must be optimized for electrical measurements, and that not all microorganisms generate an adequate amount of ionized metabolites to allow for their detection.

These limitations can be overcome by the use of surface plasmon resonance (SPR). We suitably modified an SPR apparatus for bacterial detection. Multiple strategies were used to improve the immobilization of recognition elements on sensor surfaces including the physisorption of phages and the covalent immobilization of phages via L-cysteine, glutaraldehyde and self-assembled monolayers; an article in preparation contains a fuller discussion of the interaction of these molecules with gold than is given here, as well as the optimal method for phage immobilization. We have isolated and characterized a lytic bacteriophage that can specifically recognize methicillin-resistant strains of *S. aureus*. More importantly, we report on a rapid, specific and cost-effective method of detecting $10^3$ CFU of bacteria per mL.

## 5.3 Materials and methods

### *5.3.1* Surface Plasmon Resonance

A schematic diagram of the instrument design is shown in Figure 5-1. A superluminescent light-emitting diode (SLED), operating at 650 nm, was used as the light source. This allowed for a reduction in speckle patterning and interference fringes as SLEDs present low temporal coherence, related to their large spectral bandwidth. This translates in noise reduction, which allowed for better signal processing and better sensitivity. An achromatic lens produced a collimated beam, which passed through a polarizer. The linear p-polarized light was then

focalized by a lens, and excited surface plasmons on the sensing surface, situated on top of a coupling prism.

A commercial sensing surface (Platypus technologies), consisting in a microscope glass slide (BK7) covered by an adhesion layer of 5 nm of titanium and a sensing layer of 50 nm of gold, was placed in oil immersion contact (Cargille Labs) on the top of the coupling prism (BK7 glass). For the real-time tests, a flow injection double channel-measuring cell, with 12 µl volumes, was developed. The entire system was placed on a goniometer stage with 2-D linear translation for exact beam angle and beam position, permitting surface plasmon excitation on the gold/adjacent medium interface.

The spatial distribution of the reflected light intensity was recorded by a CCD camera (Hamamatsu C4742-95), and examined by appropriate software image treatment. The SPR resonance dip is usually recorded with a linear CCD detector. In our case, a drastic reduction of both signal noise and dispersion, which are due to the non-ideality of the light beam and the sensor surface modification, was achieved by using numerical analysis of the acquired SPR curves. Both fourth order polynomial curve fitting and centroid method were used to determine accurately the position of the SPR minimum.

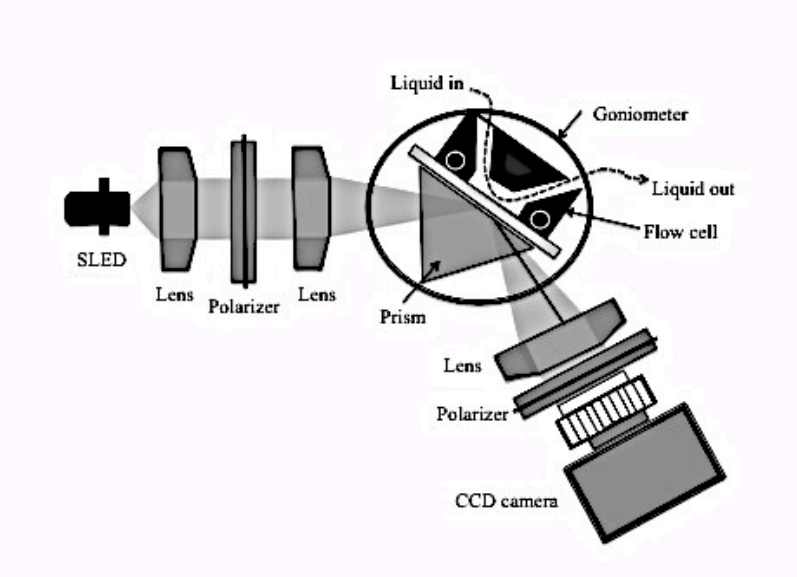


Figure 5-1: Experimental CCD camera-based SPR set-up.

Prior to SPR use, the gold surfaces of the glass slides were cleaned, using freshly prepared "piranha" solution (caution: piranha solution is a 3:1 mixture of concentrated $H_2SO_4$ and 30%

$H_2O_2$), at room temperature, for 2 min, then rinsed thoroughly using MilliQ water, and dried in a nitrogen flow. The liquid flow rate (111 μL $min^{-1}$) was controlled by a peristaltic pump (Ismatec). Phages specific for the targeted bacteria were then attached to the gold surface of the planar SPR system.

### 5.3.2 Impedance Measurements

The impedance measurements were carried out using a PDS Biosensor (Biophage Pharma). The PDS biosensor is based on Electric Cell-Substrate Impedance Sensing (ECIS) and is used to detect the total live bacterial load of a sample. Small gold electrodes, 250 μm in diameter, were placed on the bottom of individual culture wells. The sample, containing the bacteria and culture medium, was placed in the culture wells and a 4,000 Hz, 1.5 V, 1 μA current was applied between the detecting and the counter electrodes. The bacteria interfere with current flow as they occupy the free space immediately above the electrode; the impedance is monitored by a lock-in amplifier. Bacteriophages were immobilized on the gold electrode surface, following which, 400 μL of freshly prepared bacterial solutions were injected into the well containing the gold sensor chip. The chip was then placed in an incubator at 37°C. The growth of the bacteria was then monitored.

### 5.3.3 Chemicals

L-cysteine, 1-(3-imethylaminopropyl) ethylcarbodiimide hydrochloride (EDC), NHS, 11-mercaptoundecanoic acid, bovine serum albumin, sodium chloride, magnesium sulfate, and gelatin were purchased from Sigma-Aldrich. Luria-Bertani (LB) medium was purchased from Quelabs (Montréal, Québec, Canada); 25 g of LB powder were dissolved in 1 L of distilled water and autoclaved. LB-agar plates were prepared by adding 6 g of granulated agar to 400 mL of LB media. The LB-agar was autoclaved, melted and placed in Petri dishes. PBS was purchased from Fisher Scientific (Nepean, Ontario, Canada). E. coli K12 (11303) and T4 bacteriophages (11303-

B4) were purchased from American Type Culture Collection (ATCC). SaA4 MRSA bacteria and BP14 bacteriophages were isolated by Biophage Pharma.

### 5.3.4 Bacterial culture

EC12 and SaA4 bacteria were grown in an incubator-shaker at 37°C in 4 mL of LB media for 3h. The bacteria were then centrifuged at 2500 g (Sorvall RT7, 3500 rpm) for 20 min. The supernatant was discarded and the bacteria were resuspended in PBS. This was repeated twice. The concentration of bacteria was determined by plate count technique and expressed in colony forming units per milliliter (CFU/mL).

### 5.3.5 Bacteriophage preparation

Bacteriophages were amplified by pipetting 100 μL of a suspension of $10^6$ PFU/mL of bacteriophages in a solution containing 1mL of $10^6$ CFU/mL of freshly prepared bacteria. After 15 minutes of incubation at room temperature, the infection mix was added to an Erlenmeyer flask containing 250 mL LB and incubated for 6 hours, at 37°C, in an incubator-shaker. The infected culture was then centrifuged at 2500 g for 20 minutes, then filtered (0.22 μm) and titrated. For the SPR measurements, the bacteriophages were further centrifuged for 60 minutes, the supernatant was removed and the phages were resuspended in PBS. The concentration of bacteriophages was determined by plate count technique and expressed in plaque forming units per milliliter (PFU/mL).

### 5.3.6 Optical density measurements

Bacterial suspensions were vortexed. One mL of the suspension was pipette in a disposable cuvette (Sarstedt AG & Co., Numbrecht, Germany). Optical density (OD) was monitored at 595 nm on a Beckman DU-140B spectrophotometer (Beckman Coulter Inc., Fullerton, CA).

### 5.3.7 Transmission electron microscopy

The TEM used was a Hitachi H-7100, operating at 75 kV. We used copper grids (200 mesh), coated with a layer of Formvar and an overlayer of evaporated amorphous carbon. The samples were deposited on the grid by the reverse drop method (a drop of sample was deposited on Parafilm for 5 min, then the grid was deposited on top of the Parafilm, and excess was wiped up with a paper towel. The grid was then dipped, for 1 minute, in a drop of 3% aqueous phosphotungstic acid (PTA) adjusted to a pH of 7; PTA is a negative stain solution, used at neutral pH because phages will tend to dissociate at low pH. The grid was allowed to dry before the sample was used for TEM analysis.

### 5.3.8 DNA sequence analysis and bioinformatics

Open reading frame identification was performed using GeneMark.hmm [195]. Similarity searches, for nucleotide sequences and for the deduced amino acid sequences, were performed using the FASTA [196], BLAST [197], and PARALIGN [198] programs available on the Online Analysis Tools website (http://molbio-tools.ca/).

## 5.4 Results and discussion

### 5.4.1 Specificity of BP14 for MRSA

To facilitate the immobilization and detection processes, bacteriophages should possess morphological characteristics, such as small size, and a short tail. For example, the T4 phage has a 168.9 kb genome, its head dimension is 110 x 80 nm, while its tail length 98 nm [199, 200]. Because the evanescent wave of our SPR travels up to 300 nm into the substrate, only a portion of the bacterium will generate a response by interacting with it. Reducing the length of the recognition element will increase the SPR response on bacterial attachment. The transmission electron microscopic [201] image of BP14 (Figure 5-2a) shows its morphology to be very similar to that of the *S. aureus* 44AHDJ virus, allocated to the order *Caudovirales* and the family *Podoviridae*. It possesses a short, non-contractile tail measuring 25 nm (black arrow), and a small isometric head, measuring 42 nm (white arrow). It has a pre-neck appendage characteristic of the ϕ29-like phages, according to the International Committee on Taxonomy of Viruses. BP14 is 68% smaller than T4. This observation indicates that a larger portion of the target bacteria (~233 nm) can be probed by the evanescent field of the SPR, yielding an improved response (Figure 5-2b).

The complete DNA sequence of BP14 was determined. The genome of BP14 consists of 17 769 base pairs (bp), and the total G+C content is 29.6 %. Twenty-two open reading frames (ORFs) were identified, with 12 orientated in opposite directions from each other. The overall DNA sequence identity between BP14 and similar phages are 85.7% for Bacteriophage 66, 85.9% for *S. aureus* phage phiP68, 73% for *Staphylococcus* phage phi44AHJD, and 82% for *Staphylococcus* phage SAP-2. Of the 22 ORFs found, ORF-14 and 15 were identified as major and minor tail proteins, respectively, based on the overall similarity to tail proteins of the ϕ29 phage family. In particular, the sequence coding for the minor tail protein of BP14 differs from that of phage phiP68 by 11.2%, of *Staphylococcus* phage 66 by 9.8%, and of *Staphylococcus* phage SAP-2 by 63.7%. Our results suggest that phage BP14 is unique and different from other

commercially available phages. Bacterial recognition is achieved by tailed-phages through the interaction of fibers at their tails. These fibers will first recognize, and adhere to, the host bacterium in a reversible fashion, followed by the irreversible binding of a secondary minor tail protein to another receptor molecule on the surface of the bacterium. Having a short, non-contractile tail, the phage has the advantage of not being able to fold and interact with the gold substrate on which it is deposited. Moreover, BP14 has a lesser probability of adhering to the gold surface by its tail, compared to phages with larger tail/head ratios.

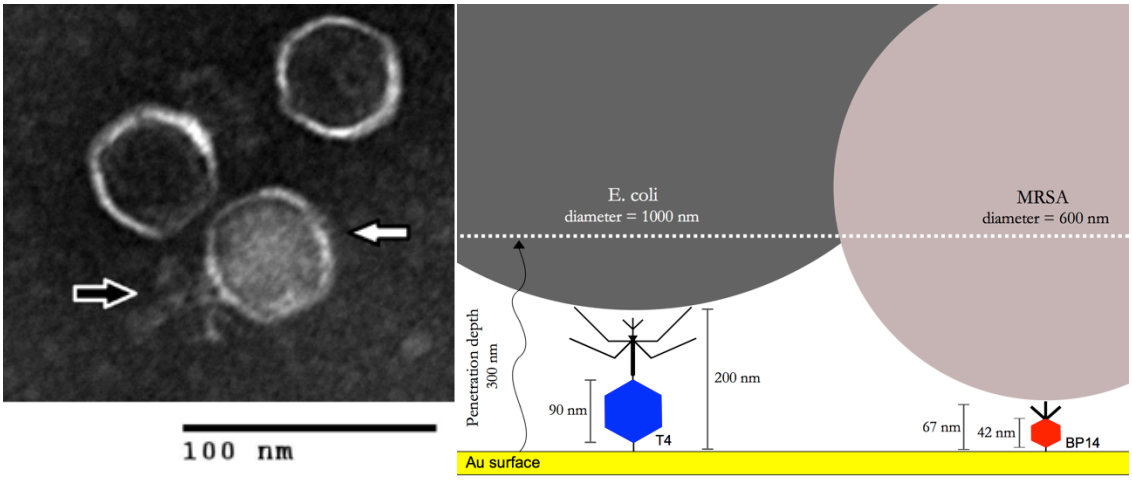


Figure 5-2: a) TEM image of bacteriophage BP14, showing an icosahedral head, measuring 42 nm in diameter (white arrow), and a 25 nm non-contractile tail (black arrow). b) Comparison between T4 and BP14 bacteriophages. The use of a smaller bacteriophage, such as BP14, allows for a larger portion of the bacterium to be probed by the evanescent field.

Moreover, phages can be further divided into two categories, depending on their life cycles and means of propagation [36]. BP14 is a member of the virulent phages, which are only capable of lytic propagation, consisting of infection of the host bacterium by the phage, replication of the phage genome, production of the phage structural components, and release of the newly assembled phages. More often than not, this process results in bacterial lysis and death. This is crucial for cost-effective production.

To establish whether bacteriophage BP14 possesses lytic capabilities, it was exposed to MRSA, and the optical density was monitored over time (Figure 5-3a). We found that the optical density of BP14+MRSA did not increase over time, indicating that BP14 specifically recognizes MRSA, binds to the bacteria and lyses them, ultimately inhibiting their growth. Solutions containing only MRSA show an increase in optical density over time, consistent with bacterial growth.

In order to ensure the specificity of the sensor, the non-specific adsorption of entities other than the bacterium of interest must be prevented. Moreover, the selected phages should discriminate between MRSA and methicillin-*sensitive S. aureus* (MSSA), which is affected by the use of antibiotics. To demonstrate that BP14 can discriminate between different types of bacteria, we used an impedance biosensor to detect the total live bacterial load on a sensor chip. Bacteria act as insulating particles, by reducing the area that the current reaches and, thus, increasing the interface impedance. Because a bacteriophage specifically recognizes a host bacterium and lyses it, the microbial growth will be reduced and, therefore, the detection time will increase in the wells containing the samples treated with phages. Here, the gold electrodes were first coated, using a solution of bovine serum albumin (BSA), to prevent non-specific binding. Following this, 400 μL of solution was pipetted into each cuvette and placed in an incubator at 37°C for 12 hours. The LB curve, in figure 5-3b, contains only culture medium and shows that there was no contamination present, while the MRSA curve contains only bacteria and shows their unhindered growth. Other wells contained bacteriophage BP14, incubated in the presence of various solutions of bacteria (EC12, O157:H7, MSSA, and MRSA), at a concentration ration of 1:5. Our results indicate that BP14 does not affect the growth of different E. coli strains, such as EC12 and O157:H7. Moreover, BP14 does not recognize, or lyse, methicillin-sensitive *S. aureus*. However,

when in the presence of MRSA, BP14 provokes a delay in the growth of the bacterium. This observation signifies that BP14 is able to specifically recognize, adhere to, replicate, and lyse MRSA. The impedance decrease that can be observed in the first 30-60 minutes is due to the fact that bacteria release molecules to prepare their environment for growth. When bacteria grow in a culture medium, they transform uncharged reactants, such as carbohydrates, into charged products, mainly carboxylic acids. These molecules render the culture medium more conductive, with a resultant decrease in impedance.

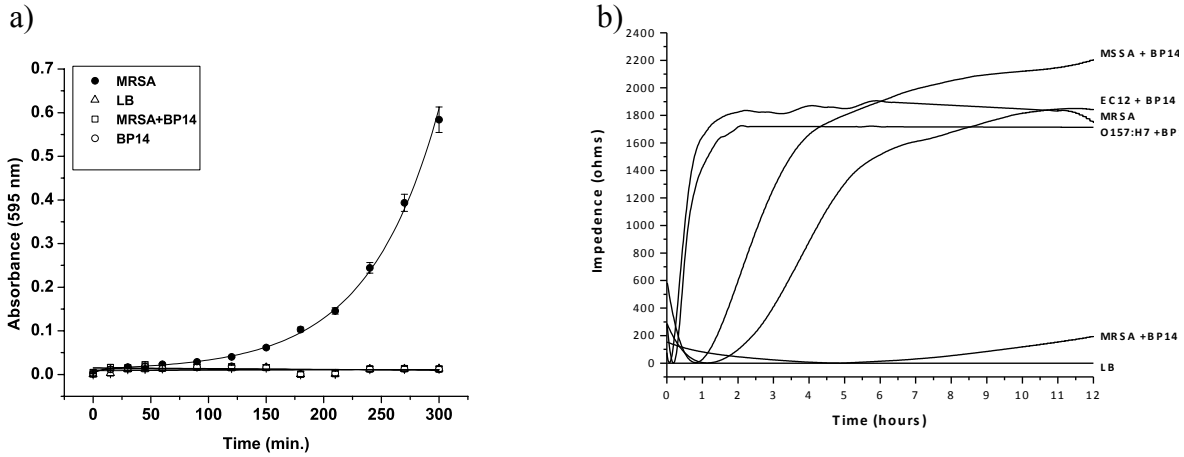


Figure 5-3: Specificity of bacteriophage BP14 to MRSA bacteria. a) Optical density of MRSA (positive control), LB (negative control), bacteriophage BP14, and MRSA and BP14 solution. b) MRSA, MSSA, *E. coli* EC12 and O157:H7 were incubated with BP14 at 37°C. Impedance was monitored for 12 h, reflecting bacterial growth. Replications of MSSA, EC12 and O157:H7 were not hindered by the presence of BP14. MRSA growth was delayed by the presence of BP14; MRSA bacteria are lysed following bacteriophage replication.

### 5.4.2 Detection of E. coli and MRSA

We used a home-built biosensor, with bacteriophages as specific recognition elements, to detect low concentrations of bacteria. Gold was coated with a self-assembled monolayer (SAM) of l-cysteine overnight at 37°C, washed and subsequently coated with mercaptoundecanoic acid (MUA), then treated with 1-(3-dimethylaminopropyl)ethylcarbodiimide hydrochloride (EDC) and N-hydroxysuccinimide (NHS). A PBS solution was injected onto the SAM-modified gold chip for 10 minutes, followed by the injection of a PBS solution containing $10^9$ PFU/mL phages for 50 minutes (Figure 5-4). PBS was then injected to wash away the unbound phages, and $10^6$ CFU/mL of the target bacterium was flowed over the sensor for 50 minutes, followed by washing. Because the lytic cycle of the phage is 30 minutes, we chose to follow the initial 20 minutes of surface plasmon response, following the injection of bacteria (dashed lines). The results are shown in pixels, with one pixel corresponding to 0.005 angle units.

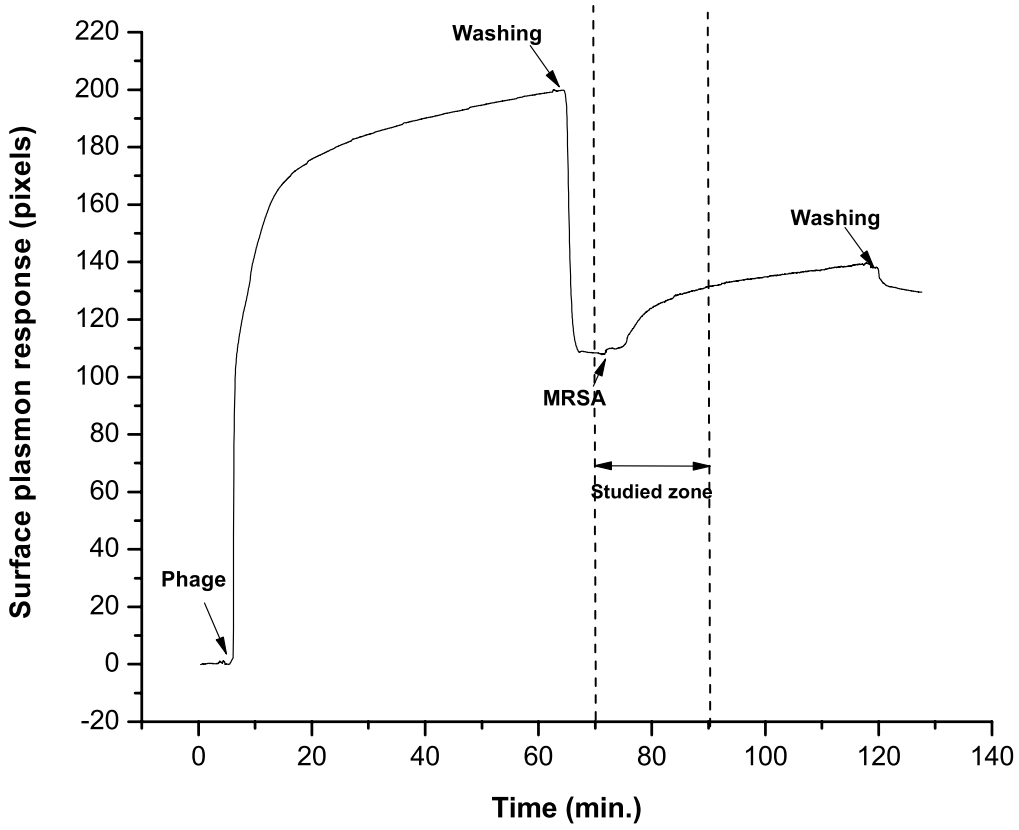


Figure 5-4: SPR response of attachment of phages, followed by specific attachment of bacteria. The dashed lines indicate the region of interest for phage assisted detection.

To determine the sensor detection limit, we coated the gold chips with bacteriophage, using the previously described method. Furthermore, the chips were coated with BSA to prevent non-specific binding, followed by the injection of different concentrations of target bacteria. A solution of PBS was injected for the first 10 minutes, to create a baseline, after which a solution of E. coli in PBS was injected onto the sensor for another 20 minutes (Figure 5-5). Bacteriophages will lyse the bacteria within 20 minutes following their attachment to their hosts. A significant change in the surface plasmon response can be seen after 10 minutes. The control consists of PBS injected onto a T4-coated gold chip.

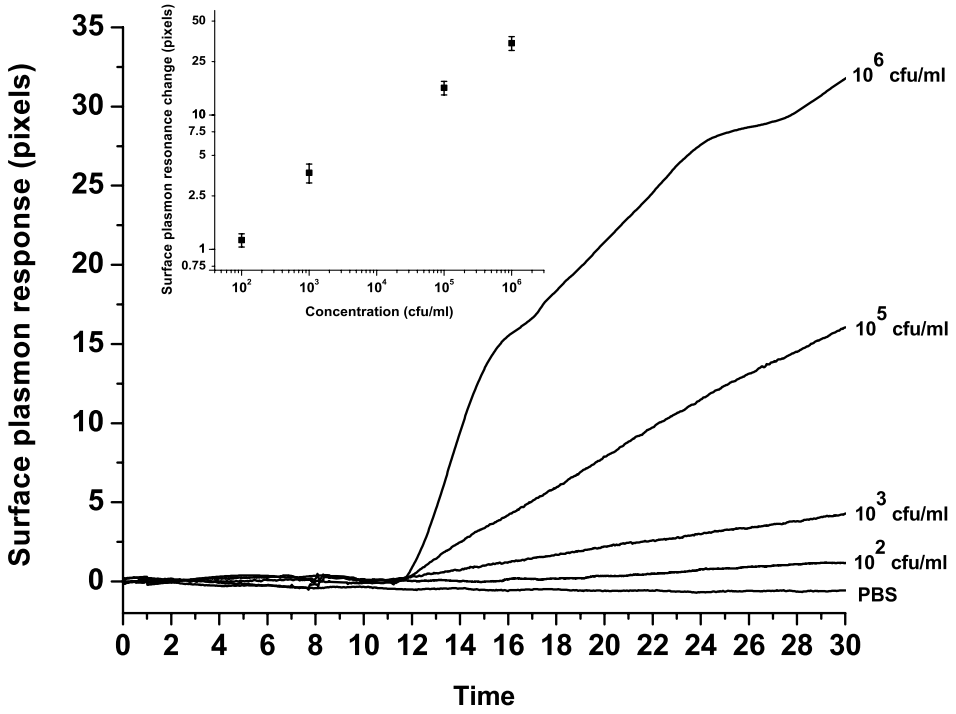


Figure 5-5: Detection of E. coli, using T4 bacteriophages. T4 bacteriophages were coated onto the gold sensor chip. A baseline was created by injecting PBS buffer for 10 minutes. Following this, known concentrations of E. coli, diluted in PBS, were flowed over the sensor surface. The surface plasmon resonance change was monitored for 20 minutes. A dose-response curve for detection of E. coli is shown, in inset, for values taken after 20 minutes following bacterial insertion.

The same experiment was repeated to establish the possibility of detecting MRSA bacteria, using BP14 combined with SPR (Figure 5-6) All slides were previously coated with BP14 bacteriophages and BSA, to prevent non-specific adhesion. The controls consist of PBS injected onto a BP14-coated slide, and a solution of $10^6$ CFU/mL of EC12 injected on a BP14-coated slide. Because EC12 are E. coli bacteria, and BP14 are not specific to this type of bacteria, we saw no significant change in SPR response. Noise was determined to be the surface plasmon response difference between the PBS baseline and the non-specific adsorption of E. coli bacteria,

corresponding to 0.835 pixels. Using the criterion of S/N ›3, the limit of detection is found to be $10^3$ CFU/mL. Figure 5-6 demonstrates that the SPR response due to bacterial detection by bacteriophages is dose-dependent. All experiments were carried out at room temperature; better results are anticipated at 37°C.

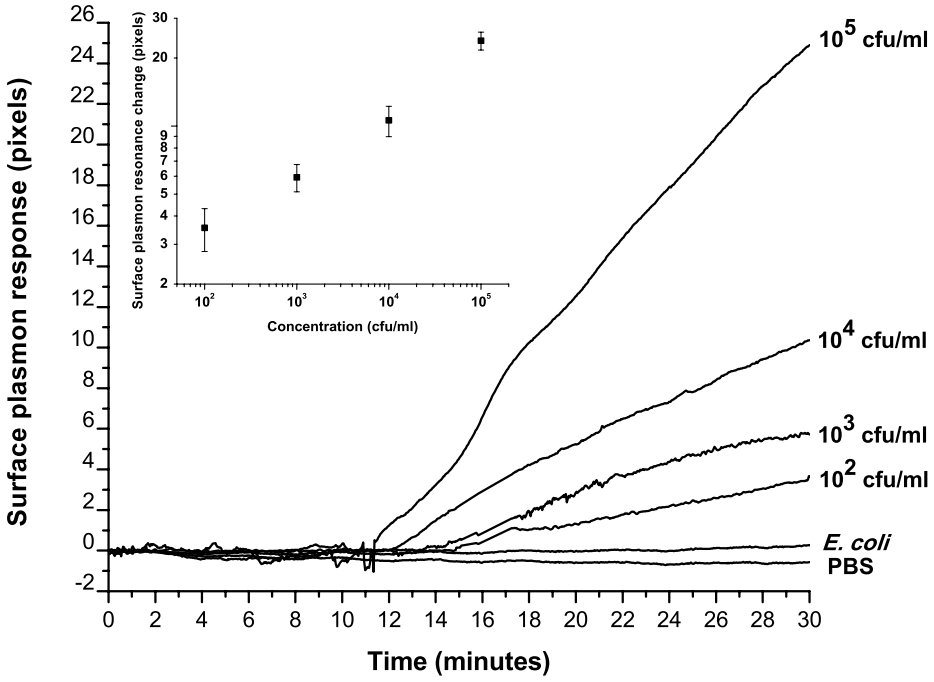


Figure 5-6: Detection of MRSA using BP14 bacteriophages. BP14 bacteriophages were immobilized on the gold sensor chip. A baseline was created by injecting PBS buffer for 10 minutes. Following this, known concentrations of MRSA diluted in PBS were flowed onto the sensor surface. Surface plasmon resonance change was monitored for 20 minutes. E. coli, at a concentration of $10^6$ CFU/mL, was also tested, and showed the high specificity of the B14 for MRSA detection. For detection of MRSA, a dose-response curve is shown, in inset, for values taken after 20 minutes.

Our results are consistent with those reported by other groups [105, 109]. The interaction between the phage and the bacterium receptor is a reversible process, which is ultimately followed by irreversible binding, coinciding with the initiation of phage DNA translocation into the bacterium. These two steps are characterized by rapid and slow exponential relaxations [37]. Given the geometrical parameters of the phage and the bacterium, the rate of adsorption of phage binding can exceed the theoretical limit of adsorption determined by diffusion models [37]. Moreover, despite the small size of the bacterial receptors and the fact that they are sparingly found on the bacterium wall, phage capture of the bacterium occurs on each collision.

## 5.5 Conclusions

Using SPR, we have demonstrated the use of T4 bacteriophage to detect E. coli, as well as the use of BP14 to detect MRSA. Our work reveals the specificity of bacteriophage BP14 for MRSA bacteria, as none of the other strains of bacteria examined show any interaction with BP14, which targets MRSA and interferes with its replication. It was possible to detect concentrations of $10^3$ CFU/mL, without prior labeling or enrichment steps, in less than 20 minutes. This method of detection is of interest not only for public health, but for other phages, which can be used to identify and target other types of bacteria, such as anthrax for bioterrorism prevention, and E. coli O157:H7 for the food and water industries.

## 5.6 Acknowledgements

We thank NanoQuébec for their financial support, R. Allain (INRS-Institut Armand Frappier, Montréal) for TEM assistance, V. Latendresse for art work on Figure 5-2b, and M. Maisonneuve and S. Patskovsky for SPR assistance.

# CHAPTER 6 ARTICLE 5 : THE DIFFERENTIAL DETECTION OF METHICILLIN-RESISTANT, METHICILLIN-SUSCEPTIBLE AND BORDERLINE OXACILLIN-RESISTANT STAPHYLOCOCCUS AUREUS BY SURFACE PLASMON RESONANCE

The diagnosis and monitoring of various infections necessitate intensive efforts for the routine examination of blood samples and other associated tests. Novel diagnostic systems have traditionally been developed in response to the needs of the medical community. With the advent of nosocomial infection outbreaks, a major challenge for the biomedical engineering community is to develop diagnostic tests that can distinguish between the rapidly evolving plethoras of resistant bacterial strains. *S. aureus* infections exemplify this problem with an ever-increasing heterogeneous spectrum of resistance. In addition, while substantial efforts have been directed towards distinguishing the resistance patterns of highly pathogenic strains from those of antibiotically susceptible ones, conventional microbiological and DNA-based genotyping techniques have largely failed to address the problem, and to provide adequate treatment to patients.

In this fifth article, we characterize 250 different *S. aureus* clinical isolates provided by the LSPQ, and determine their pattern of resistance. We then adapt our SPR biosensor to effectively differentiate among MSSA, CA-MRSA, HA-MRSA and BORSA strains. Our proposed assay permits the rapid and accurate detection of these strains an less than 20 minutes, for concentrations as low as 10 CFU/mL.

# The Differential Detection of Methicillin-Resistant, Methicillin-Susceptible and Borderline Oxacillin-Resistant *Staphylococcus aureus* by Surface Plasmon Resonance.

*Nancy Tawil[1,2,4], Flaviana Mouawad[2], Simon Lévesque[3], Edward Sacher[1], Rosemonde Mandeville[2], Michel Meunier[1,4]*

[1]Laboratory for the Analysis of the Surfaces of Materials, Department of Engineering Physics, École Polytechnique de Montreal, Case Postale 6079, succursale Centre-Ville, Montreal, Québec, H3C 3A7, Canada

[2]Biophage Pharma Inc, 6100 Royalmount, Montreal, Quebec, H4P 2R2, Canada

[3]Laboratoire de santé publique du Québec (LSPQ) / Institut national de santé publique du Québec (INSPQ), 20045 chemin Ste-Marie, Sainte-Anne-de-Bellevue, Québec, H9X 3R5, Canada

[4]Laser Processing and Plasmonics Laboratory, Department of Engineering Physics, École Polytechnique de Montreal, Case Postale 6079, succursale Centre-Ville, Montreal, Quebec, H3C 3A7, Canada

Received : March 19, 2013 Published : May 20, 2013

dx.doi.org/10.1016/j.bios.2013.05.031 Biosensors Bioelectronics 2013, 49, 334-340

KEYWORDS: penicillin-binding protein (PBP), biosensor, methicillin-resistant *Staphylococcus aureus* (MRSA), methicillin-sensitive *Staphylococcus aureus* (MSSA), borderline oxacillin-resistant *Staphylococcus aureus* (BORSA), surface plasmon resonance (SPR)

## 6.1 Abstract

Two hundred fifty *Staphylococcus aureus* clinical isolates were studied to determine their susceptibilities to β-lactam antibiotics. Among these isolates, 16 were methicillin-sensitive *S. aureus* (MSSA), 207 were methicillin-resistant *S. aureus* (MRSA) and 27 were borderline oxacillin-resistant *S. aureus* (BORSA). Currently, the reported mechanism of methicillin resistance in *S. aureus* is the production of a distinctive penicillin binding protein 2a (PBP2a), which exhibits low affinity toward β-lactams. A surface plasmon resonance biosensor was evaluated for its ability to identify MRSA and to distinguish these strains from MSSA and BORSA, by specifically detecting PBP2a. We found that the system permits label-free, real-time, specific detection of pathogens for concentrations as low as 10 colony forming units/milliliter (CFU/mL), in less than 20 min. This system promises to become a diagnostic tool for bacteria that cause major public concern in clinical settings.

# 6.2 Introduction

Nosocomial infections are the primary cause of mortality for hospitalized patients[187]. Methicillin-resistant *Staphylococcus aureus* (MRSA) is the leading cause of nosocomial and community-acquired infections worldwide with MRSA accounting for up to 40% of all *S. aureus* isolates[202, 203]. It has been estimated that nearly 50% of adults are carriers of *S. aureus*[15]. Thus, *S. aureus* ranks amongst the primary causes of skin[204-206] and bloodstream bacterial infections[16, 207], as well as nosocomial pneumonia[208-210]. The development of resistance to methicillin and vancomycin has been a cause of concern among the medical community. MRSA infections have been associated with accelerated deterioration of pulmonary function, leading to increased hospitalization, and increased antibiotic usage and mortality[211]. The problem resides in the fact that therapeutic options to cure MRSA infections are scarce and that MRSA has the ability to acquire resistance to novel antibiotics.

Methicillin is a β-lactam, a member of a broad class of antibiotics characterized by the presence of a β-lactam ring in their chemical structures, which disrupts bacterial cell wall synthesis. They are the most prescribed antibiotics due to their specificity and non-toxicity to host cells. MRSA has acquired resistance to such antibiotics due to the production of altered penicillin binding proteins (PBPs)[212] that have low affinity for β-lactams, and are encoded by the chromosomal *mecA* gene[211].

Substantial efforts have been directed at properly distinguishing this resistance pattern from those of susceptible strains. Current guidelines call for antibiotic susceptibility testing of *S. aureus* by agar dilution, disk diffusion tests, latex agglutination tests, and molecular methods, such as PCR and radio-labeled DNA probes[203, 213]. MRSA is defined as having an oxacillin minimum inhibitory concentration (MIC) ≥4μg/ml[214]. However, heterogeneous expression of oxacillin resistance in multiple strains of *S. aureus*[203, 215] has complicated the identification of MRSA via conventional microbiological procedures. Strains with extremely low-level methicillin resistance are susceptible to most of the non-β-lactam antibiotics[212], and routine tests may lead to false positive results. For instance, borderline oxacillin-resistant *S. aureus* (BORSA) strains exhibit oxacillin MICs at, or just above, the susceptibility breakpoint (≥2μg/ml)[215], but lack the *mecA* gene. Optimal conditions for the identification of BORSA and their differentiation from MRSA have not been determined[216]. Moreover, a novel gene coding for methicillin resistance (*mecC*) has recently been identified in *S. aureus* clinical isolates from humans and animals. These strains, which have a variable resistance profile to oxacillin, cannot be detected by standard molecular techniques, such as PCR and slide agglutination tests, and are thus falsely identified as BORSA[217].

Rapid assays for detecting methicillin resistance in Staphylococci, such as BD geneOhm MRSA[218], Xpert MRSA[218], BBL Crystal MRSA ID[219], Velogene Rapid MRSA Identification[220] and MRSA-Screen[221], are commercially available. However, these methods lack accuracy for MRSA identification and differentiation from BORSA. For these methods, heavy inoculums are still needed, false negative results can still occur[203], and they are inappropriate for *mecC* gene detection. Other DNA-based genotyping techniques, such as

polymerase chain reaction (PCR), pulsed-field gel electrophoresis (PFGE) and multi-locus sequence typing (MLST), are time-consuming (6h to 3 days) and require highly trained personnel. A bioluminescent assay was recently developed, using biotinylated firefly luciferase to detect PBP2a[222]. However, the assay suffered from requiring an extraction step, as well as having a low sensitivity (0.5 x $10^6$ CFU/mL). Chen et al. recently developed an integrated microfluidic system that could effectively differentiate community–acquired MRSA (CA-MRSA) from hospital-acquired MRSA (HA-MRSA) in less than 40 min[223]. However, this system requires PCR amplification and a labeling step. Similarly, another study demonstrated the possibility of detecting the *mecA* gene by EIS, after PCR has been carried out on genomic DNA from bacterial isolates[224].

Thus, it is our aim to respond to the pressing need for the development of a rapid and sensitive biosensing method to specifically detect and differentiate MRSA from both BORSA and methicillin susceptible *Staphylococcus aureus* (MSSA), allowing for a better management of the bacterial infection. Furthermore, we aim to reduce the time of diagnosis, which is crucial for effective treatment and the prevention of disease spread[223], and will result in reduced morbidity and mortality rates[189]. Here, we studied two hundred fifty *Staphylococcus aureus* clinical isolates to determine their susceptibilities to β-lactam antibiotics. A surface plasmon resonance (SPR) biosensor was used to differentiate among CA-MRSA, HA-MRSA, BORSA and MSSA strains by specifically detecting PBP2a on whole bacterial cells, without labeling, without recourse to PCR or enrichment steps.

## 6.3 Materials and methods

### 6.3.1 Bacterial Cultures

Bacteria were either isolated by Biophage Pharma (Saa1 to Saa 29) or provided by the Laboratoire National de Santé Publique du Québec (LSPQ) (Saa 30 to Saa 250). At LSPQ, the presence of *nuc* gene to confirm *S. aureus* was detected using PCR with the following primers: SN1 5'-CGAAAGGGCAATACGCAAAG-3' and SN2 5'-ATCAGCGTTGTCTTCGCTCC-3'. The presence of *mecA* genes was detected using PCR as previously described. Susceptibility confirmation to oxacillin was done at LSPQ according to the CLSI standards[214]. The presence of PVL genes, lukS-PV and lukF-PV, were assessed by PCR amplification as previously described[225]. Molecular typing was done by *spa* typing[226] and epidemic type determination was determined according to the guideline for Canadian epidemic type[227]. MRSA, BORSA and MSSA bacteria were grown in 4 mL of Luria-Bertani (LB) medium in an incubator-shaker, for 3h at 37°C. The bacteria were then centrifuged at 2500 g (Sorvall RT7, 3500 rpm) for 20 min. The supernatant was discarded and the bacteria were resuspended in phosphate-buffered saline (PBS). This was repeated twice. The concentration of bacteria was determined by plate count technique, and expressed as colony forming units per milliliter (CFU/mL).

### 6.3.2 Chemicals

L-cysteine, 1-(3-dimethylaminopropyl)ethylcarbodiimide hydrochloride (EDC), N-hydroxysuccinimide (NHS), 11-mercaptoundecanoic acid (MUA), bovine serum albumin (BSA), sodium chloride, magnesium sulfate, and gelatin were purchased from Sigma-Aldrich. LB medium was purchased from Quelabs (Montréal, Québec, Canada); 25 g of LB powder were dissolved in 1 L of distilled water and autoclaved. LB-agar plates were prepared by adding 6 g of granulated agar to 400 mL of LB media. The LB-agar was autoclaved, melted and placed in Petri dishes. Phosphate buffered saline (PBS) was purchased from Fisher Scientific (Nepéan, Ontario, Canada).

### 6.3.3 Extraction of genomic DNA from *S. aureus* isolates

After centrifugation of 5 ml of cultured bacteria (4000 rpm, 15 min), pellets were resuspended in 564 µl of TE buffer (10 mM Tric-HCl pH8 / 1 mM EDTA pH8) , frozen at -80°C and thawed at 45°C. After addition of 6µl of Proteinase K in 30 µl of 10% of sodium dodecyl sulfate (SDS) (2 hours, 45 °C), 80 µl of CTAB/NaCl (10% hexadecyltrimethyl ammonium bromide/0.7M NaCl) (30 min, 65°C), and 750 µl chloroform/iso-amyl alcohol (ratio of 24:1), the mixed solution was centrifuged at 15000G for 15 min. The supernatant was then subjected to the addition of 600 µl phenol/chloroform/iso-amyl alcohol (25:24:1) and centrifugation (15000 G, 15 min). DNA was precipitated, using 600 µl of isopropyl alcohol. After centrifugation, the pellet was allowed to dry and, then, resuspended in 20 µl of TE buffer.

### 6.3.4 Polymerase chain reaction (PCR)

Total *Staphylococcus aureus* and MRSA DNAs were prepared, as previously described[228]. The primer mixes used for the multiplex PCR for SCCmec I, II, II, and IV are listed in Table 6.1. The monoplex PCR primers used for SCCmec IV detection are listed in Table 6.2. The PCR was carried out with Taq DNA Polymerase (New England Biolabs, Ipswich, MA), using 30 cycles, under the following conditions: 30 seconds at 95°C, 30 seconds at 57°C, 90 seconds at 70°C.

Table 6.1 Multiplex PCR mixes for SCC*mec I, II, III, V* and *mec*A typing

| | Primer | Length | Forward | Reverse |
|---|---|---|---|---|
| 1 | SCCmec I | 613 bp | GCTTTAAAGAGTGTCGTTACAGG | GTTCTCTCATAGTATGACGTCC |
| | SCCmec II | 287 bp | CGTTGAAGATGATGAAGCG | CGAAATCAATGGTTAATGGACC |
| | Sa442 | 108 bp | AATCTTTGTCGGTACACGATATTCTTCACG | CGTAATGAGATTTCAGTAGATAATACAACA |
| 2 | SCCmec V | 325 bp | GAACATTGTTACTTAAATGAGCG | TGAAAGTTGTACCCTTGACACC |
| | MecA | 162 bp | TCCAGATTACAACTTCACCAGG | CCACTTCATATCTTGTAACG |
| 3 | SCCmecIII | 243 bp | CATTTGTGAAACACAGTACG | GTTATTGAGACTCCTAAAGC |
| | Sa442 | 108 bp | AATCTTTGTCGGTACACGATATTCTTCACG | CGTAATGAGATTTCAGTAGATAATACAACA |

Table 6.2: Monoplex PCR primers for SCC*mec IV* typing

| SCCmec IV type | Length | Forward | Reverse |
|---|---|---|---|
| IVa | 776 bp | GCCTTATTCGAAGAAACCG | CTACTCTTCTGAAAAGCGTCG |
| IVb | 1000 bp | AGTACATTTTATCTTTGCGTA | AGTCATCTTCAATATGGAGAAAGTA |
| IVc | 677 bp | TCTATTCAATCGTTCTCGTATT | TCGTTGTCATTTAATTCTGAACT |
| IVd | 1242 bp | AATTCACCCGTACCTGAGAA | AGAATGTGGTTATAAGATAGCTA |

### 6.3.5 Extraction and isolation of Staphylococcus aureus PBP2a membrane protein

A total of $2.0x10^{10}$ CFU/mL of cultured bacteria (Saa4, 5, 30, and 226) were used. Membranous protein extraction was performed, using a ReadyPrep Protein Extraction kit (Membrane I) (BioRad), according to the manufacturer's protocol. After centrifugation (16000 G, 5 min at room temperature), hydrophobic and hydrophilic phases were separated, and the hydrophobic protein concentration was determined, using RC DC protein assays (Bio-Rad). Proteins in each sample were purified, using ReadyPrep 2-D Cleanup kits (BioRad), following the manufacturer's protocol. Equal amounts of proteins were separated by SDS-PAGE, under reducing conditions, and electrophoretically transferred to nitrocellulose membranes. The membranes were blocked with 5% BSA and incubated with primary antibody (monoclonal PBP2a antibodies, Fitzgerald) overnight at 4°C. After five washes with PBS Tween-20 (PBST), membranes were incubated overnight, at 4°C, with secondary antibodies (Cell Signaling, Beverly, MA), conjugated with horseradish peroxidase. Immunoreactive proteins were then detected by an Opti-4CN detection kit (BioRad). Dried membranes were scanned and densitometric analyses were carried, using the Image J software. The following antibody dilutions were used: anti-PBP2a, 1:10 000, anti-IgG HRP, 1:3000.

### 6.3.6 Au Surface Preparation

Biacore Platypus biosensor chips, to be described below, were used as the gold surface. Prior to modification, they were placed in freshly prepared "Piranha" solution, a 7:3 (v/v) mixture of concentrated $H_2SO_4$ and 30% $H_2O_2$ (caution: piranha solution reacts vigorously with organics, and can splatter), at room temperature, for 30 min, then rinsed thoroughly with MilliQ water (Millipore, Mississauga, Ont.), ultrasonicated in water for 15 min and dried in a nitrogen flow. The gold substrate was coated with a self-assembled monolayer (SAM) of L-cysteine overnight at 37°C, washed with PBS and subsequently coated with mercaptoundecanoic acid (MUA) to

create mixed self-assembled monolayers[19]; these were treated with 1-(3-dimethylaminopropyl)ethylcarbodiimide hydrochloride (EDC) and N-hydroxysuccinimide (NHS). Anti-PBP2a antibodies were then exposed to the surface for an hour, followed by BSA for 15 min, to prevent non-specific adhesion.

### 6.3.7 Surface Plasmon Resonance Apparatus

We used a homemade highly sensitive surface plasmon resonance (SPR) system. Briefly, a superluminescent light-emitting diode (SLED), emitting at 650 nm, was used as the light source. An achromatic lens produced a collimated beam, which passed through a polarizer. The linearly *p*-polarized light was focused by a lens, and then used to excite surface plasmons on the sensing surface, situated on top of a coupling prism. A commercial sensing surface (Platypus Technologies), consisting of a glass microscope slide (BK7), covered by an adhesion layer of 5 nm of titanium and a sensing layer of 50 nm of gold, was placed in oil immersion contact (Cargille Labs) on the top of the coupling prism. For the real-time tests, a flow injection double channel-measuring cell, with a 12 µl volume, was developed. The entire system was placed on a goniometer stage, with 2-D linear translation for exact beam angle and position, permitting surface plasmon excitation at the gold/adjacent medium interface. The spatial distribution of the reflected light intensity was recorded by a CCD camera (Hamamatsu C4742-95), and examined by appropriate software image treatment. A more detailed description of the system can be found in references [3, 229].

### 6.3.8 DNA sequence analysis and bioinformatics

Open reading frame identification was performed, using GeneMark.hmm[195]. Similarity searches, for nucleotide sequences and for the deduced amino acid sequences, were performed using the FASTA[196], BLAST[197], and PARALIGN[198] programs available on the Online Analysis Tools website (http://molbio-tools.ca/).

## 6.4 Results and discussion

### 6.4.1 Characterization of Staphylococcus aureus resistance cassettes

Current methods employed to type bacteria are based on genotypic characteristics of the strains. The staphylococcal cassette chromosome, *mec* (SCC*mec*), is a mobile genetic element that contains the *mec*A gene, which encodes methicillin resistance in *S. aureus*. SCC*mec* typing is used to differentiate strains or lineages within the MRSA population. Eleven SCC*mec* types and several variants have been described, with types I to V being the most common[230].

From a bacteriological standpoint, CA-MRSA differs from HA-MRSA owing to various characteristics. CA-MRSA is typically susceptible to most non-β-lactam antibiotics and comprises a SCC*mec* element of type IV, type V or of the newly described type VII. On the other hand, HA-MRSA is usually multidrug-resistant and contains a SCC*mec* element of type I, II or III[230].

A study by the Society for Healthcare Epidemiology of America [231], surveying both community and hospitalized patients in Canada demonstrated the incidence and the changing epidemiology of *S. aureus* infections. This study demonstrates the emergence of CA-MRSA strains in Canada and, in particular, the presence of CMRSA-10 (USA300) and CMRSA-7 (USA400) in the Province of Quebec[231]

Table 6.3: Microbiological Characteristics of *S. aureus* Isolates

| Identification (nb of isolates) | Oxacillin MIC µg/ml (nb of isolates) | *mecA* PCR | SCC*mec* type | Epidemiologic type | PVL (nb of isolates) |
|---|---|---|---|---|---|
| MRSA (207) | ≥ 32 (207) | Positive | HA-MRSA (55/194) | CMRSA-1/USA600 (2/184)<br>CMRSA-2/USA100/USA800 (43/184) | Positive (134/196)<br>Negative (62/196) |
| | | | CA-MRSA (139/194) | MRSA-7/USA400 (10/184)<br>CMRSA-10 /USA 300 (121/184)<br>USA700 (4/184)<br>USA1100 (4/184) | |
| MSSA (16) | ≤0.25 (6)<br>≤0.5 (7)<br>≤1 (3) | Negative | - | - | Negative |
| BORSA (27) | 1-4 (16)<br>4-8 (11) | Negative | - | - | Negative |

MRSA infections are endemic in hospitals worldwide. In recent years, infections have emerged in the community and livestock, and thus, MRSA is no longer exclusively considered as a healthcare associated problem. Validation of the current SPR platform was carried out on 250 well-characterized *S. aureus* strains (82.8% MRSA, 10.8% BORSA, and 6.4% MSSA). *S. aureus* isolates were characterized by multiplex PCR amplification of the Panton-Valentine leukocidin (PVL) and *mecA* genes, staphylococcal cassette chromosome *mec* (SCC*mec*) typing and oxacillin susceptibility. The results are summarized in Table 6.3. Amongst these isolates, 28.9% were HA-

MRSA, and 71.1% were CA-MRSA. Further analysis of the LSPQ isolates determined that the strains belonged to 6 epidemiologic types, with CMRSA-10 (USA300) accounting for 65.7% of isolates, CMRSA-2 (USA100/800) for 23.4%, CMRSA-7 (USA400) for 5.4%, USA700 for 2.2%, USA1100 for 2.2% and CMRSA-1 (USA600) for 1.1%.

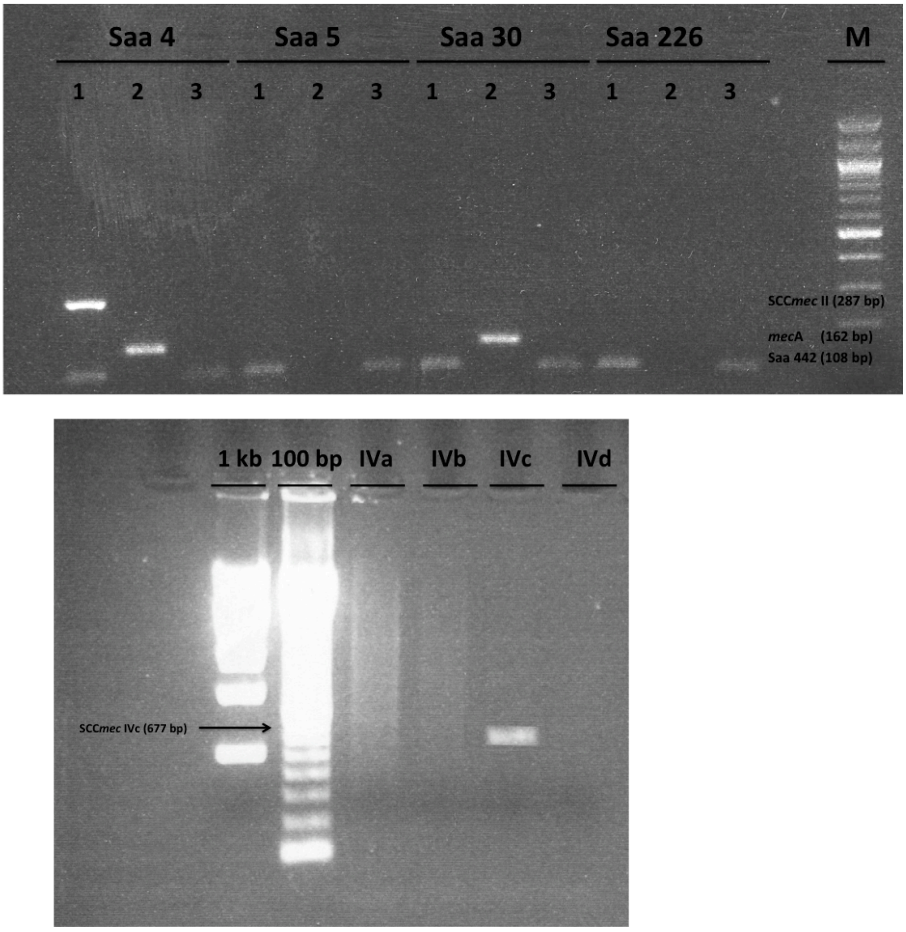


Figure 6-1: a) Multiplexed PCR SCC*mec* and *mec*A typing. Representative Biophage Pharma isolates (Saa 4 and 5) and representative LSPQ isolates (Saa 30 and 226). Lanes marked with the number 1 contain primers for SCC*mec* I, II and Sa442, a positive control to confirm *S. aureus* strain. Lanes marked with the number 2 contain primers for SCC*mec* V, and *mec*A. Lanes marked with the number 3 contain primers for SCC*mec* III, and Sa442. Lane marked with the letter M contains the molecular marker. b) monoplex PCR for SCCmec IV typing for the Saa 30 strain. Lanes marked with 1kb and 100 bp are molecular markers, while lanes marked with IVa, IVb, IVc and IVd contain primers for SCCmec IVa, IVb, IVc and IVd, respectively.

As previously noted, *mec*A resides in the large mobile genetic element, SCC*mec.* Methicillin resistance is known to be inducible, and the *mecA* gene, which codes for PBP2a, is under the control of the *mec*I and *mec*R1 regulatory genes. These genes encode, respectively, for a repressor and for a β-lactam sensing signal transducer. In an antibiotic-free environment, *mec*I represses the transcription of *mec*A and *mec*R1. However, when β-lactams are introduced, *mec*R1 is cleaved, thus freeing the metalloprotease domain and inducing *mec*A transcription[232]. The presence of *mec*A and the production of PBP2a provide methicillin resistance in *S. aureus*. Thus, testing with both SCC*mec* and *mec*A gene markers provides conclusive proof of resistance in MRSA.

We arbitrarily selected Saa 4 as a representative strain for HA-MRSA, Saa 5 for MSSA, Saa 30 for CA-MRSA and Saa 226 for BORSA to carry on biosensing studies. Amplification of the *mecA* gene and SCCmec types for selective *S. aureus* isolates included in Table 6.2 are shown in Figure 6-1. MSSA and BORSA strains (Saa 5 and 226) were negative for the 162-bp internal fragment of the *mecA* gene, while Saa 4 and Saa 30 were positive, confirming that these strains are MRSA . The Saa 4 strain showed resistance to oxacillin, cefazolin, ceftriaxone, ciprofloxacin, and ampicillin (MIC > 32 μg/ml for all antibiotics tested), but was susceptible to vancomycin (MIC = 2 μg/ml). PCR SCC*mec* typing showed that it was type II, making it a HA-MRSA strain. Saa 5 was chosen as representative of MSSA strains, with susceptibility to all antibiotics tested (MIC≤ 1 μg/ml); it was also negative for all SCC*mec*s and *mec*A genes tested. Saa30 was chosen as representative of CA-MRSA, as it was resistant to β-lactams, positive for *mec*A, positive for PVL, and was a SCC*mec* IV. For BORSA, Saa 226 was chosen, as it was negative for *mec*A and SCC*mec*s but showed borderline susceptibility to oxacillin (MIC = 8 μg/ml).

Although PCR, spa typing, and SCCmec subtyping are suitable for epidemiological studies, risk assessment and surveillance, there is still a paramount need for a highly discriminatory, inexpensive, and rapid technology for point-of-care diagnosis.

### 6.4.2 Expression of protein PBP2a

Currently, the reported mechanism of methicillin resistance in *S. aureus* is the production of a distinctive cell wall protein, PBP2a, which exhibits low affinity toward β-lactams[17]. In contrast, susceptible strains of *S. aureus* have normal PBPs that function as transpeptidases, endopepitdases or carboxypeptidases in the crosslinking of macromolecules in the cell wall during cell division. MRSA PBP2a has a slightly different molecular size than PBP, and is controlled by a repressor gene also confined within the *mec* gene. Various other PBPs can be found in both resistant and susceptible strains of *S .aureus*, but only PBP2a remains active in the presence of high concentrations of β-lactams. On the other hand, BORSA strains do not exhibit PBP2a in their cell wall membranes but appear to produce large amounts of staphylococcal penicillinase that slowly degrades methicillin and oxacillin[233].

Due to the fact that multiple genes are involved in cell-wall precursor formation, regulation, transport and signal transduction, different MRSA strains appear to be heterogeneous in their level of resistance[232]. Thus, different strains of MRSA may not only manifest a wide range of resistance to β-lactams, but also different concentrations of PBP2a in the cell wall membranes. The inset of Figure 6-2 shows SDS-PAGE of total cell lysate protein (10 μg) derived from Saa 4, 5, 30 and 226.

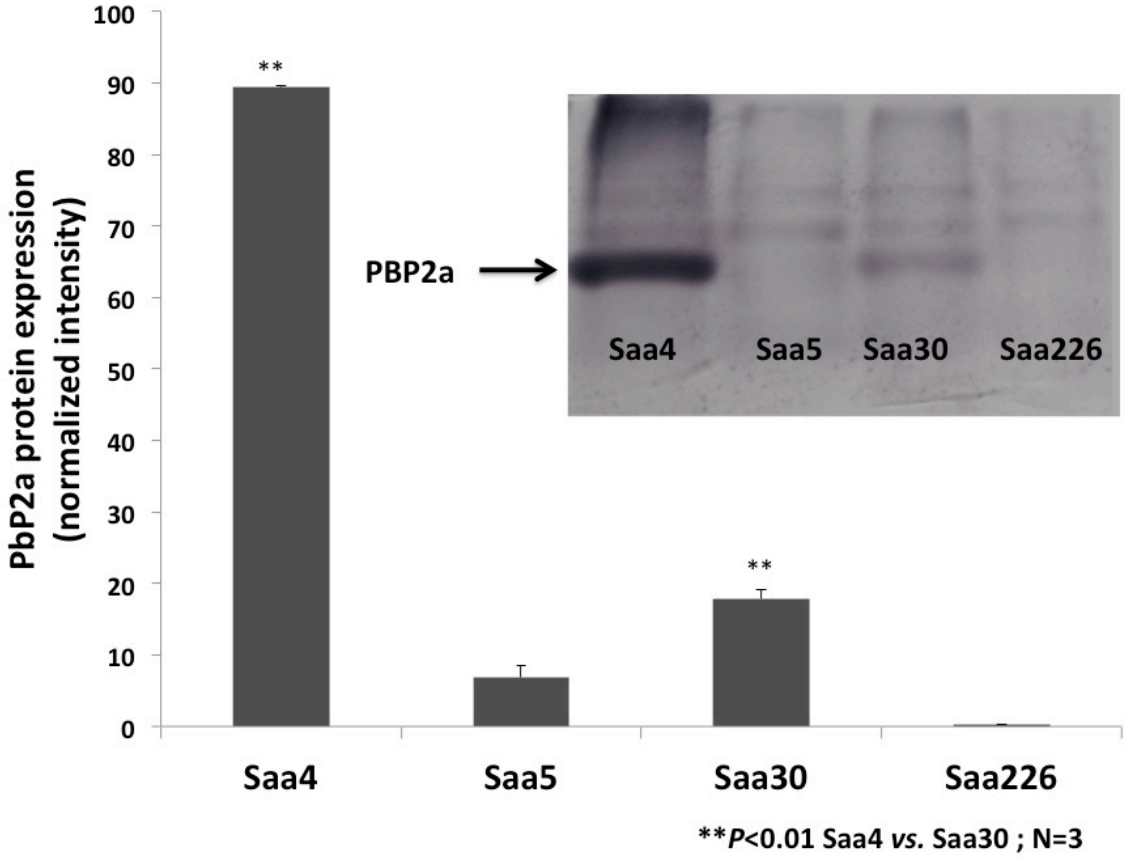


Figure 6-2: PBP2a protein expression in *S. aureus*. Expression of PBP2a from membranes of Saa 4 (HA-MRSA), Saa 5 (MSSA), Saa 30 (CA-MRSA) and Saa 226 (BORSA). Significant heterogeneous expression of PBP2a was found for Saa 4 MRSA strains compared to Saa 30 ($P<0.01$, $N=3$). The inset shows SDS-PAGE of total membranous protein expression of *S. aureus* lysates. The arrow indicates PBP2a expression (82kDa).

In this experiment, membranous proteins were extracted from $2.0x10^{10}$ CFU/mL of freshly cultured bacteria (Saa4, 5, 30, and 226) in order to determine the PBP2a concentration in different S. aureus strains. The normalized PBP2a concentrations were found to be 89.4 ±0.2 % for HA-MRSA Saa 4 strain, 6.9±1.7 % for MSSA Saa5, 17.9±1.3 % for CA-MRSA strain Saa 30, and 0.3±0.1 % for BORSA strain Saa 226, respectively. As expected, no significant PBP2a expression was found in the MSSA and BORSA strains, whereas MRSA strains (Saa4 and Saa

30) expressed heterogeneous amounts of PBP2a ($P<0.01$, $N=3$). In fact there is approximately 5 times more PBP2a in Saa 4 than in Saa 30.

Resistance levels in MRSA depend on PBP2a production, which is regulated by chromosomal factors and is dependent on controlled cell wall synthesis and chemical structure of the peptidoglycan precursor. The regulation of genes that govern resistant levels may, in turn, be contingent on control by global regulators whose fine-tuning may vary from strain to strain. Thus, resistance levels in different MRSA strains range from phenotypically susceptible to highly resistant. In the following section, we propose an SPR assay, which can prove efficient at determining the level of membranous PBP2a in different MRSA strains.

### 6.4.3 Differential detection of MRSA, MSSA and BORSA

One of the major objectives of our work is to develop a rapid and sensitive technique, using a SPR biosensor, to specifically detect and differentiate between MRSA, BORSA and MSSA strains. To meet this objective, we used a home-built biosensor, with anti-PBP2a antibodies as specific recognition elements, to detect low concentrations of methicillin-resistant bacteria. A PBS solution was injected onto the gold chip for 10 minutes, followed by a 20 minute injection of a PBS solution containing different concentrations of *S. aureus* Saa4 and Saa5 strains. PBS was then injected to wash away the unbound bacteria (Figure 6-3a). Results are shown in pixel units, with one pixel corresponding to 0.005 angle units. All experiments were carried out at room temperature and were performed in triplicates. The SPR responses for Saa 4 were 26.1± 1.2 pixels for $10^2$ CFU/mL and 6.4± 0.9 pixels for 10 CFU/mL (inset of Figure 6-3). Noticeably a small, but measurable, response was noted for $10^4$ CFU/mL Saa 5 (1.1± 1.1 pixels). These results confirm the specificity of the antibody to PBP2a and the presence of the PBP2a protein on the membranes of MRSA strains (Saa4) and not on the antibiotic susceptible strain (Saa 5).

a)

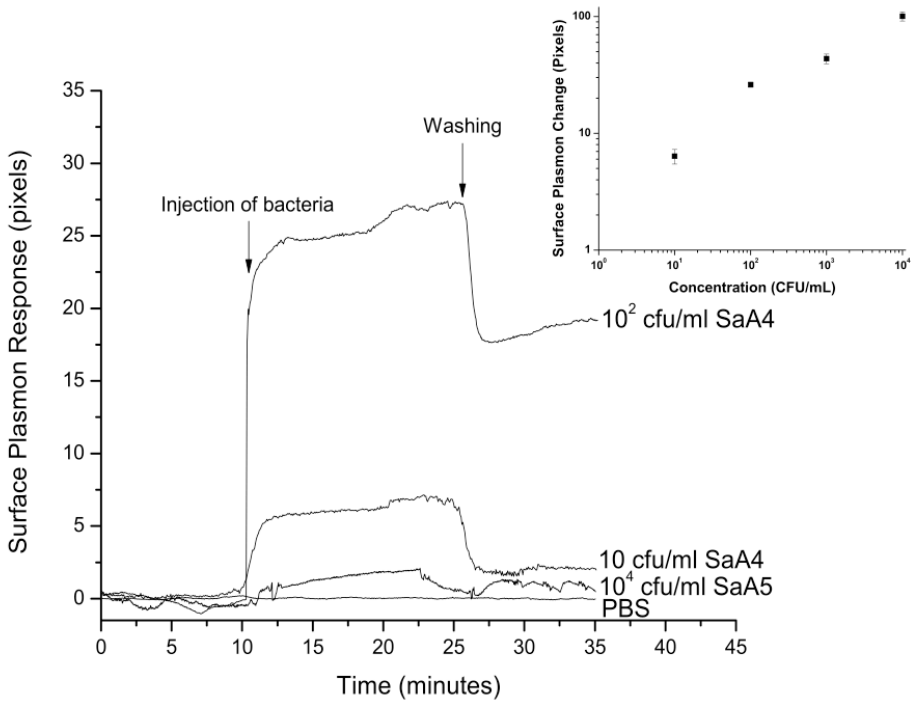
Surface Plasmon Response (pixels)
Time (minutes)
Injection of bacteria
Washing
10^2 cfu/ml SaA4
10 cfu/ml SaA4
10^4 cfu/ml SaA5
PBS
Surface Plasmon Change (Pixels)
Concentration (CFU/mL)

b)

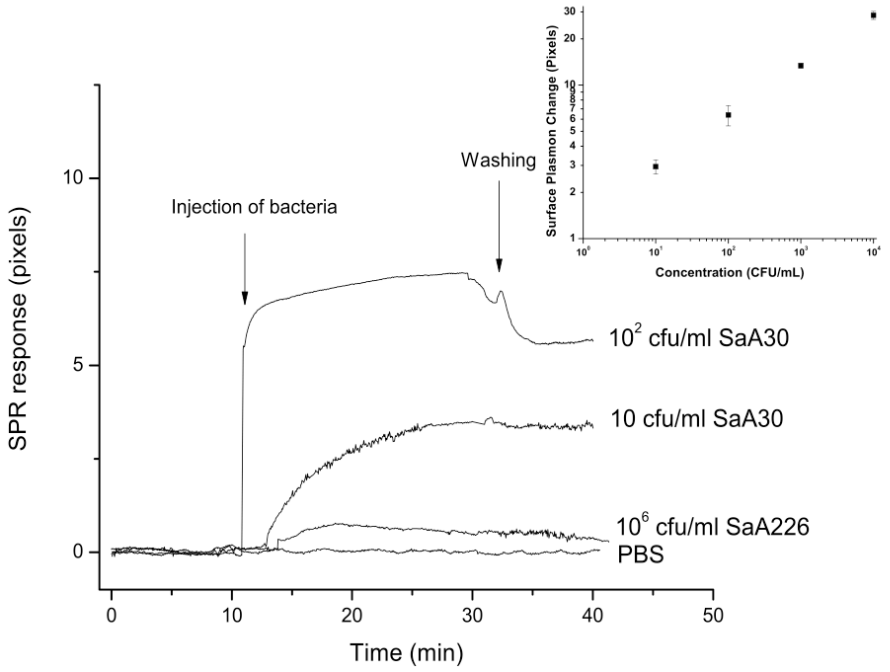
SPR response (pixels)
Time (min)
Injection of bacteria
Washing
10^2 cfu/ml SaA30
10 cfu/ml SaA30
10^6 cfu/ml SaA226
PBS
Surface Plasmon Change (Pixels)
Concentration (CFU/mL)

Figure 6-3: Detection of MRSA, using anti-PBP2a antibodies, immobilized on the gold sensor chip. A baseline was created by injecting PBS buffer for 10 minutes. PBS was used as negative control. a) Known concentrations of HA-MRSA (Saa 4) diluted in PBS were flowed onto the sensor surface. MSSA (Saa 5), at a concentration of $10^4$ CFU/mL, was also tested, and manifested the high specificity of the anti-PBP2a antibody for MRSA detection. For detection of Saa4 MRSA strain, a dose-response curve is shown, in inset, for values taken after 20 minutes. b) Known concentrations of CA-MRSA (Saa 30), diluted in PBS, were flowed onto the sensor surface. Surface plasmon responses for MRSA strains (Saa 30) showed the high specificity of the antibody for PBP2a. On the contrary, BORSA strains (Saa 226), at a concentration of $10^4$ CFU/mL, did not show any significant SPR response. For detection of Saa30 MRSA strain, a dose-response curve is shown, in inset.

The same experiment was repeated to establish the possibility of detecting CA-MRSA (Saa 30) bacteria using PBP2a antibody. All slides were previously coated with anti-PBP2a antibody and BSA, to prevent non-specific adhesion. The controls consisted of a solution of $10^6$ CFU/mL of BORSA (Saa 226), injected on an anti-PBP2a-coated slide (Figure 6-3b). SPR responses for predetermined concentrations of Saa 30 were 6.4± 1.0 pixels for $10^2$ CFU/mL and 2.9±0.3 for 10 CFU/mL. A concentration of $10^6$ CFU/mL of Saa 226 produced a noticeably small, but measurable, response (0.4±0.3 pixels). As anticipated, because MSSA and BORSA do not exhibit PBP2a on their cell wall membranes, we did not observe a significant change in SPR response. Any surface plasmon response difference between the PBS baseline and the non-specific adsorption of MSSA was determined to be due to noise. Using the criterion of S/N ›3, the limit of detection is found to be 10 CFU/mL (inset of Figure 6-3b). Moreover, the SPR responses for Saa 30 were 5 times lower than those of Saa 4, which is consistent with the SDS-PAGE results, where PBP2a expression was found to be approximately 5 times greater in Saa 4 than in Saa 30 strains. This shows that the SPR assay can effectively assess the amount of PBP2a in MRSA cell walls.

Our results demonstrate that, when the SPR biosensor assay was used to test *S. aureus* samples, it could effectively differentiate among MRSA, MSSA, and BORSA strains. The methicillin resistance measured was in total agreement with standard microbiological approaches. The chemical and optical components of the biosensing surface have excellent sensitivity, as evidenced by a detection limit of 10 CFU/mL, when MRSA strain response was compared to that of BORSA strains. This analytical limit of sensitivity is adequate to detect the numbers of organisms in positive isolates. Furthermore, the surface configuration is designed to be chemically inert, thereby limiting nonspecific interactions. The SPR assay was able to differentiate among *S. aureus* strains without the need for a culture step, target amplification, or PCR products. Thus, this approach has the advantages of being simple and rapid, allowing for identification of resistant strains of *Staphylococcus aureus* up to 48 hours earlier than conventional microbiological techniques. This method could have a significant impact on hospital costs, effective infection control, and patient mortality.

## 6.5 Conclusions

Our proposed SPR assay allows rapid and accurate detection of MRSA, eliminating the necessity for specialized reference laboratories. This assay is easy to perform, can accurately differentiate MRSA from BORSA and MSSA isolates, and provides a rapid (less than 20 min) alternative for the detection of methicillin resistance in *S. aureus* in clinical laboratories, especially when *mecA* PCR gene detection is unavailable. This will permit clinicians to more effectively manage patients and to control the spread of MRSA. This new test shows great promise in providing rapid, sensitive and specific alternatives, when neither PCR nor DNA hybridization for the *mec*A gene is available.

## 6.6 Acknowledgements

We thank NanoQuébec and NSERC for their financial supports, P. Lamarche for help with molecular biology protocols, K. Benhamioud for technical assistance, and S. Patskovsky for SPR assistance.

# CHAPTER 7 ARTICLE 6 : X-RAY PHOTOELECTRON SPECTROSCOPIC AND TRANSMISSION ELECTRON MICROSCOPIC CHARACTERIZATIONS OF BACTERIOPHAGE-NANOPARTICLE COMPLEXES FOR PATHOGEN DETECTION

The need for a more flexible, reliable and sensitive targeting of pathogens has directed our research towards the synthesis of bacteriophage-nanoparticles systems. The unique properties of NPs may increase the sensitivity of pathogen detection, while opening up new possibilities for point-of-care, multiplexed devices. Moreover, these nano-bio hybrids hold great promise for further applications, such as in other sensing systems, imaging and therapy.

In this article, we take advantage of the previous knowledge we acquired, about functionalization chemistries and conventional SPR detection, to design a sensing platform where gold NPs were functionalized and bioconjugated to bacteriophages, and studied with XPS and TEM.

# X-Ray Photoelectron Spectroscopic and Transmission Electron Microscopic Characterizations of Bacteriophage-Nanoparticle Complexes for Pathogen Detection

*Nancy Tawil*[1,2,3], *Edward Sacher*[1], *Etienne Boulais*[3], *Rosemonde Mandeville*[2], *Michel Meunier*[1,3]

[1] Regroupement Québécois de Matériaux de Pointe, Department of Engineering Physics, École Polytechnique de Montréal, Case Postale 6079, succursale Centre-Ville, Montréal, Québec, H3C 3A7, Canada

[2] Biophage Pharma, 6100 Royalmount, Montréal, Québec, H4P 2R2, Canada

[3] Laser Processing and Plasmonics Laboratory, Department of Engineering Physics, École Polytechnique de Montréal, Case Postale 6079, succursale Centre-Ville, Montréal, Québec, H3C 3A7, Canada

Received : June 21, 2013 Published : September 15, 2013

dx.doi.org/10.1021/jp406148h J. Phys. Chem. C 2013, 117, 20656-20665

**Keywords**

*Bacteriophage, Gold Nanoparticles, Polyethylene glycol, Transmission Electron Microscopy, X-ray Photoelectron Spectroscopy*

## 7.1 Abstract

We report the synthesis and characterization of gold-bacteriophage hybrids for biodetection purposes. The physical and optical properties of gold nanoparticles (AuNPs) and the biological features of the phages offer a multifunctional scaffold with great potential for nanotechnologically based biomedical applications. AuNPs stabilized (PEGylated) using heterobifunctional polyethylene glycol (PEG), were coupled to methicillin-resistant *S. aureus*-specific phages. The PEG ligands contain a thiol group for stable anchoring to the gold surface, and a terminal carboxylic acid group for further coupling to the outside of the PEG shell by carbodiimide chemistry. Transmission electron microscopic analysis showed that the NP-phage bioconjugates are highly stable, with a median diameter of 90 nm. X-ray photoelectron spectroscopy was used to chemically characterize the surfaces of the PEG-functionalized AuNPs, the bacteriophages, and the gold-phage hybrids. The role of the interface and the covalent coupling chemistry employed to attach the phages to the AuNPs have been delineated. Successful attachment of phages to AuNPs was confirmed by the presence of amide between the primary amines of the phage and the carboxylic acid terminal groups of the NPs and by the presence of carboxyl and amine species, which form hydrogen bonds.

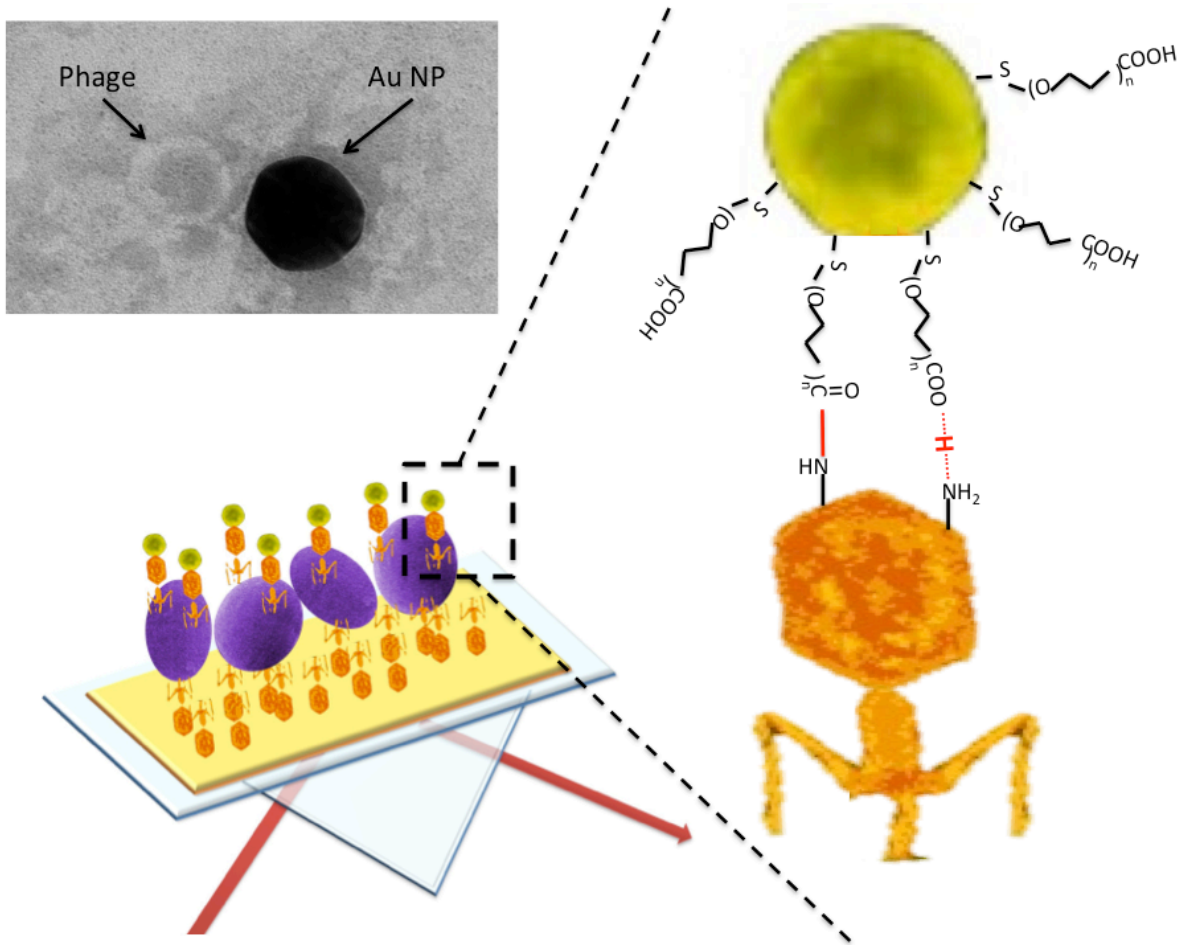


Figure 7-1: Graphical Abstract : Nanoparticle-Bacteriophage interaction for LSPR applications

## 7.2 Introduction

Conventional microbiological techniques for the detection of harmful bacteria, such as methicillin-resistant *Staphylococcus aureus* (MRSA), often require up to two days[234] to obtain results. Many groups have devoted significant efforts toward the development of rapid, sensitive, and specific methods for the detection of such pathogens[9, 126, 185, 191, 235-240]. The past few decades have seen the advent of biosensors, based on surface plasmon resonance (SPR), for the study of the chemical and biological reactions that occur at the interface of a metal and its biochemical environment[3, 107, 241, 242]. A surface plasmon (SP) is a charge density oscillation, propagating along the boundary between a dielectric and a metal[94, 100, 243]. However, the requirement for detection by attenuated total reflectance requires a rather complex

optical setup. Here we use localized surface plasmon resonance (LSPR), where the plasmon is produced by metal nanoparticles (NPs). In accordance with the Mie theory, the movement of electrons through the internal metal framework of the NPs is confined in three dimensions[244]. When the frequency of the incident light matches that of the resonance of the collectively oscillating electrons, the energy of the incident photons is absorbed, corresponding to a peak in the absorbance spectrum. The use of localized SPs permits increased resolution and sensitivity of the optical probes and therefore the amplification of the detection signal[245].

In the case of LSPR for bacterial detection, recent findings show that the contact area between a bacterial cell and a single NP may be too small to result in a detectable plasmon peak shift[245]. This prompted us to explore the possibility of attaching numerous NPs to a single bacterial cell by exploiting the specificity of bacteriophage-bacteria interactions. Bacteriophages are among the most promising candidates for biosensing scaffolds due to their specificity, robustness and unique display system. Au–phage fractal networks have previously been shown to effectively integrate the unique signal-reporting properties of AuNPs while preserving the biological properties of phages[6]. Moreover, the use of these NP-phage hybrids can be extended to the targeted separation of specific bacteria from heterogeneous samples as well as a wide range of biotechnological applications, such as labels for enhanced fluorescence and dark-field microscopy and surface-enhanced Raman scattering detection[6].

In a previous paper, using bacteriophages immobilized on planar gold surfaces, we studied the bacteriophage-MRSA specificity[3]. The phages were covalently attached to the gold through amide bonds via a mixed self-assembled monolayer of L-cysteine and 11-mercaptoundecanoic acid[107]. We present here a novel method to immobilize phages on AuNPs that are functionalized with heterobifunctional PEG molecules, consisting of a thiol anchor group on one end and a carboxylic acid group on the other end, for further reaction.

The use of these PEG linkers has the dual functions of readily substituting weakly adsorbed surface molecules and stabilizing the NPs during synthesis. The linker is there to provide a high density of docking sites for bacteriophages through carbodiimide amidization reactions between the carboxy terminal of PEG and the amine groups at the phage surface.

Together with the NP shape and size and the specificity of the bacteriophage, the immobilization

chemistry of the nanohybrid defines the performance and stability of the system. Although self-assembled monolayer (SAM) characterization on gold platforms has been extensively studied[149, 152, 159, 163], a detailed quantitative characterization of PEG-functionalized AuNPs is lacking[246]. Furthermore, a detailed physicochemical analysis for the reliable interpretation of observed biointerfacial interactions of NPs and lytic phage conjugates has not been published. The characterization of such intentionally designed nanohybrids is a crucial step in the development of novel nanomaterials.

X-ray photoelectron spectroscopy (XPS) and transmission electron microscopy (TEM) are widely used techniques for the characterization of nanobiomaterials[247]. TEM was used to determine the morphology of PEG-AuNPs, and XPS was used to determine surface chemistries of the PEG-AuNPs, MRSA-specific bacteriophages, and phage-AuNPs nanohybrids.

## 7.3 Materials and Methods

### 7.3.1 Chemicals

1-(3-dimethylaminopropyl) ethylcarbodiimide hydrochloride (EDC), N-hydroxy-succinimide (NHS), glutaraldehyde, sodium chloride, magnesium sulfate, and gelatin were purchased from Sigma-Aldrich. Luria-Bertani (LB) medium was purchased from Quelabs (Montréal, Québec, Canada). Phosphate-buffered saline (PBS) was purchased from Fisher Scientific (Nepean, Ontario, Canada). Sixty nanometer diameter heterobifunctional PEG-AuNPs (cat # CGC3K-60-25) were provided by Cytodiagnostics (Burlington, Ontario, Canada). MRSA bacteria and bacteriophages were provided by Biophage Pharma (Montréal, Québec, Canada). Uranyl acetate (UA) was purchased from Canemco Inc. (Lakefield, Québec, Canada).

### 7.3.2 Bacterial culture

MRSA bacteria were isolated by Biophage Pharma and were grown in an incubator-shaker at 37°C in 4 mL of LB medium for 3h. The bacteria were then centrifuged at 2500 *g* (Sorvall RT7, 3500 rpm) for 20 min. The supernatant was discarded, and the bacteria were washed twice and resuspended in water. Their concentration was determined by plate count technique and expressed in colony forming units per milliliter (CFU/mL).

### 7.3.3 Bacteriophage preparation

Bacteriophages were isolated by Biophage Pharma and amplified by pipetting 100 µL of a suspension of $10^6$ PFU/mL of bacteriophages into a solution containing 1 mL of $10^6$ CFU/mL of freshly prepared bacteria. The bacteriophage concentration was determined by plate count technique and expressed in plaque forming units per milliliter (PFU/mL). After 15 minutes of incubation at room temperature, the infection mix was added to an Erlenmeyer flask containing 250 mL LB medium and incubated for 6 hours, at 37°C, in an incubator-shaker. The infected culture was then centrifuged at 2500 g for 20 minutes, filtered (0.22 µm) and titrated. For XPS and TEM, the bacteriophages were further centrifuged for 60 minutes, the supernatant was removed, and the phages were washed 3 times and resuspended in water.

### 7.3.4 Preparation of phage-AuNPs hybrids

One milliliter of nanoparticle stock solution (9.80 x $10^{11}$ particles/ml, 50 OD) was mixed with 49 mL of a solution consisting of 1 mol $L^{-1}$ EDC and 0.1 mol $L^{-1}$ NHS, for 15 min. The PEGylated NPs were then added to the phage solution (1.2 x $10^6$ PFU/mL) and mixed overnight in an incubator shaker at 37°C. Gold-phage hybrids slowly precipitated, sank to the bottom of the tube, and were centrifuged at 10 000 *g* for 1 min. The pellet was resuspended in 1 mL of water.

### 7.3.5 Transmission electron microscopy

The TEM employed was a Hitachi H-7100, operating at 75 kV. Copper grids (200 mesh), coated with a layer of Formvar and an overlayer of evaporated amorphous carbon, were used. A 10 μL drop of sample was deposited onto the grid by the reverse drop method: a drop of sample was deposited on Parafilm for 5 min, then the grid was deposited on top of the Parafilm, and excess liquid was removed with filter paper. The grid was then dipped, for 5 minutes, in a drop of 2% gluteraldehyde. The excess solution was again wicked from the edge of the grid with filter paper, and the specimen was washed twice with water. A drop of 1% UA was applied to the grid for 1 min, and excess was removed with the edge of a filter paper. The grid was allowed to dry before the sample was used for TEM analysis.

### 7.3.6 X-ray photoelectron spectroscopy

The XPS apparatus was a VG ESCALAB 3 Mark II using a non-monochromated Mg Kα X-ray source (1253.6 eV) at a base pressure below $10^{-10}$ Torr. For sample preparation, drops of the colloidal solution were placed on undoped, undiced, polished, Piranha-cleaned silicon wafers and dried overnight in a pumped desiccator. High-resolution spectra were obtained at a perpendicular takeoff angle using a pass energy of 20 eV and 0.05 eV steps. Spectral peaks were separated using the VG Avantage software; the peak widths used were those established in our laboratory, and are held constant for any element. The components were separated after a Shirley background was subtracted. The energy was calibrated by setting the major C1s peak, attributed to hydrocarbon, to 285.0 eV.

### 7.3.7 DNA sequence analysis and bioinformatics

Open reading frame identification was performed using GeneMark.hmm [195]. Similarity searches, for nucleotide sequences and for the deduced amino acid sequences, were performed using the FASTA [196], BLAST [197], and PARALIGN [198] programs available on the Online Analysis Tools website (http://molbio-tools.ca/).

## 7.4 Results and Discussion

### 7.4.1 Silicon wafer characterization

All samples were deposited onto a silicon wafer. As can be seen from Figure 7-1, where the XPS survey scan of a silicon wafer is presented, the surface has, in addition to silicon (22.55%), the expected presence of natural oxide (67.33 %) and lower but significant amounts of carbon (8.92 %) and fluorine (1.20%). The presence of carbon indicates the existence of organic contaminants, arising from the ambient atmosphere and perhaps human handling. Fluorine contamination is certainly due to the etching process[248] used in the original cleaning of the silicon wafer surface. The presence of silicon was not detected in further experiments due to the thicknesses of the phages, NPs and phage-NP hybrid layers and will not be discussed.

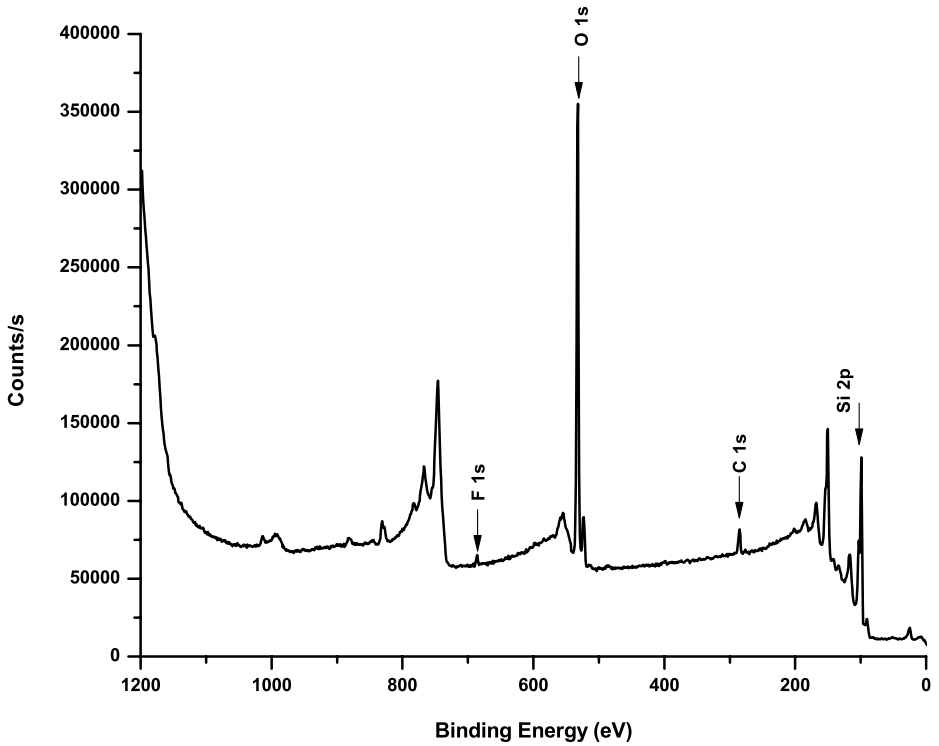


Figure 7-2: XPS survey spectrum of the silicon wafer

### 7.4.2 Bacteriophage characterization

Taking into account that a typical layer thickness measured by XPS ranges from around 4 to 5 nm (three times the attenuation length) for C, N and O, we expected to see the chemical constituents of the outer layer of the phage capsid, primarily composed of amino acids. Figure 7-2a shows a bacteriophage survey spectrum. A molecular characterization [3] of the podoviral bacteriophages virulent for *S. aureus* revealed the open reading frame six (ORF 6) codes for the major coat proteins containing 30 amino acids (MEKIYTAVLLYNVSINEIYEHEIEQFEKNK). Major XPS peaks account for the presence of C1s, O1s, and N1s, at 62.22, 23.26, and 14.45%, respectively. A minor S2p peak (163.66 eV) is found, at 0.06%, corresponding to sulfur present in methionine. No Si was detected, indicating that the wafer was thickly covered with bacteriophages.

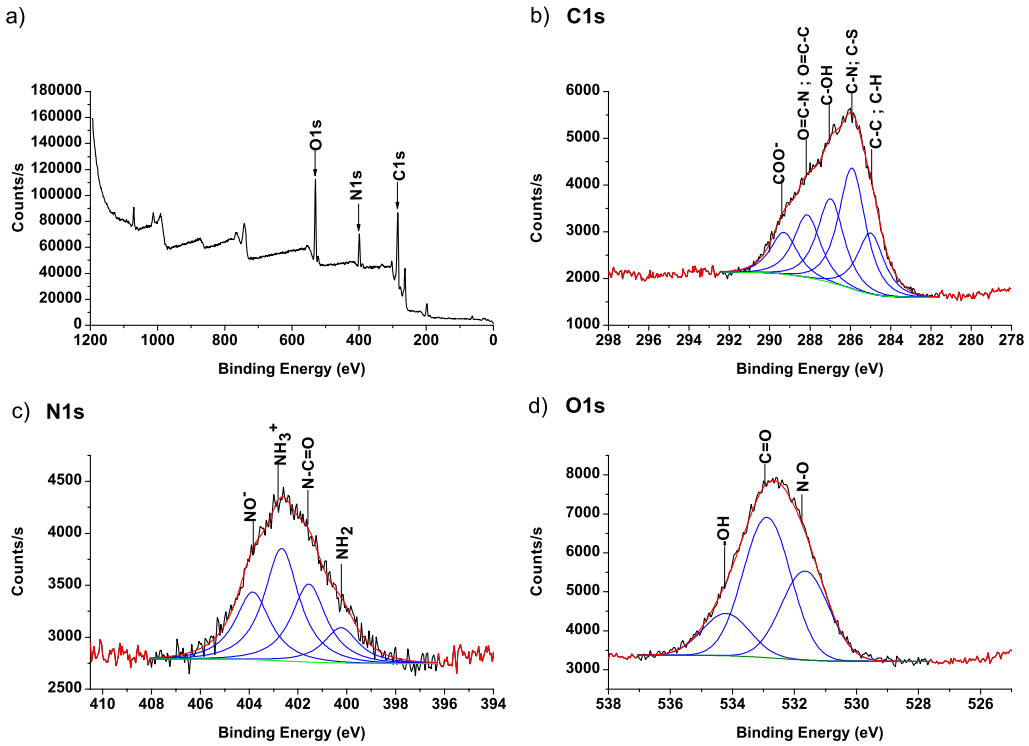


Figure 7-3: XPS spectra of MRSA-specific bacteriophage (a) XPS survey spectrum of bacteriophages showing carbon, nitrogen and oxygen species. (b) C1s high-resolution spectrum. (c) N1s high-resolution spectrum. (d) O1s high-resolution spectrum.

Table 7.1 presents the binding energies of the component peaks. The high resolution C1s spectrum was separated into five peaks (Figure 7-2b). The first, at 284.99 eV, is attributed to aliphatic carbon present in all amino acids, bound only to carbon or hydrogen[249-251]. The second, at 285.91 eV, is attributed to carbon singly bound to nitrogen (C-N)[251, 252], present in all amino acids, as well as carbon singly bound to sulfur (C-S)[253], present in methionine. The third, at 286.98 eV, is attributed to C-OH[252, 254] present in serine and threonine residues. The fourth, at 288.14 eV, is attributed to carbonyl carbon (O=C-C, O=C-N)[250, 252]. The highest binding energy component in the C1s spectra, at 289.29 eV, is attributed to carboxylate or carboxylic acid groups ($R\text{-}COO^-$ ; HO-C=O)[250, 255].

Table 7.1: C1s, N1s and O1s peaks detected for bacteriophage samples

| Name | Peak BE (eV) | FWHM (eV) | At. % (%) | Suggested attributions |
|---|---|---|---|---|
| C 1s | 284.99 | 1.60 | 9.87 | Aliphatic carbon |
| | 285.91 | | 19.63 | C-N; C-S |
| | 286.98 | | 13.68 | C-OH |
| | 288.14 | | 10.21 | O=C-N; O=C-C |
| | 289.29 | | 6.79 | COOH |
| N 1s | 400.24 | 1.70 | 1.88 | Amine |
| | 401.55 | | 4.16 | Amide |
| | 402.67 | | 6.00 | Protonated nitrogen |
| | 403.85 | | 3.62 | Oxidized nitrogen |

| Name | Peak BE (eV) | FWHM (eV) | At. % (%) | Suggested attributions |
|---|---|---|---|---|
| O 1s | 531.69 | 1.80 | 8.32 | Oxidized nitrogen |
| | 532.92 | | 12.37 | Carbonyl |
| | 534.26 | | 3.45 | Hydroxyl |

High-resolution N1s spectra, obtained from the sample, are found in Figure 7-2c. The spectra were separated into four peaks, representing contributions from neutral nitrogen, mainly amines, at 400.24 eV[256], and amides from asparagine and glutamine, at 401.55 eV[257]. The peak at 402.67 eV is attributed to protonated amino acid residues[256]. This is in agreement with Helgstrand et al. [258], where some amino acids of the major capsid proteins involved in the formation of the icosahedral capsid of phages are in a highly polar region and are protonated, forming hydrogen bonds with carboxylate groups. The fourth peak, at 403.85 eV, is due to a higher oxidation state, such as an amine N-oxide [255] .

Finally, the O1s spectrum was separated into three peaks (Figure 7-2d). The first, at 531.69 eV, is attributed to oxidized nitrogen. The second (532.92 eV) is attributed to carbonyl groups and the third, at 534.26 eV, is attributed to hydroxyl groups.

From the TEM image in Figure 7-3, the MRSA-specific bacteriophage is seen to be very similar to other *S. aureus* phages, such as the 44AHDJ virus, and is most probably from the *Podoviridae* family. As seen in Figure 7-3, it possesses a small isometric head, measuring 42 nm and, at its lower left a short, non-contractile tail, measuring 25 nm; the tail is responsible for its ability to adhere to and infect its bacterial host. The length of the phage (recognition element) is of critical importance to LSPR and will be discussed later.

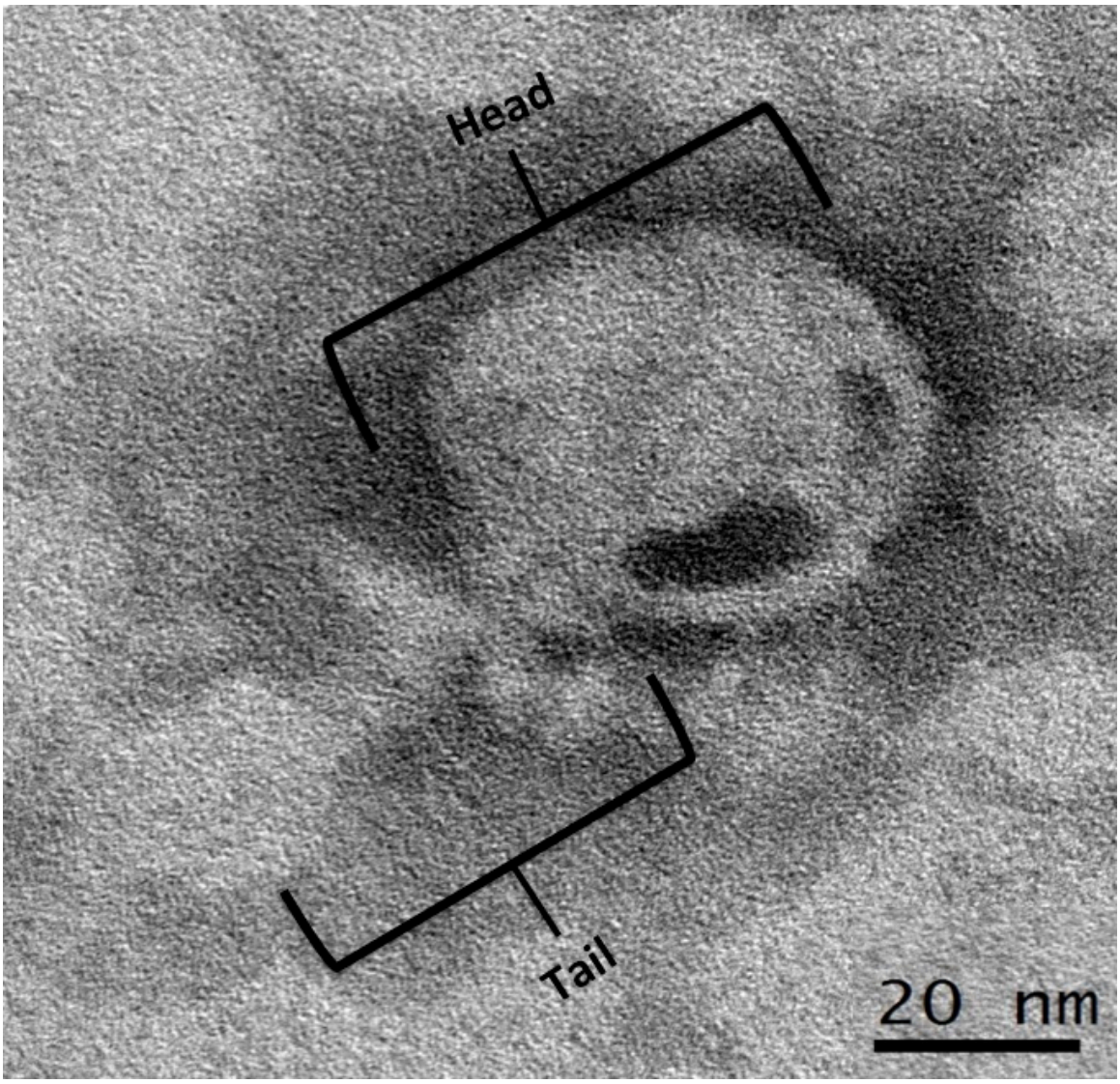


Figure 7-4: TEM photomicrograph of an MRSA bacteriophage

### 7.4.3 Heterobifunctional PEG-functionalized gold nanoparticles

Previous studies showed that the chemical synthesis of the gold NPs, through the reduction of a precursor salt by a reducing agent, often leads to surface contamination [259]. An XPS survey of the 60 nm PEGylated nanoparticles shows, as expected, the presence of gold, sulfur, carbon and oxygen (Figure 7-4a). The relative concentrations were, respectively, 26.04, 2.46, 37.87, and 23.26%. Silicon was not detected, indicating a thick, homogenous coverage of the wafer. No other contaminants, such as chlorine, fluorine or sodium were detected.

Our XPS resultsshow that the PEG linker is composed of seven repeat units, which is not in accordance with the manufacturer [260], who claims that the PEG functional group has a molecular weight of 3000 Da (~70 repeat units). We can still see the gold through the PEG surface layer; because XPS can probe up to 4.5 nm (three times the attenuation length of Au, 15Å), the PEG surface layer must be < 4.5 nm in thickness. For S-(O-C-C)$_n$-COOH with n=7, we should have 15 times the amount of carbon relative to that of sulfur (i.e. 36.9%) and nine times the amount of oxygen (i.e. 22.14%). A comparison with what we found experimentally leads us to believe that there is very little, if any, carbon and oxygen contamination.

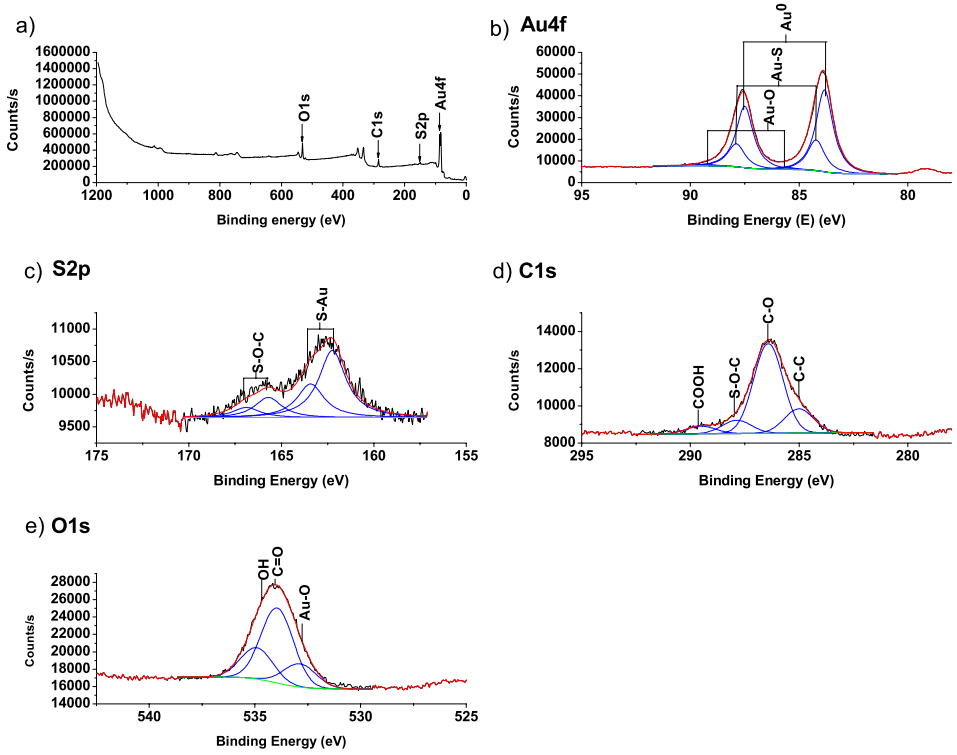


Figure 7-5: XPS spectra of heterobifunctionalized PEGylated gold nanoparticles. a) XPS survey spectrum. b) Au 4f high-resolution spectrum. c) S2p high-resolution spectrum. d) C1s high-resolution spectrum. e) O1s high-resolution spectrum.

A detailed chemical analysis of the high-resolution Au4f spectrum showed that the NPs may be partially oxidized by the oxygen present in solution (Figure 7-4b). High-resolution gold spectra are characterized by three pairs of peaks contained in the $Au4f_{7/2}$ and $Au4f_{5/2}$ doublet. The positions of the first and most important pair (BEs of 83.83 and 87.5 eV) are due to elemental gold ($Au^0$); those of the other pairs are due to Au-S (BE 84.22 and 87.89 eV), and oxidized gold (Au-O) (BEs of 85.63 and 89.30 eV) (Table 7.2). Our results clearly indicate that gold is present at the interface in several oxidation states, explaining the low energy O1s components of O-Au species. On the basis of relative peak areas, their respective atomic percentages were estimated as 18.94% for $Au^0$, 7.04% for Au-S, and 0.52% for Au-O.

Table 7.2: Au 4f, S2p, C1s and O1s peaks detected for PEGylated nanoparticle samples

| Name | Peak BE (eV) | FWHM (eV) | At. % (%) | Suggested attributions |
|---|---|---|---|---|
| Au 4f doublets | 83.83 – 87.50 | 0.95 | 18.94 | $Au^0$ |
| | 84.22 – 87.89 | | 7.04 | Au-S |
| | 85.63 – 89.30 | | 0.52 | Au-O |
| S2p doublets | 162.24 – 163.42 | 1.75 | 4.15 | S-Au |
| | 165.71 – 166.89 | | 1.14 | S-O-C |
| C 1s | 285.02 | 1.60 | 5.67 | Hydrocarbon |
| | 286.42 | | 21.01 | O-C-C |
| | 287.86 | | 3.12 | S-O-C |
| | 289.53 | | 1.82 | COOH |
| O 1s | 532.87 | 1.80 | 5.86 | Au-O |
| | 533.82 | | 22.85 | Carbonyl |
| | 534.92 | | 7.87 | Hydroxyl |

The S2p high-resolution spectrum (Figure 7-4c) consists of two pair of peaks, attributed to S-Au (BEs 162.24 and 163.42 eV) and S-O-C (BEs 165.71 and 166.89 eV), with respective atomic percentages of 4.15 and 1.14.

The high-resolution C1s spectrum (Figure7- 4d) consists of four peaks attributed to hydrocarbon (285.02 eV), $(O\text{-}C)_n$ (286.42 eV), S-O-C (287.86 eV), and COOH (289.53 eV). Respective atomic percentages were found to be 5.67, 21.01, 3.12, and 1.82 of the total.

The high-resolution O1s spectrum (Figure 7-4e) contains three peaks attributed to Au-O (532.87 eV), carbonyl (BE 533.95 eV), and hydroxyl components of PEG (534.92 eV). Respective atomic percentages were found to be 5.86, 22.85, and 7.87.

From Figure 7-5, it can be seen that the Au NPs are approximately cuboctahedral and reasonably monodisperse. From the TEM images, we obtain an average particle diameter and standard deviation of 62 ± 6 nm. The size of the NPs is of critical importance for biodetection purposes using LSPR and will be further discussed in the following section.

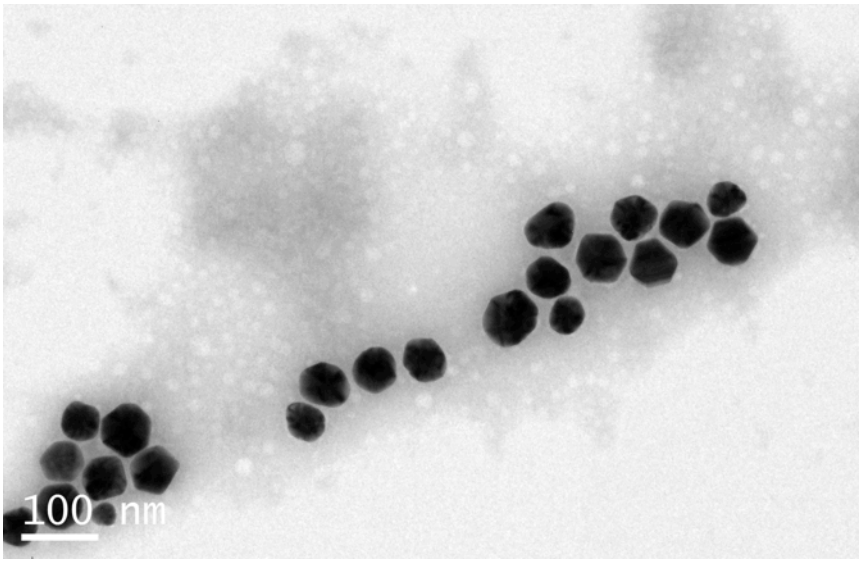


Figure 7-6: TEM photomicrograph of heterobifunctional PEG-functionalized gold nanoparticles.

### 7.4.4 Bacteriophage-gold nanoparticle nanohybrids

We recently investigated several coupling strategies aimed at attaching lytic bacteriophages to gold surfaces[107]. It is of paramount importance that phages retain their native conformation and binding activity while being stably immobilized to a sensor surface. Thus, an understanding of the interface between the gold surface and the systems to be studied is fundamental to all surface-sensitive sensor systems.

Phages were coupled to heterobifunctional PEGylated NPs using carbodiimide chemistry through reaction of the phage amino groups with EDC/NHS and the carboxylic acid terminations of the PEG deposited onto the gold NP surfaces. Chemical alterations of the sample surfaces, leading to the formation of an amide bond between the bacteriophages and the AuNPs, were studied by XPS. An elemental survey of the samples shows the presence of carbon, oxygen and nitrogen, contributed by the presence of phages as well as small but detectable amounts of gold and sulfur, contributed by the PEGylated NPs (Figure 7-6a). The low atomic percentages of gold (0.32) and sulfur (0.77) indicate that Au NPs were densely covered by phages. Thus, we expect relatively similar carbon, nitrogen, and oxygen percentages for phage-NPs hybrids when compared to phages. The atomic percentages of carbon were 60.72 for phage-NPs hybrids, compared to 60.18 for phages. Similarly, the nitrogen and oxygen contributions remained very similar, at 15.4 and 22.82%, respectively, for phage-NPs hybrids, compared to 15.60 and 24.16 % for phage species. There was, however, an increase in sulfur components (0.77%) for phage-NP when compared to phages alone (0.06%) due to the presence of thiolated heterobifunctional PEG nanoparticles.

A detailed chemical analysis of the high resolution Au4f spectrum showed a component composition pattern similar to that of the PEGylated NPs (Figure 7-6b). Gold was characterized by three $Au4f_{7/2}$ and $Au4f_{5/2}$ doublets. The relative atomic percentage of elemental gold ($Au^0$) (0.10%, BEs 83.88 and 87.55 eV) as well as Au-S (0.12%, BEs 84.86 and 88.53 eV) diminished when compared to PEGylated NPs . This is due to the high density coverage of the NPs with phages, lowering the relative atomic percentage of the gold species, compared to the C, N and O contributions of the phages. The presence of Au-O species (BEs of 85.71 and 89.38 eV) was also detectable (0.08%). The S2p high-resolution spectra again consisted of two pair of $S2p_{3/2}$ and $S2p_{1/2}$ doublets (Figure 7-6c). The first pair, attributed to S-Au (0.53% BEs 162.56 and 163.74 eV), is derived from PEG attachment to NPs; the second peak, less electronegative than that

reported for S-O-C component of PEGylated AuNPs, is attributed to oxidized sulfur at 0.28 % with BEs of 163.72 and 164.90 eV.

High-resolution C1s spectra (Figure 7-6d), showed a decrease of the relative atomic percentage of aliphatic carbons in phage-NPs hybrids (6.38%, BE 284.99 eV), compared to phages (9.87%). This decrease was also noted for the peak attributed to C-N and C-S (15.77%, BE 285.98 eV) compared with 19.63% in phages. There was an increase in the relative atomic percentages of C-OH (16.82%, BE 286.95 eV), when compared to phages (13.68%). The peak attributed to the amide contribution (288.79 eV) showed a slight increase (12.52%, compared with 10.20% for phages), due to bond formation between the NP and the phage surface amines. The peak corresponding to the carboxylic acid components of phages remained stable (6.85%, 289.31 eV). A sixth peak appeared at BE 290.54 eV, at 2.37%. This peak may be due to the EDC/NHS complex used to form active ester functionalities with carboxylate groups.

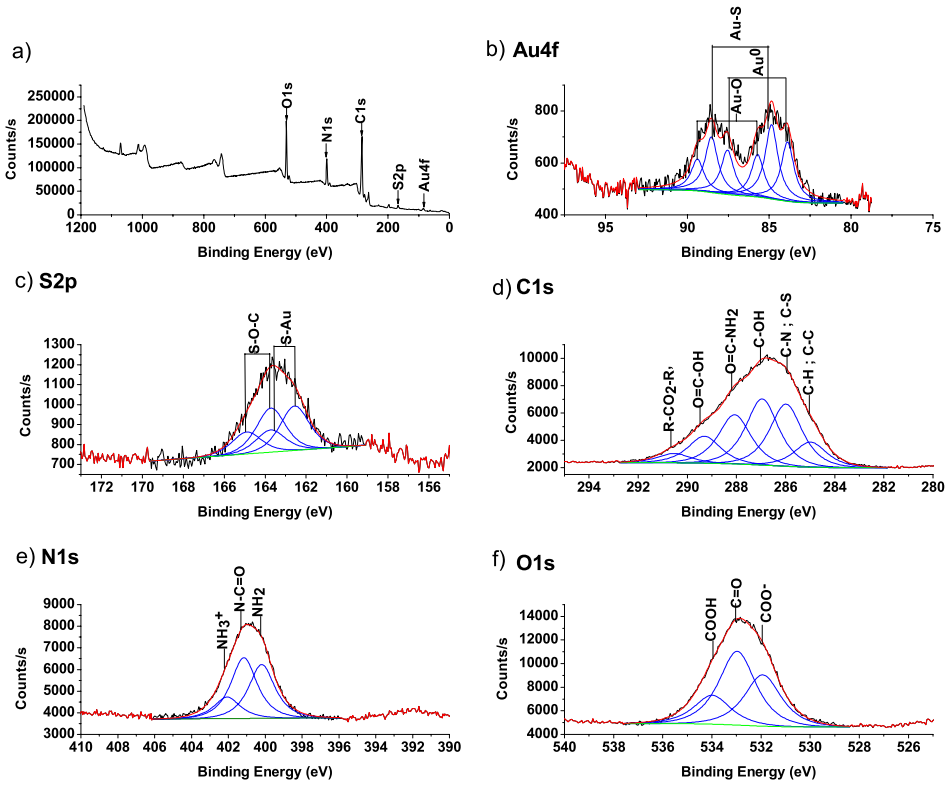


Figure 7-7: XPS spectra of phage-NPs hybrids. a) XPS survey spectrum. b) Au 4f high-resolution spectrum. c) S2p high-resolution spectrum. d) C1s high-resolution spectrum. e) N1s high-resolution spectrum. f) O1s high-resolution spectrum.

Although the relative percentages of the N1s, O1s and C1s components remained the same in phage-NPs samples compared with phages, high resolution N1s spectra were different, with only three peaks for phage-NPs compared to four for phages (Figure 7-6e). Moreover, we see an increase in amine concentration (6.28%, 400.20 eV) and amide groups (6.86%, 401.18 eV) when compared with phages (1.88 and 4.16%, respectively), reflecting the formation of a peptide bond between the PEGylated gold and the phage. Our N1s XPS results reveal the presence of both amine ($-NH_2$) and ammonium ion ($-NH_3^+$) in phage samples. However, following the covalent attachment of phages to AuNPs, N1s spectra show a marked decrease in protonated amine (2.27 %, 402.10 eV, compared to 6.00% in phage samples) and a complete disappearance of the peak attributed to N-oxides compared with 3.62% for the phage samples. This indicates that the $-NH_2$

covalently binds to the AuNPs, while the -$NH_3^+$ electrostatically binds to the negatively charged silicon surface. These results are consistent with previously published work [259]: although amines do not generally react with bulk Au, they do react with nanosized Au, in solution, to form a weak covalent bond [261, 262]. Moreover, amine oxides are very reactive and can be readily converted to amine, in the presence of reducing agents, such as NHS. We note the presence of –$NH_2$ species at 400.20 eV, while –$NH_3^+$ species are present at 402.10 eV;–$COO^-$ are found at lower binding energy (531.93 eV) than –COOH groups (533.99 eV). These are consistent with recent findings, where core level shifts larger than 1 eV in the N1s and O1s spectra are induced by the formation of strong intermolecular H bonds with opposite sign for the proton donor and the proton acceptor[263]. Positions and atomic percentages for the high-resolution peaks of the O1s spectrum remained essentially the same (Figure 7-6f).

Table 7.3: Au4f, S2p, C1s, N1s and O1s peaks detected for bacteriophage-NP hybrids

| Name | Peak BE | FWHM eV | At. % | Suggested attributions |
|---|---|---|---|---|
| Au 4f doublets | 83.88 – 87.55 | 0.95 | 0.10 | $Au^0$ |
| | 84.86 – 88.53 | | 0.12 | Au-S |
| | 85.71 – 89.38 | | 0.08 | Au-O |
| S 2p doublets | 162.56 – 163.74 | 1.75 | 0.53 | S-Au |
| | 163.72 – 164.90 | | 0.28 | S-O-C |
| C 1s | 284.99 | 1.60 | 6.38 | Aliphatic carbon |
| | 285.98 | | 15.77 | C-N; C-S |
| | 286.95 | | 16.82 | C-OH |
| | 288.07 | | 12.51 | O=C-N; O-C-C |
| | 289.31 | | 6.85 | COOH |
| | 290.54 | | 2.37 | Carbonate |
| N 1s | 400.20 | 1.70 | 6.28 | Amine |
| | 401.18 | | 6.85 | Amide |
| | 402.10 | | 2.27 | Protonated nitrogen |
| O 1s | 531.93 | 1.80 | 7.63 | $COO^-$ |
| | 532.97 | | 10.94 | Carbonyl |
| | 533.99 | | 4.25 | Carboxyl |

TEM was used it to directly visualize the nanohybrid complex at high resolution (Figure 7-7). Negative staining was required to verify the presence of the bacteria and bacteriophages. To date, very few studies have investigated negative staining factors affecting these types of complexes. Recent studies show that phosphotungstic acid (PTA) solution interrupts the interactions between Au NPs and phage particles, resulting in the detachment of the NPs from phages [246]. To avoid this, we used a 2% UA solution. Although the NP-phage hybrids were darkened, lytic bacteriophages are still recognizable. Moreover, phage-nanoparticle hybrids can be seen to still adhere to their host bacterium, implying that the phage remains active. Further studies are needed to confirm this.

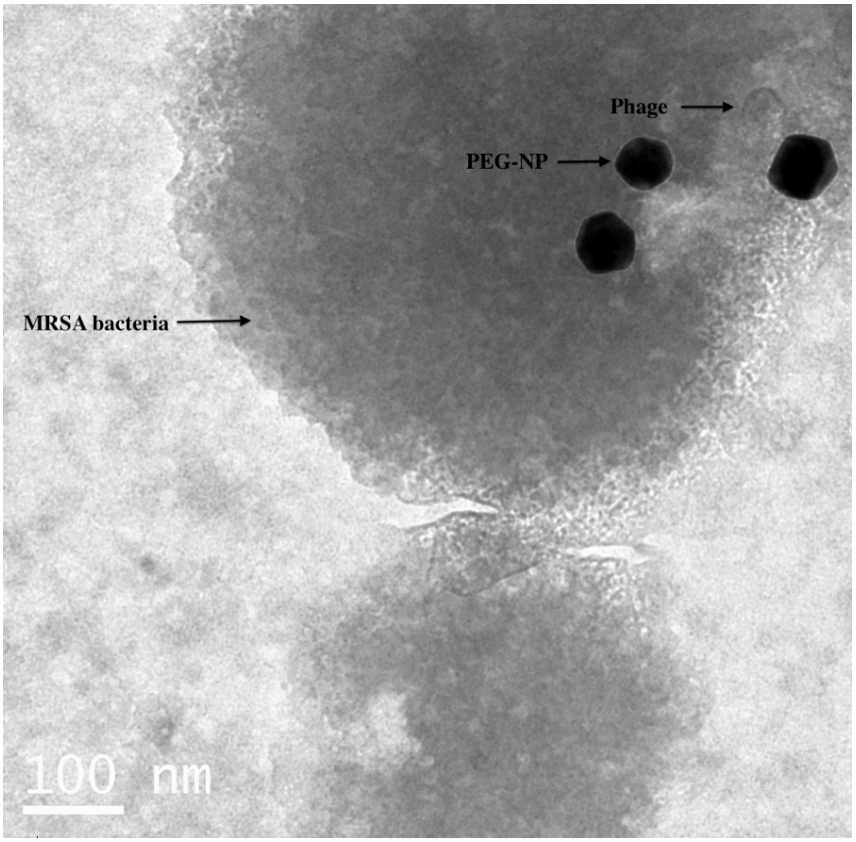


Figure 7-8: TEM photomicrograph of phage-NP nanohybrids adhering to MRSA bacteria

We have used a finite-element model that solves for Maxwell's equations in the time-harmonic regime[264] to support our views and to estimate the optimum size of NPs to be used for the field enhancement of LSPR in biodetection. The distribution of the amplification of the electric field in space was obtained by solving for the Helmholtz equation and using the dielectric function of gold given by Johnson and Christy[265]. Figure 7-8a presents the near-field enhancement ($|\mathbf{E}|^2$) around our 60 nm AuNPs suspended in a PBS solution (refractive index ≈1.334), following linearly polarized irradiation at 680 nm. Calculations (Figure 7-8b) show that the enhanced field intensity reaches well beyond the size of an average phage (≈ 42 nm[3])confirming the possibility of phage-NP hybrid-based biodetection. Varying the AuNPs diameter, Figure 7-8c also reveals the dependence of the enhanced near-field intensity, at the phage-bacterium interface, relative to the size of the NPs and shows that the greatest intensity is predicted for 150 nm NPs; unfortunately, this could not be verified because PEGylated Au NPs of this dimension are not available at the time. However, those NPs would be, as a consequence, the most promising candidates for the development of efficient phage-NP hybrids.

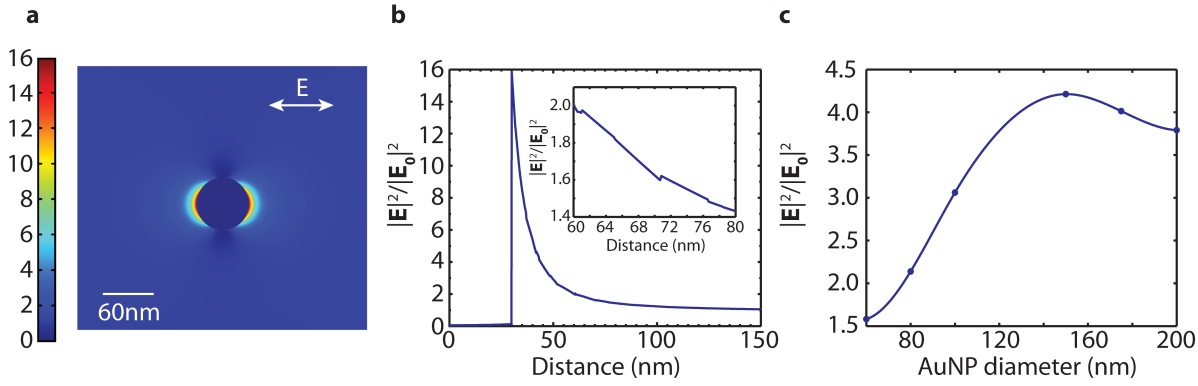


Figure 7-9: a. Enhancement of the field intensity ($|E|^2$) around a 60 nm diameter AuNPs suspended in PBS medium, on irradiation at 680 nm. The laser polarization direction is indicated on the figure. b. Enhancement of the field intensity along the horizontal axis. The NP-phage boundary is situated at 30nm, and the phage-bacteria boundary is at 72nm. An enlargement near the phage-bacteria boundary is shown in inset. c. Enhancement of the field intensity at the phage-bacteria boundary as a function of AuNP diameter.

## 7.5 Conclusion

Gold nanoparticles, functionalized with a heterobifunctional PEG, were successfully coupled to lytic bacteriophages specific to MRSA, via carbodiimide chemistry, for biodetection purposes. XPS has been used to study the interface between the metal and the bacteriophage. XPS characterization of the lytic phage showed the presence of protonated nitrogen species attributed to the major capsid proteins. PEGylated gold nanoparticles were shown to efficiently bind to phages through the formation of amide bonds between the primary amines of the phage and the carboxylic acid terminal groups of the NP platforms. Our results also showed the formation of strong intermolecular hydrogen bonds between carboxyl and amine species, as shown by N1s and O1s core level shifts.

## 7.6 Acknowledgements

We thank NanoQuébec and the National Science and Engineering Research Council of Canada for financial support, S. Patskovsky for insightful discussions regarding LSPR, and Cytodiagnostics for providing NPs.

# GENERAL DISCUSSION

The ever-increasing incidence of multidrug-resistant infections has created a global public health crisis. It is difficult to go a week without hearing about the deteriorating state of health care. The CDC estimates that there are 1.7 million people infected by nosocomial bacteria in the US. This translates into excess health costs, reaching $20 billion, with 8 million days of additional hospital occupancy, and $35 billion in societal costs annually. Of these nosocomial infections, MRSA is by far, the most important and constitutes one of the biggest therapeutic hurdles of our time. According to the CDC, more people in the US died from MRSA infections than from AIDS in 2005. The situation is alarming, and we need to find suitable ways to tackle this problem. The pressing need for novel technologies to detect and, thus, better treat these infections, has paved the way for a worldwide effort in biosensor research and development. The significant number of publications and patents, presenting improvements in sensor performance in terms of selectivity and sensitivity, suggests a continuing interest for biosensing technologies targeting health, drug discovery, agro-food industries and homeland security. The world market for *in vitro* diagnostics was estimated to be about $17 billion in 2003, with the biosensor market expected to reach $8.2 billion by 2009 [266]. Nonetheless, the commercialization of biosensor technology is lagging behind research efforts. The technology transfer to a clinical setting seems to be circumvented by cost, sensitivity, and reliability considerations. In order to respond to these limitations, we turned our attention to bacteriophages whose multivalent, fast and specific interaction with target bacteria, combined with their low production costs, make them a promising alternative to antibodies in a biosensing scheme.

One of the key steps in the construction of a sensing platform is to select a pertinent method for the immobilization of the recognition element to the surface. We chose to study the self-assembly of thiols to generate functionalized surfaces which selectively attach bacteriophages to gold. Although alkanethiol SAMs are commonly used in biosensing technologies, little is known about their real-time assembly. In particular, the monolayer formation of amino acids, such as L-cysteine, has been largely overlooked. The importance of L-cysteine resides in the fact that the molecules have both carboxyl and amino terminal endgroups that confer broader possibilities for metal-molecule and molecule-molecule interactions. Moreover, its zwitterionic state results in

various intermolecular forces governing its interaction with the metal surface. We chose to use SPR to determine the binding mechanisms of both L-cysteine and MUA on gold, and introduced numerical models to describe the assembly of both higher and lower concentrations of the thiolated molecules. Our results were deemed necessary to improve strategies for the attachment of recognition elements, such as bacteriophages, to the functionalized surface.

The self-assembly technique offers an interesting perspective in developing a sensitive sensor. It is widely accepted that generating functionalized surfaces, through modification of thiols, permits the attachment of biomolecules onto gold. However, there is a lack of systematic investigation of the relationship between the immobilization conditions and the resulting orientation and bioactivity of adhered bacteriophages. Our SPR investigations relating to bacteriophage attachment to gold using various chemistries, including physisorption, gluteraldehyde fixation, and L-cysteine, combined with MUA and EDC/NHS, show that it is possible to attach bacteriophages with a reasonable density for all methods. However, high phage coverage did not necessarily translate into preserved phage lytic activity. These results suggest that density of immobilized phages cannot solely account for an increased binding of host bacteria or a better sensitivity of detection. To circumvent the problem of steric hindrance, we prepared a mixed SAM consisting of a long chain alkanethiol (MUA) combined with a shorter-chain amino acid (L-cysteine). AFM results show the resulting formation of a more uniform surface with vacancy cavities permitting the oriented positioning of bacteriophages. This correlates with increased binding affinities of the phages immobilized with this method, suggesting a tail-up deposition and availability of their caudal proteins to the external medium containing the host bacteria. The results of the present study confirm that oriented immobilization of phages allow for the capture and detection of their host bacteria with high sensitivity.

Market viability and applicability of a biosensor in a clinical setup depends on its cost, which is related to its shelf life and stability. Most biosensors cannot fulfill this requirement due to the fragility of the biorecognition element (i.e. antibodies). Moreover, the biosensor should accurately assay a biological sample in less than a few minutes. Most devices presently available have analysis times ranging from hours to several days. We successfully report on the detection of *E. coli* (Gram negative) and MRSA (Gram positive), using a phage-based SPR sensor, for bacterial concentrations of $10^3$ CFU/mL in less than 20 minutes. What is more, bacteriophages

are extremely stable and can survive at room temperature for more than a month. The proposed biodetection approach could be extended further to other phages targeting different types of bacteria of particular interest for health care, food, and homeland security.

The failed technology transfer of biosensors can be attributed in part by their inadequacy to effectively probe clinical samples; biosensors are usually tested under controlled environments, and only subjected to the evaluation of pristine, homogeneous laboratory samples. Moreover, successful biosensors must be versatile enough to support interchangeable biorecognition elements. We evaluated 250 clinical samples, provided by the LSPQ, for their susceptibility to antibodies. We found that these samples displayed a wide range of antimicrobial resistance or susceptibility. We then modified our SPR assay in order to selectively detect and differentiate between MSSA, CA-MRSA, HA-MRSA and BORSA strains, by targeting PBP2a proteins exclusive to MRSA, but present in different concentrations on the membranes of community or hospital acquired strains. We found that the system permits the label-free, real time, specific detection of pathogens for concentrations as low as 10 CFU/mL, in less than 20 minutes. We found that the highest sensitivity of detection was achieved by using antibodies as recognition elements owing to their smaller size when compared to that bacteriophage. Smaller recognition elements tend to increase the sensitivity of the platform due to the fact that the probing depth of the evanescent field is approximately 300nm in the direction perpendicular to the detection surface. This system promises to become a diagnostic tool for bacterial pathogens in clinical settings and should be further tested for clinical samples in biological fluids, such as serum.

Nanoparticles have been reported to significantly enhance detections sensitivities of SPR sensors. Recent advances in nanofabrication have prompted us to immobilize bacteriophages to heterobifunctional nanoparticles. The chemical functionalization of nanomaterials and the subsequent attachment of phages are expected to pave the way for improved biosensing assays. We used XPS and TEM to delineate the role of the interface and covalent coupling chemistry to attach phages to gold nanoparticles. This study is of interest for LSPR biosensing and can be extended to other applications, such as targeted separation of bacteria from heterogeneous samples, dark-field microscopy and surface-enhanced Raman scattering detection.

# CONCLUSIONS

Pathogen detection is of utmost importance in many sectors, such as in the food industry, environmental quality control, clinical diagnostics, bio-defence and counter-terrorism. Failure to appropriately, and specifically, detect pathogenic bacteria can lead to serious consequences, and may ultimately be lethal. Public safety, new legislation, recent outbreaks in food contamination, and the ever-increasing prevalence of multidrug-resistant infections have fostered a worldwide research effort targeting novel biosensing strategies. Phage-based SPR biosensors could become a powerful diagnostic tool for the detection of emerging infectious diseases in a clinical setting.

We have developed a phage-based biosensing SPR system suited to the specific and sensitive detection of bacterial pathogens in a rapid and inexpensive fashion. The first part of this work was devoted to deciphering the self-assembly of L-cysteine and MUA and derive better strategies for the oriented immobilization of the phages to the gold sensing platform. A mixed self-assembled layer of these two molecules permitted a favorable positioning of the phages where the caudal recognition proteins are facing the surrounding medium containg the bacterial pathogens. Optimization of surface immobilization chemistry and finding bacteriophage candidates suitable for SPR permitted the detection of low concentrations of pathogens in real time for concentrations < $10^3$ CFU/mL in 20 minutes, without prior labeling or enrichment steps. Clinical applicability of the sensor was demonstrated by investigating 250 clinical *S. aureus* samples displaying a large spectrum of resistance. Finally, phages were immobilized to heterobifunctional nanoparticles with the intent of improving the sensitivity of biodectection, as well as extending their use to a wide range of biotechnological applications.

Although this body of work reports on the development of a fast, easy to use, specific and inexpensive biosensor, many important challenges remain before it can be efficiently used in a point of care setting. Of these challenges, the biosensor should include an apparatus for sample collection, which is compatible with blood serum and other heterogeneous environmental

samples. Moreover, the system should be miniaturized to allow for a wireless, handheld apparatus.

In conclusion, phage-based SPR sensing offers many promising features and has a great potential for pathogen detection. A multidisciplinary research effort is of essence to bring about the commercialization and introduction of this system in a clinical setting.

# BIBLIOGRAPHY

[1] Tawil N, Hatef A, Sacher E, Maisonneuve M, Gervais T, Mandeville R, et al. Surface Plasmon Resonance Determination of the Binding Mechanisms of L-Cysteine and Mercaptoundecanoic Acid on Gold. Journal of Physical Chemistry C. 2013;117:6712-8.

[2] Tawil N, Sacher E, Mandeville R, Meunier M. Strategies for the Immobilization of Bacteriophages on Gold Surfaces Monitored by Surface Plasmon Resonance and Surface Morphology. Journal of Physical Chemistry C. 2013;117:6686-91.

[3] Tawil N, Sacher E, Mandeville R, Meunier M. Surface plasmon resonance detection of E. coli and methicillin-resistant S. aureus using bacteriophages. Biosensors & Bioelectronics. 2012;37:24-9.

[4] Tawil N, Mouawad F, Levesque S, Sacher E, Mandeville R, Meunier M. The differential detection of methicillin-resistant, methicillin-susceptible and borderline oxacillin-resistant Staphylococcus aureus by surface plasmon resonance. Biosensors & Bioelectronics. 2013;49:334-40.

[5] Tawil N, Sacher E, Boulais E, Mandeville R, Meunier M. X-ray Photoelectron Spectroscopic and Transmission Electron Microscopic Characterizations of Bacteriophage–Nanoparticle Complexes for Pathogen Detection. Journal of Physical Chemistry C. 2013;117:20656-65.

[6] Souza GR, Christianson DR, Staquicini FI, Ozawa MG, Snyder EY, Sidman RL, et al. Networks of gold nanoparticles and bacteriophage as biological sensors and cell-targeting agents. Proceedings of the National Academy of Sciences of the United States of America. 2006;103:1215-20.

[7] Arias CA, Murray BE. Antibiotic-Resistant Bugs in the 21st Century -- A Clinical Super-Challenge. New England Journal of Medicine. 2009;360:439-43.

[8] Roberts RR, Hota B, Ahmad I, Scott RD, II, Foster SD, Abbasi F, et al. Hospital and Societal Costs of Antimicrobial-Resistant Infections in a Chicago Teaching Hospital: Implications for Antibiotic Stewardship. Clinical Infectious Diseases. 2009;49:1175-84.

[9] Dover JE, Hwang GM, Mullen EH, Prorok BC, Suh S-J. Recent advances in peptide probe-based biosensors for detection of infectious agents. Journal of Microbiological Methods. 2009;78:10-9.

[10] Gravitz L. Turning a new phage. Nature Medicine. 2012;18:1318-20.

[11] Pennington H. Penicillin: Triumph and tragedy. Nature. 2007;446:981-.

[12] Kohanski MA, Dwyer DJ, Collins JJ. How antibiotics kill bacteria: from targets to networks. Nature Reviews Microbiology. 2010;8:423-35.

[13] Typas A, Banzhaf M, Gross CA, Vollmer W. From the regulation of peptidoglycan synthesis to bacterial growth and morphology. Nature Reviews Microbiology. 2012;10:123-36.

[14] Boucher HW, Talbot GH, Bradley JS, Edwards JE, Jr., Gilbert D, Rice LB, et al. Bad Bugs, No Drugs: No ESKAPE! An Update from the Infectious Diseases Society of America. Clinical Infectious Diseases. 2009;48:1-12.

[15] Wertheim HFL, Melles DC, Vos MC, van Leeuwen W, van Belkum A, Verbrugh HA, et al. The role of nasal carriage in Staphylococcus aureus infections. Lancet Infectious Diseases. 2005;5:751-62.

[16] Biedenbach DJ, Moet GJ, Jones RN. Occurrence and antimicrobial resistance pattern comparisons among bloodstream infection isolates from the SENTRY Antimicrobial Surveillance Program (1997-2002). Diagnostic Microbiology and Infectious Disease. 2004;50:59-69.

[17] Pantosti A, Venditti M. What is MRSA? European Respiratory Journal. 2009;34:1190-6.

[18] Lim D, Strynadka NCJ. Structural basis for the beta-lactam resistance of PBP2a from methicillin-resistant Staphylococcus aureus. Nature Structural Biology. 2002;9:870-6.

[19] Schofield DA, Sharp NJ, Westwater C. Phage-based platforms for the clinical detection of human bacterial pathogens. US Pubmed Central. 2012;2:105-283.

[20] Klevens RM, Morrison MA, Nadle J, Petit S, Gershman K, Ray S, et al. Invasive methicillin-resistant Staphylococcus aureus infections in the United States. Jama-Journal of the American Medical Association. 2007;298:1763-71.

[21] Prevention CfDCa. HIV/AIDS Surveillance report, 2005. In: US Department of Health and Human Services CfDCaP, editor. Atlanta2007.

[22] Organization WH. Human plague: review of regional morbidity and mortality, 2004–2009. Weekly epidemiological record. 2010;85:37-48.

[23] Williamson ED, Oyston PCF. Protecting against plague: towards a next-generation vaccine. Clinical and Experimental Immunology. 2013;172:1-8.

[24] dos Santos MB, Agusil JP, Prieto-Simon B, Sporer C, Teixeira V, Samitier J. Highly sensitive detection of pathogen Escherichia coli O157:H7 by electrochemical impedance spectroscopy. Biosensors & Bioelectronics. 2013;45:174-80.

[25] Hernandez-Reyes C, Schikora A. Salmonella, a cross-kingdom pathogen infecting humans and plants. Fems Microbiology Letters. 2013;343:1-7.

[26] Prevention CfDCa. Vital Signs: Incidence and Trends of Infection with Pathogens Transmitted Commonly Through Food --- Foodborne Diseases Active Surveillance Network, 10 U.S. Sites, 1996--2010. Morbidity and Mortality Weekly Report (MMWR). 2011;60:749-55.

[27] da Silva EP, De Martinis ECP. Current knowledge and perspectives on biofilm formation: the case of Listeria monocytogenes. Applied Microbiology and Biotechnology. 2013;97:957-68.

[28] Organization WH. Risk assessment of Listeria monocytogenes in ready-to-eat foods: interpretative summary. 2012.

[29] Griffiths G, Nystroem B, Sable SB, Khuller GK. Nanobead-based interventions for the treatment and prevention of tuberculosis. Nature Reviews Microbiology. 2010;8:827-34.

[30] Kutter E, Sulakvelidze A. Bacteriophages: Biology and Applications. Boca Raton, Florida: CRC Press; 2005.

[31] Twort F. An investigation on the nature of ultramicroscopic viruses. Lancet. 1915;11:1241.

[32] D'Herelle F. Sur un microbe invisible antagoniste des bacilles dysentériques. Comptes rendusde l'Académie des Sciences. 1917;165:373-5.

[33] D'Herelle F. Du rôle du microbe filtrant bacteriophage dans la fièvre thyphoide. Compte rendu de l'Académie des Sciences. 1919;168:631.

[34] D'Herelle F. Sur une épizooric de thyphose aviaire. Compte rendu de l'Académie des Sciences. 1919;169:817.

[35] Cherry WB, Davis BR, Edwards PR, Hogan RB. A simple procedure for the identification of the genus Salmonella by means of a specific bacteriophage. J Lab Clin Med. 1954;44:51-5.

[36] Mandeville R, Griffiths M, Goodridge L, McIntyre L, Henchuk TT. Diagnostic and Therapeutic Applications of Lytic Phages. Analytical Letters. 2003;36:3241-59.

[37] Moldovan R, Chapman-McQuiston E, Wu XL. On kinetics of phage adsorption. Biophysical Journal. 2007;93:303-15.

[38] Sidhu S. Phage display in biotechnology and drug discovery: CRC Press; 2005.

[39] Lu TK, Collins JJ. Engineered bacteriophage targeting gene networks as adjuvants for antibiotic therapy. Proceedings of the National Academy of Sciences of the United States of America. 2009;106:4629-34.

[40] Lu TK, Collins JJ, Ieee. Engineering Synthetic Bacteriophage to Combat Antibiotic-Resistant Bacteria2009.

[41] Lu TK, Bowers J, Koeris MS. Advancing bacteriophage-based microbial diagnostics with synthetic biology. Trends in Biotechnology. 2013;31:325-7.

[42] Zakeri B, Lu TK. Synthetic Biology of Antimicrobial Discovery. Acs Synthetic Biology. 2013;2:358-72.

[43] Tawil N, Sacher E, Boulais E, Mandeville R, Meunier M. X-ray Photoelectron Spectroscopic and Transmission Electron Microscopic Characterizations of Bacteriophage-Nanoparticle Complexes for Pathogen Detection. Journal of Physical Chemistry C. 2013;117:20656-65.

[44] Minion J, Pai M. Bacteriophage assays for rifampicin resistance detection in Mycobacterium tuberculosis: updated meta-analysis. International Journal of Tuberculosis and Lung Disease. 2010;14:941-51.

[45] Sergueev KV, He YX, Borschel RH, Nikolich MP, Filippov AA. Rapid and Sensitive Detection of Yersinia pestis Using Amplification of Plague Diagnostic Bacteriophages Monitored by Real-Time PCR. Plos One. 2010;5.

[46] Zhu CT, Cui ZL, Zheng RJ, Yang H, Jin RL, Qin LH, et al. A Multi-Center Study to Evaluate the Performance of Phage Amplified Biologically Assay for Detecting TB in Sputum in the Pulmonary TB Patients. Plos One. 2011;6.

[47] Biswas D, Deb A, Gupta P, Prasad R, Negi KS. Evaluation of the usefulness of phage amplification technology in the diagnosis of patients with paucibacillary tuberculosis. Indian Journal of Medical Microbiology. 2008;26:75-8.

[48] Zaki MES, Goda T. Rapid phenotypic assay of antimycobacterial susceptibility pattern by direct mycobacteria growth indicator tube and phage amplified biological assay compared to BACTEC 460 TB. Tuberculosis. 2007;87:102-8.

[49] Simboli N, Takiff H, McNerney R, Lopez B, Martin A, Palomino JC, et al. In-house phage amplification assay is a sound alternative for detecting rifampin-resistant Mycobacterium tuberculosis in low-resource settings. Antimicrobial agents and chemotherapy. 2005;49:425-7.

[50] Stewart G, Jassim SAA, Denyer SP, Newby P, Linley K, Dhir VK. The specific and sensitive detection of bacterial pathogens within 4 h using bacteriophage amplification. Journal of Applied Microbiology. 1998;84:777-83.

[51] Pierce CL, Rees JC, Fernandez FM, Barr JR. Detection of Staphylococcus aureus Using N-15-Labeled Bacteriophage Amplification Coupled with Matrix-Assisted Laser Desorption/Ionization-Time-of-Flight Mass Spectrometry. Analytical Chemistry. 2011;83:2286-93.

[52] Pierce CL, Rees JC, Fernandez FM, Barr JR. Viable Staphylococcus aureus Quantitation using N-15 Metabolically Labeled Bacteriophage Amplification Coupled with a Multiple Reaction Monitoring Proteomic Workflow. Molecular & Cellular Proteomics. 2012;11.

[53] Cox CR, Rees JC, Voorhees KJ. Modeling bacteriophage amplification as a predictive tool for optimized MALDI-TOF MS-based bacterial detection. Journal of Mass Spectrometry. 2012;47:1435-41.

[54] Albert H, Heydenrych A, Mole R, Trollip A, Blumberg L. Evaluation of FASTPlaqueTB-RIF (TM), a rapid, manual test for the determination of rifampicin resistance from Mycobacterium tuberculosis cultures. International Journal of Tuberculosis and Lung Disease. 2001;5:906-11.

[55] Mole RJ, Maskell TWO. Phage as a diagnostic - the use of phage in TB diagnosis. Journal of Chemical Technology and Biotechnology. 2001;76:683-8.

[56] Albert H, Trollip A, Seaman I, Mole RJ. Simple, phage-based (FASTPlaque) technology to determine rifampicin resistance of Mycobacterium tuberculosis directly from sputum. International Journal of Tuberculosis and Lung Disease. 2004;8:1114-9.

[57] Eltringham IJ, Wilson SM, Drobniewski FA. Evaluation of a bacteriophage-based assay (phage amplified biologically assay) as a rapid screen for resistance to isoniazid, ethambutol, streptomycin, pyrazinamide, and ciprofloxacin among clinical isolates of Mycobacterium tuberculosis. Journal of Clinical Microbiology. 1999;37:3528-32.

[58] Hance KR, Smith BC, Steinmark TD, Rees JC. Rapid identification of Staphylococcus aureus in blood cultures by bacteriophage-enhanced immunoassay. American Journal of Clinical Pathology. 2005;124:644-5.

[59] Kutin RK, Alvarez A, Jenkins DM. Detection of Ralstonia solanacearum in natural substrates using phage amplification integrated with real-time PCR assay. Journal of Microbiological Methods. 2009;76:241-6.

[60] Reiman RW, Atchley DH, Voorhees KJ. Indirect detection of Bacillus anthracis using real-time PCR to detect amplified gamma phage DNA. Journal of Microbiological Methods. 2007;68:651-3.

[61] Tiwari RP, Hattikudur NS, Bharmal RN, Kartikeyan S, Deshmukh NM, Bisen PS. Modern approaches to a rapid diagnosis of tuberculosis: Promises and challenges ahead. Tuberculosis. 2007;87:193-201.

[62] Favrin SJ, Jassim SA, Griffiths MW. Application of a novel immunomagnetic separation-bacteriophage assay for the detection of Salmonella enteritidis and Escherichia coli O157 : H7 in food. International Journal of Food Microbiology. 2003;85:63-71.

[63] Goodridge L, Gallaccio A, Griffiths MW. Morphological, host range, and genetic characterization of two coliphages. Applied and Environmental Microbiology. 2003;69:5364-71.

[64] Ulitzur N, Ulitzur S. New rapid and simple methods for detection of bacteria and determination of their antibiotic susceptibility by using phage mutants. Applied and Environmental Microbiology. 2006;72:7455-9.

[65] Madonna AJ, Van Cuyk S, Voorhees KJ. Detection of Escherichia coli using immunomagnetic separation and bacteriophage amplification coupled with matrix-assisted laser desorption/ionization time-of-flight mass spectrometry. Rapid Communications in Mass Spectrometry. 2003;17:257-63.

[66] de Siqueira RS, Dodd CER, Rees CED. Phage amplification assay as rapid method for salmonella detection. Brazilian Journal of Microbiology. 2003;34:118-20.

[67] Favrin SJ, Jassim SA, Griffiths MW. Development and optimization of a novel immunomagnetic separation-bacteriophage assay for detection of Salmonella enterica serovar enteritidis in broth. Applied and Environmental Microbiology. 2001;67:217-24.

[68] Foddai A, Elliott CT, Grant IR. Optimization of a Phage Amplification Assay To Permit Accurate Enumeration of Viable Mycobacterium avium subsp paratuberculosis Cells. Applied and Environmental Microbiology. 2009;75:3896-902.

[69] Schofield DA, Molineux IJ, Westwater C. Diagnostic Bioluminescent Phage for Detection of Yersinia pestis. Journal of Clinical Microbiology. 2009;47:3887-94.

[70] Ripp S, Jegier P, Birmele M, Johnson CM, Daumer KA, Garland JL, et al. Linking bacteriophage infection to quorum sensing signalling and bioluminescent bioreporter monitoring for direct detection of bacterial agents. Journal of Applied Microbiology. 2006;100:488-99.

[71] Ripp S, Jegier P, Johnson CM, Brigati JR, Sayler GS. Bacteriophage-amplified bioluminescent sensing of Escherichia coli O157 : H7. Analytical and Bioanalytical Chemistry. 2008;391:507-14.

[72] Schofield DA, Westwater C. Phage-mediated bioluminescent detection of Bacillus anthracis. Journal of Applied Microbiology. 2009;107:1468-78.

[73] Chen J, Griffiths MW. Salmonella detection in eggs using Lux(+) bacteriophages. Journal of Food Protection. 1996;59:908-14.

[74] Thouand G, Vachon P, Liu S, Dayre M, Griffiths MW. Optimization and validation of a simple method using P22 :: luxAB bacteriophage for rapid detection of Salmonella enterica serotypes A, B, and D in poultry samples. Journal of Food Protection. 2008;71:380-5.

[75] Loessner MJ, Rudolf M, Scherer S. Evaluation of luciferase reporter bacteriophage A511::luxAB for detection of Listeria monocytogenes in contaminated foods. Applied and Environmental Microbiology. 1997;63:2961-5.

[76] Kodikara CP, Crew HH, Stewart G. Near online detection of enteric bacteria using lux recombinant bacteriophage. Fems Microbiology Letters. 1991;83:261-6.

[77] Tetart F, Repoila F, Monod C, Krisch HM. Bacteriophage T4 host range is expanded by duplications of a small domain of the tail fiber adhesin. Journal of Molecular Biology. 1996;258:726-31.

[78] Wolber PK, Green RL. Detection of bacteria by transduction of ice nucleation genes. Trends in Biotechnology. 1990;8:276-9.

[79] Banaiee N, Bobadilla-Del-Valle M, Riska PF, Bardarov S, Small PM, Ponce-De-Leon A, et al. Rapid identification and susceptibility testing of Mycobacterium tuberculosis from MGIT cultures with luciferase reporter mycobacteriophages. Journal of Medical Microbiology. 2003;52:557-61.

[80] Kumar V, Loganathan P, Sivaramakrishnan G, Kriakov J, Dusthakeer A, Subramanyam B, et al. Characterization of temperate phage Che12 and construction of a new tool for diagnosis of tuberculosis. Tuberculosis. 2008;88:616-23.

[81] Namura M, Hijikata T, Miyanaga K, Tanji Y. Detection of Escherichia coli with fluorescent labeled phages that have a broad host range to E-coli in sewage water. Biotechnology Progress. 2008;24:481-6.

[82] Funatsu T, Taniyama T, Tajima T, Tadakuma H, Namiki H. Rapid and sensitive detection method of a bacterium by using a GFP reporter phage. Microbiology and Immunology. 2002;46:365-9.

[83] Piuri M, Jacobs WR, Hatfull GF. Fluoromycobacteriophages for Rapid, Specific, and Sensitive Antibiotic Susceptibility Testing of Mycobacterium tuberculosis. Plos One. 2009;4.

[84] Zourob M, Elwary S, Turner A. Principles of Bacterial Detection. New-York: Springer; 2008.

[85] Stanley PE. A review of bioluminescent ATP techniques in rapid microbiology. Journal of Bioluminescence and Chemiluminescence. 1989;4:375-80.

[86] Kannan P, Yong HY, Reiman L, Cleaver C, Patel P, Bhagwat AA. Bacteriophage-Based Rapid and Sensitive Detection of Escherichia coli O157:H7 Isolates from Ground Beef. Foodborne Pathogens and Disease. 2010;7:1551-8.

[87] Laczka O, Garcia-Aljaro C, del Campo FJ, Pascual FXM, Mas-Gordi J, Baldrich E. Amperometric detection of Enterobacteriaceae in river water by measuring beta-galactosidase activity at interdigitated microelectrode arrays. Analytica Chimica Acta. 2010;677:156-61.

[88] Blasco R, Murphy MJ, Sanders MF, Squirrell DJ. Specific assays for bacteria using phage mediated release of adenylate kinase. Journal of Applied Microbiology. 1998;84:661-6.

[89] Wu Y, Brovko L, Griffiths MW. Influence of phage population on the phage-mediated bioluminescent adenylate kinase (AK) assay for detection of bacteria. Letters in Applied Microbiology. 2001;33:311-5.

[90] Minikh O, Tolba M, Brovko LY, Griffiths MW. Bacteriophage-based biosorbents coupled with bioluminescent ATP assay for rapid concentration and detection of Escherichia coli. Journal of Microbiological Methods. 2010;82:177-83.

[91] Neufeld T, Schwartz-Mittelmann A, Biran D, Ron EZ, Rishpon J. Combined phage typing and amperometric detection of released enzymatic activity for the specific identification and quantification of bacteria. Analytical Chemistry. 2003;75:580-5.

[92] Yemini M, Levi Y, Yagil E, Rishpon J. Specific electrochemical phage sensing for Bacillus cereus and Mycobacterium smegmatis. Bioelectrochemistry. 2007;70:180-4.

[93] Kenzaka T, Utrarachkij F, Suthienkul O, Nasu M. Rapid monitoring of Escherichia coli in southeast Asian urban canals by fluorescent-bacteriophage assay. Journal of Health Science. 2006;52:666-71.

[94] Davies J. Surface plasmon resonance*the technique and its applications to biomaterial processes. Nanobiology. 1994;3:5-16.

[95] Wood RW. A suspected case of the electrical resonance of minute metal particles for light-waves. A new type of absorption. Philosophical Magazine Series 6. 1902;3:396 - 410.

[96] Fano U. The Theory of Anomalous Diffraction Gratings and of Quasi-Stationary Waves on Metallic Surfaces (Sommerfelds Waves). J Opt Soc Am. 1941;31:213-22.

[97] Turbadar T. Complete Absorption of Light by Thin Metal Films. Proc Phys Soc. 1959;73:5.

[98] Otto A. Excitation of nonradiative surface plasma waves in silver by the method of frustrated total relection. Zeitschrift für Physik A Hadrons and Nuclei. 1968;216:398-410.

[99] E Kretschmann HR. Radiative decay of non radiative surface plasmons excited by light (Surface plasma waves excitation by light and decay into photons applied to nonradiative modes). Zeitschrift fuer naturforschung. 1968;23A:2135-6.

[100] Homola J. Surface Plasmon Resonance Based Sensors. Berlin: Springer Berlin Heidelberg; 2006.

[101] De Crescenzo G, Boucher C, Durocher Y, Jolicoeur M. Kinetic characterization by surface plasmon resonance-based biosensors : principle and emerging trends. Cellular and Molecular Bioengineering. 2008;1:204-15.

[102] Leonard P, Hearty S, Quinn J, O'Kennedy R. A generic approach for the detection of whole Listeria monocytogenes cells in contaminated samples using surface plasmon resonance. Biosensors & Bioelectronics. 2004;19:1331-5.

[103] Taylor AD, Ladd J, Yu QM, Chen SF, Homola J, Jiang SY. Quantitative and simultaneous detection of four foodborne bacterial pathogens with a multi-channel SPR sensor. Biosensors & Bioelectronics. 2006;22:752-8.

[104] Subramanian A, Irudayaraj J, Ryan T. Mono and dithiol surfaces on surface plasmon resonance biosensors for detection of Staphylococcus aureus. Sensors and Actuators B-Chemical. 2006;114:192-8.

[105] Balasubramanian S, Sorokulova IB, Vodyanoy VJ, Simonian AL. Lytic phage as a specific and selective probe for detection of Staphylococcus aureus- A surface plasmon resonance spectroscopic study. Biosensors and Bioelectronics. 2007;22:948-55.

[106] Guntupalli R, Sorokulova I, Krumnow A, Pustovyy O, Olsen E, Vodyanoy V. Real-time optical detection of methicillin-resistant Staphylococcus aureus using lytic phage probes. Biosensors and Bioelectronics. 2008:151-4.

[107] Tawil N, Sacher E, Mandeville R, Meunier M. Strategies for the Immobilization of Bacteriophages on Gold Surfaces, Monitored by Surface Plasmon Resonance and Surface Morphology. Journal of Physical Chemistry C. 2013.

[108] Arya SK, Singh A, Naidoo R, Wu P, McDermott MT, Evoy S. Chemically immobilized T4-bacteriophage for specific Escherichia coli detection using surface plasmon resonance. Analyst. 2011;136:486-92.

[109] Singh A, Arya SK, Glass N, Hanifi-Moghaddam P, Naidoo R, Szymanski CM, et al. Bacteriophage tailspike proteins as molecular probes for sensitive and selective bacterial detection. Biosensors & Bioelectronics. 2010;26:131-8.

[110] Singh A, Arutyunov D, McDermott MT, Szymanski CM, Evoy S. Specific detection of Campylobacter jejuni using the bacteriophage NCTC 12673 receptor binding protein as a probe. Analyst. 2011;136:4780-6.

[111] Balasubramanian S, Sorokulova IB, Vodyanoy VJ, Simonian AL. Lytic phage as a specific and selective probe for detection of Staphylococcus aureus - A surface plasmon resonance spectroscopic study. Biosensors & Bioelectronics. 2007;22:948-55.

[112] Guntupalli R, Sorokulova I, Krumnow A, Pustovyy O, Olsen E, Vodyanoy V. Real-time optical detection of methicillin-resistant Staphylococcus aureus using lytic phage probes. Biosensors & Bioelectronics. 2008;24:151-4.

[113] Nanduri V, Bhunia AK, Tu SI, Paoli GC, Brewster JD. SPR biosensor for the detection of L-monocytogenes using phage-displayed antibody. Biosensors & Bioelectronics. 2007;23:248-52.

[114] Sharma H, Mutharasan R. Review of biosensors for foodborne pathogens and toxins. Sensors and Actuators B-Chemical. 2013;183:535-49.

[115] Wang XD, Wolfbeis OS. Fiber-Optic Chemical Sensors and Biosensors (2008-2012). Analytical Chemistry. 2013;85:487-508.

[116] Anderson GP, Lingerfelt BM, Taitt CR. Eight analyte detection using a four-channel optical biosensor. Sensor Letters. 2004;2:18-24.

[117] Mazhorova A, Markov A, Ng A, Chinnappan R, Skorobogata O, Zourob M, et al. Label-free bacteria detection using evanescent mode of a suspended core terahertz fiber. Optics Express. 2012;20:5344-55.

[118] Smietana M, Bock WJ, Mikulic P, Ng A, Chinnappan R, Zourob M. Detection of bacteria using bacteriophages as recognition elements immobilized on long-period fiber gratings. Optics Express. 2011;19:7971-8.

[119] Tripathi SM, Bock WJ, Mikulic P, Chinnappan R, Ng A, Tolba M, et al. Long period grating based biosensor for the detection of Escherichia coli bacteria. Biosensors & Bioelectronics. 2012;35:308-12.

[120] Brewster JD, Gehring AG, Mazenko RS, VanHouten LJ, Crawford CJ. Immunoelectrochemical assays for bacteria: Use of epifluorescence microscopy and rapid-scan electrochemical techniques in development of an assay for Salmonella. Analytical Chemistry. 1996;68:4153-9.

[121] Gervais L, Gel M, Allain B, Tolba M, Brovko L, Zourob M, et al. Immobilization of biotinylated bacteriophages on biosensor surfaces. Sensors and Actuators B. 2007;125:615-21.

[122] Neufeld T, Mittelman AS, Buchner V, Rishpon J. Electrochemical phagemid assay for the specific detection of bacteria using Escherichia coli TG-1 and the M13KO7 phagemid in a model system. Analytical Chemistry. 2005;77:652-7.

[123] Benhar I, Eshkenazi I, Neufeld T, Opatowsky J, Shaky S, Rishpon J. Recombinant single chain antibodies in bioelectrochemical sensors. Talanta. 2001;55:899-907.

[124] Shabani A, Zourob M, Allain B, Marquette CA, Lawrence MF, Mandeville R. Bacteriophage-Modified Microarrays for the Direct Impedimetric Detection of Bacteria. Analytical Chemistry. 2008;80:9475-82.

[125] Yao L, Lamarche P, Tawil N, Khan R, Aliakbar AM, Hassan MH, et al. CMOS Conductometric System for Growth Monitoring and Sensing of Bacteria. Ieee Transactions on Biomedical Circuits and Systems. 2011;5:223-30.

[126] Mejri MB, Baccar H, Baldrich E, Del Campo FJ, Helali S, Ktari T, et al. Impedance biosensing using phages for bacteria detection: Generation of dual signals as the clue for in-chip assay confirmation. Biosensors & Bioelectronics. 2010;26:1261-7.

[127] Dadarwal R, Namvar A, Thomas DF, Hall JC, Warriner K. Organic conducting polymer electrode based sensors for detection of Salmonella infecting bacteriophages. Materials Science & Engineering C-Biomimetic and Supramolecular Systems. 2009;29:761-5.

[128] Zhang HK, Li X, Bai YP, Niu RF, Jia YF, Zhang CZ, et al. Metastatic cell detection using a phage-peptide-modified light-addressable potentiometric sensor. Biotechnology and Applied Biochemistry. 2009;53:185-92.

[129] Falahee MB, Park SF, Adams MR. Detection and enumeration of Campylobacer jejuni and Campylobacter coli by indirect impedimetry with an oxygen scavenging system. Journal of Food Protection. 2003;66:1724-6.

[130] Shabani A, Zourob M, Allain B, Lawrence M, Mandeville R, Ieee. Electrochemical detection of bacteria using bacteriophage2007.

[131] Yao L, Haj-Hassan M, Ghafar-Zadeh E, Shabani A, Chodavarapu V, Zourob M, et al. CMOS capactive sensor system for bacteria detection using phage organisms. 2008 Canadian Conference on Electrical and Computer Engineering, Vols 1-42008. p. 836-9.

[132] Tawil N, Sacher E, Mandeville R, Meunier M. Surface plasmon resonance detection of E. coli and methicillin-resistant S. aureus using bacteriophages. Biosensors & Bioelectronics. 2012;37:24-9.

[133] Olsen EV, Sorokulova IB, Petrenko VA, Chen IH, Barbaree JM, Vodyanoy VJ. Affinity-selected filamentous bacteriophage as a probe for acoustic wave biodetectors of Salmonella typhimurium. Biosensors & Bioelectronics. 2006;21:1434-42.

[134] Fu LL, Li SQ, Zhang KW, Chen IH, Barbaree JM, Zhang AX, et al. Detection of Bacillus anthracis Spores Using Phage-Immobilized Magnetostrictive Milli/Micro Cantilevers. Ieee Sensors Journal. 2011;11:1684-91.

[135] Fu LL, Li SQ, Zhang KW, Chen IH, Petrenko VA, Cheng ZY. Magnetostrictive microcantilever as an advanced transducer for biosensors. Sensors. 2007;7:2929-41.

[136] Horikawa S, Bedi D, Li SQ, Shen W, Huang SC, Chen IH, et al. Effects of surface functionalization on the surface phage coverage and the subsequent performance of phage-immobilized magnetoelastic biosensors. Biosensors & Bioelectronics. 2011;26:2361-7.

[137] Horikawa S, Vaglenov KA, Gerken DM, Chai YT, Park MK, Li SQ, et al. Rapid, enhanced detection of Salmonella Typhimurium on fresh spinach leaves using micron-scale, phage-coated magnetoelastic biosensors. In: Kim MS, Tu SI, Chao K, editors. Sensing for Agriculture and Food Quality and Safety Iv2012.

[138] Johnson ML, Wan JH, Huang SC, Cheng ZY, Petrenko VA, Kim DJ, et al. A wireless biosensor using microfabricated phage-interfaced magnetoelastic particles. Sensors and Actuators a-Physical. 2008;144:38-47.

[139] Lakshmanan RS, Guntupalli R, Hu J, Kim DJ, Petrenko VA, Barbaree JM, et al. Phage immobilized magnetoelastic sensor for the detection of Salmonella typhimurium. Journal of Microbiological Methods. 2007;71:55-60.

[140] Lakshmanan RS, Guntupalli R, Hu J, Petrenko VA, Barbaree JM, Chin BA. Detection of Salmonella typhimurium in fat free milk using a phage immobilized magnetoelastic sensor. Sensors and Actuators B-Chemical. 2007;126:544-50.

[141] Lakshmanan RS, Guntupalli R, Huang S, Johnson ML, Mathison LC, Chen IH, et al. Magnetoelastic Material as a Biosensor for the Detection of Salmonella Typhimurium. In: Su J, Wang LP, Furuya Y, TrolierMcKinstry S, Leng J, editors. Materials and Devices for Smart Systems Iii2009. p. 131-6.

[142] Lakshmanan RS, Hu J, Guntupalli R, Wan JH, Huang SC, Yang H, et al. Detection of of Salmonella typhimurium using phage based magnetostrictive sensor - art. no. 62180Z. In: Gardner PJ, Fountain AW, editors. Chemical and Biological Sensing VII2006. p. Z2180-Z.

[143] Park MK, Oh JH, Chin BA. The effect of incubation temperature on the binding of Salmonella typhimurium to phage-based magnetoelastic biosensors. Sensors and Actuators B-Chemical. 2011;160:1427-33.

[144] Wan JH, Johnson ML, Guntupalli R, Petrenko VA, Chin BA. Detection of Bacillus anthracis spores in liquid using phage-based magnetoelastic micro-resonators. Sensors and Actuators B-Chemical. 2007;127:559-66.

[145] Huang S, Yang H, Lakshmanan RS, Johnson ML, Wan J, Chen IH, et al. Sequential detection of Salmonella typhimurium and Bacillus anthracis spores using magnetoelastic biosensors. Biosensors & Bioelectronics. 2009;24:1730-6.

[146] Dubois LH, Nuzzo RG. Synthesis, structure, and properties of model organic-surfaces. Annual Review of Physical Chemistry. 1992;43:437-63.

[147] Schreiber F. Structure and growth of self-assembling monolayers. Progress in Surface Science. 2000;65:151-256.

[148] Bieri M, Burgi T. Adsorption kinetics, orientation, and self-assembling of N-acetyl-L-cysteine on gold: A combined ATR-IR, PM-IRRAS, and QCM study. Journal of Physical Chemistry B. 2005;109:22476-85.

[149] Tielens F, Santos E. AuS and SH Bond Formation/Breaking during the Formation of Alkanethiol SAMs on Au(111): A Theoretical Study. Journal of Physical Chemistry C. 2010;114:9444-52.

[150] Hu K, Bard AJ. In Situ Monitoring of Kinetics of Charged Thiol Adsorption on Gold Using an Atomic Force Microscope. Langmuir. 1998;14:4790-4.

[151] DeBono RF, Loucks GD, DellaManna D, Krull UJ. Self-assembly of short and long-chain n-alkyl thiols onto gold surfaces: A real-time study using surface plasmon resonance techniques. Canadian Journal of Chemistry-Revue Canadienne De Chimie. 1996;74:677-88.

[152] Pan W, Durning CJ, Turro NJ. Kinetics of Alkanethiol Adsorption on Gold. Langmuir. 1996;12:4469-73.

[153] Subramanian R, Lakshminarayanan V. A study of kinetics of adsorption of alkanethiols on gold using electrochemical impedance spectroscopy. Electrochimica Acta. 2000;45:4501-9.

[154] Alves CA, Smith EL, Porter MD. Atomic scale imaging of alkanethiolate monolayers at gold surfaces with atomic force microscopy. Journal of the American Chemical Society. 1992;114:1222-7.

[155] Prato M, Alloisio M, Jadhav SA, Chincarini A, Svaldo-Lanero T, Bisio F, et al. Optical Properties of Disulfide-Functionalized Diacetylene Self-Assembled Monolayers on Gold: a Spectroscopic Ellipsometry Study. Journal of Physical Chemistry C. 2009;113:20683-8.

[156] Prato M, Moroni R, Bisio F, Rolandi R, Mattera L, Cavalleri O, et al. Optical characterization of thiolate self-assembled monolayers on Au(111). Journal of Physical Chemistry C. 2008;112:3899-906.

[157] Baralia GG, Duwez AS, Nysten B, Jonas AM. Kinetics of exchange of alkanethiol monolayers self-assembled on polycrystalline gold. Langmuir. 2005;21:6825-9.

[158] Pensa E, Carro P, Rubert AA, Benitez G, Vericat C, Salvarezza RC. Thiol with an Unusual Adsorption-Desorption Behavior: 6-Mercaptopurine on Au(111). Langmuir. 2010;26:17068-74.

[159] Vericat C, Vela ME, Benitez G, Carro P, Salvarezza RC. Self-assembled monolayers of thiols and dithiols on gold: new challenges for a well-known system. Chemical Society Reviews. 2010;39:1805-34.

[160] Carr JA, Wang H, Abraham A, Gullion T, Lewis JP. L-Cysteine Interaction with Au-55 Nanoparticle. Journal of Physical Chemistry C. 2012;116:25816-23.

[161] Cavalleri O, Oliveri L, Dacca A, Parodi R, Rolandi R. XPS measurements on L-cysteine and 1-octadecanethiol self-assembled films: a comparative study. Applied Surface Science. 2001;175:357-62.

[162] Valiokas R, Ostblom M, Svedhem S, Svensson SCT, Liedberg B. Thermal stability of self-assembled monolayers: Influence of lateral hydrogen bonding. Journal of Physical Chemistry B. 2002;106:10401-9.

[163] Love JC, Estroff LA, Kriebel JK, Nuzzo RG, Whitesides GM. Self-assembled monolayers of thiolates on metals as a form of nanotechnology. Chemical Reviews. 2005;105:1103-69.

[164] Abraham A, Mihaliuk E, Kumar B, Legleiter J, Gullion T. Solid-State NMR Study of Cysteine on Gold Nanoparticles. Journal of Physical Chemistry C. 2010;114:18109-14.

[165] Gervais T, and Klavs F. Jensen. Mass transport and surface reactions in microfluidic systems. Chemical Engineering Science 2006;61:1102-21.

[166] Kuhnle A, Linderoth TR, Hammer B, Besenbacher F. Chiral recognition in dimerization of adsorbed cysteine observed by scanning tunnelling microscopy. Nature. 2002;415:891-3.

[167] Cavalleri O, Gonella G, Terreni S, Vignolo M, Floreano L, Morgante A, et al. High resolution X-ray photoelectron spectroscopy of L-cysteine self-assembled films. Physical Chemistry Chemical Physics. 2004;6:4042-6.

[168] Gonella G, Terreni S, Cvetko D, Cossaro A, Mattera L, Cavalleri O, et al. Ultrahigh vacuum deposition of L-cysteine on Au(110) studied by high-resolution X-ray photoemission: From early stages of adsorption to molecular organization. Journal of Physical Chemistry B. 2005;109:18003-9.

[169] Ihs A, Liedberg B. Chemisorption of l-cysteine and 3-mercaptopropionic acid on gold and copper surfaces - an infrared reflection absorption study. Journal of colloid and Interface Science. 1991;144:282-92.

[170] Uvdal K, Bodo P, Liedberg B. L-cysteine adsorbed on gold and copper - an x-ray photoelectron-spectroscopy study. Journal of colloid and Interface Science. 1992;149:162-73.

[171] Voet DaV, J.G. Biochemistry. Biochemistry. Third ed: John Wiley & Sons; 2004. p. 1178.

[172] Hakkinen H. The gold-sulfur interface at the nanoscale. Nature Chemistry. 2012;4:443-55.

[173] Bain CD, Evall J, Whitesides GM. Formation of monolayers by the coadsorption of thiols on gold - variation in the head group, tail group, and solvent. Journal of the American Chemical Society. 1989;111:7155-64.

[174] Damos FS, Luz RCS, Kubota LT. Determination of thickness, dielectric constant of thiol films, and kinetics of adsorption using surface plasmon resonance. Langmuir. 2005;21:602-9.

[175] Karpovich DS, Blanchard GJ. Direct measurement of the adsorption-kinetics of alkanethiolate self-assembled monolayers on a microcrystalline gold surface. Langmuir. 1994;10:3315-22.

[176] Poirier GE. Characterization of organosulfur molecular monolayers on Au(111) using scanning tunneling microscopy. Chemical Reviews. 1997;97:1117-27.

[177] De Renzi V, Lavagnino L, Corradini V, Biagi R, Canepa M, del Pennino U. Very low energy vibrational modes as a fingerprint of H-bond network formation: L-cysteine on Au(111). Journal of Physical Chemistry C. 2008;112:14439-45.

[178] Mateo-Marti E, Rogero C, Gonzalez C, Sobrado JM, de Andres PL, Martin-Gago JA. Interplay between Fast Diffusion and Molecular Interaction in the Formation of Self-Assembled Nanostructures of S-Cysteine on Au(111). Langmuir. 2010;26:4113-8.

[179] Tolba M, Minikh O, Brovko LY, Evoy S, Griffiths MW. Oriented Immobilization of Bacteriophages for Biosensor Applications. Applied and Environmental Microbiology. 2010;76:528-35.

[180] Singh A, Glass N, Tolba M, Brovko L, Griffiths M, Evoy S. Immobilization of bacteriophages on gold surfaces for the specific capture of pathogens. Biosensors and Bioelectronics. 2009;24:3645-51.

[181] Sun W, Brovko L, Griffiths M. Use of bioluminescent Salmonella for assessing the efficiency of constructed phage-based biosorbent. Journal of Industrial Microbiology & Biotechnology. 2000;25:273-5.

[182] Sun W, Brovko L, Griffiths M. Use of bioluminescent Salmonella for assessing the efficiency of constructed phage-based biosorbent (Reprinted from Journal Industrial Microbiology & Biotechnology, vol 25, pg 273-275, 2000). Journal of Industrial Microbiology & Biotechnology. 2001;27:126-8.

[183] Poshtiban SS, Amit; Fitzpatrick, Glen; Evoy, Stephane. Bacteriophage Tail-Spike Protein Derivitized Microresonator Arrays for Specific Detection of Pathogenic Bacteria. Sensors and Actuators B: Chemical. 2013.

[184] Rao S, Anderson K, Bachas L. Oriented immobilization of proteins. Mikrochemica Acta. 1998;128:127-43.

[185] Lazcka O, Campo FJD, Munoz FX. Pathogen detection: A perspective of traditional methods and biosensors. 2007.

[186] Handa H, Gurczynski S, Jackson MP, Mao GZ. Immobilization and Molecular Interactions between Bacteriophage and Lipopolysaccharide Bilayers. Langmuir. 2010;26:12095-103.

[187] Burke JP. Infection control - A problem for patient safety. New England Journal of Medicine. 2003;348:651-6.

[188] Roberts RR, Scott RD, Cordell R, Solomon SL, Steele L, Kampe LM, et al. The use of economic modeling to determine the hospital costs associated with nosocomial infections. Clinical Infectious Diseases. 2003;36:1424-32.

[189] Lindsey WC, Woodruff ES, Weed D, Ward DC, Jenison RD. Development of a rapid diagnostic assay for methicillin-resistant Staphylococcus aureus and methicillin-resistant coagulase-negative Staphylococcus. Diagnostic Microbiology and Infectious Disease. 2008;61:273-9.

[190] Easton L. Escherichia coli O157: Occurrence, transmission and laboratory detection. Br J Biomed Sci. 1997;54:57-64.

[191] Kissinger PT. Biosensors-A perspective. Biosens Bioelectron. 2005;20:2512-6.

[192] Nanduri V, Sorokuvola IB, SAmoylov AM, Simonian AL, Petrenko VA, Vodyanoy V. Phage as a molecular recognition element in biosensors immobilized by physical adsorption. Biosensors and Bioelectronics. 2007;22:986-92.

[193] Oh BK, Lee W, Kim YK, Lee WH, Choi JW. Surface plasmon resonance immunosensor using self-assembled protein G for the detection of Salmonella paratyphi. Journal of Biotechnology. 2004;111:1-8.

[194] Caron E, Luong JHT, Male KB, Mandeville R, Mazza A, Male K. Apparatus, for detecting viable microorganisms, comprises a detecting electrode comprising gold nanoparticles deposited, a counter electrode and a capture molecule. Nat Res Council Canada (Cana).

[195] Lukashin AV, Borodovsky M. GeneMark.hmm: new solutions for gene finding. Nucleic Acids Research. 1998;26:1107-15.

[196] Pearson WR. Rapid and sensitive sequence comparison with fastp and fasta. Methods in Enzymology. 1990;183:63-98.

[197] Altschul SF, Gish W, Miller W, Myers EW, Lipman DJ. Basic local alignment search tool. Journal of Molecular Biology. 1990;215:403-10.

[198] Rognes T, Seeberg E. Six-fold speed-up of Smith-Waterman sequence database searches using parallel processing on common microprocessors. Bioinformatics. 2000;16:699-706.

[199] Abuladze NK, Gingery M, Tsai J, Eiserling FA. Tail Length Determination in Bacteriophage T4. Virology. 1994;199:301-10.

[200] Comeau AM, Bertrand C, Letarov A, Tétart F, Krisch HM. Modular architecture of the T4 phage superfamily: A conserved core genome and a plastic periphery. Virology. 2007;362:384-96.

[201] Lustemberg PG, Vericat C, Benitez GA, Vela ME, Tognalli N, Fainstein A, et al. Spontaneously formed sulfur adlayers on gold in electrolyte solutions: Adsorbed sulfur or gold sulfide? Journal of Physical Chemistry C. 2008;112:11394-402.

[202] Panlilio AL, Culver DH, Gaynes RP, Banerjee S, Henderson TS, Tolson JS, et al. Methicillin-resistant staphylococcus-aureus in united-states hospitals, 1975-1991. Infection control and hospital epidemiology. 1992;13:582-6.

[203] Louie L, Matsumura SO, Choi E, Louie M, Simor AE. Evaluation of three rapid methods for detection of methicillin resistance in Staphylococcus aureus. Journal of Clinical Microbiology. 2000;38:2170-3.

[204] Stefani S, Chung DR, Lindsay JA, Friedrich AW, Kearns AM, Westh H, et al. Meticillin-resistant Staphylococcus aureus (MRSA): global epidemiology and harmonisation of typing methods. International Journal of Antimicrobial Agents. 2012;39:273-82.

[205] Tong SYC, Chen LF, Fowler VG. Colonization, pathogenicity, host susceptibility, and therapeutics for Staphylococcus aureus: what is the clinical relevance? Seminars in Immunopathology. 2012;34:185-200.

[206] Krishna S, Miller LS. Innate and adaptive immune responses against Staphylococcus aureus skin infections. Seminars in Immunopathology. 2012;34:261-80.

[207] Adam HJ, DeCorby M, Rennie R, Karlowsky JA, Hoban DJ, Zhanel GG, et al. Prevalence of antimicrobial resistant pathogens from blood cultures from Canadian hospitals: results of the CANWARD 2007-2009 study. Diagnostic Microbiology and Infectious Disease. 2011;69:307-13.

[208] Hoban DJ, Biedenbach DJ, Mutnick AH, Jones RN. Pathogen of occurrence and susceptibility patterns associated with pneumonia in hospitalized patients in North America: results of the SENTRY Antimicrobial Surveillance Study (2000). Diagnostic Microbiology and Infectious Disease. 2003;45:279-85.

[209] Ramirez P, Fernandez-Barat L, Torres A. New therapy options for MRSA with respiratory infection/pneumonia. Current Opinion in Infectious Diseases. 2012;25:159-65.

[210] Parker D, Prince A. Immunopathogenesis of Staphylococcus aureus pulmonary infection. Seminars in Immunopathology. 2012;34:281-97.

[211] Leahy TR, Yau YCW, Atenafu E, Corey M, Ratjen F, Waters V. Epidemiology of Borderline Oxacillin-Resistant Staphylococcus aureus in Pediatric Cystic Fibrosis. Pediatric Pulmonology. 2011;46:489-96.

[212] Liu H, Buescher G, Lewis N, Snyder S, Jungkind D. Detection of borderline oxacillin-resistant staphylococcus-aureus and differentiation from methicillin-resistant strains. European Journal of Clinical Microbiology & Infectious Diseases. 1990;9:717-24.

[213] Hackbarth CJ, Chambers HF. Methicillin-resistant staphylococci - detection methods and treatment of infections. Antimicrobial agents and chemotherapy. 1989;33:995-9.

[214] CLSI. Performance standards for antimicrobial susceptibility testing; twenty-third informational supplement. M100-S23 Pennsylvania: Wayne; 2013.

[215] Chambers HF. Methicillin resistance in staphylococci: Molecular and biochemical basis and clinical implications. Clinical Microbiology Reviews. 1997;10:781-&.

[216] Hiramatsu K, Kihara H, Yokota T. Analysis of borderline-resistant strains of methicillin-resistant staphylococcus-aureus using polymerase chain-reaction. Microbiology and Immunology. 1992;36:445-53.

[217] Garcia-Alvarez L, Holden MTG, Lindsay H, Webb CR, Brown DFJ, Curran MD, et al. Meticillin-resistant Staphylococcus aureus with a novel mecA homologue in human and bovine populations in the UK and Denmark: a descriptive study. Lancet Infectious Diseases. 2011;11:595-603.

[218] Kelley PG, Grabsch EA, Howden BP, Gao W, Grayson ML. Comparison of the Xpert Methicillin-Resistant Staphylococcus aureus (MRSA) Assay, BD GeneOhm MRSA Assay, and Culture for Detection of Nasal and Cutaneous Groin Colonization by MRSA. Journal of Clinical Microbiology. 2009;47:3769-72.

[219] Knapp CC, Ludwig MD, Washington JA. EVALUATION OF BBL CRYSTAL MRSA ID SYSTEM. Journal of Clinical Microbiology. 1994;32:2588-9.

[220] Bekkaoui F, McNevin JP, Leung CH, Peterson GJ, Patel A, Bhatt RS, et al. Rapid detection of the mecA gene in methicillin resistant staphylococci using a colorimetric Cycling Probe Technology. Diagnostic Microbiology and Infectious Disease. 1999;34:83-90.

[221] Cavassini M, Wenger A, Jaton K, Blanc DS, Bille J. Evaluation of MRSA-screen, a simple anti-PBP 2a slide latex agglutination kit, for rapid detection of methicillin resistance in Staphylococcus aureus. Journal of Clinical Microbiology. 1999;37:1591-4.

[222] Shiga KG, K.; Nishimura, M.; Watanabe, M.; Nomura F.; Kajiyama N. Discrimination of methicillin-resistant Staphylococcus aureus from methicillin-susceptible Staphylococcus aureus or coagulase-negative staphylococci by detection of penicillin-binding protein 2 and penicillin-binding protein 2' using a bioluminescent enzyme immunoassay. J Immunol Methods. 2013;388.

[223] Chen YWW, H.; Hupert, M.; Soper, S. A. Identification of methicillin-resistant Staphylococcus aureus using an integrated and modular microfluidic system. Analyst. 2013;138:1075-83.

[224] Corrigan DK, Schulze H, Henihan G, Ciani I, Giraud G, Terry JG, et al. Impedimetric detection of single-stranded PCR products derived from methicillin resistant Staphylococcus aureus (MRSA) isolates. Biosensors & Bioelectronics. 2012;34:178-84.

[225] Lina G, Piemont Y, Godail-Gamot F, Bes M, Peter MO, Gauduchon V, et al. Involvement of Panton-Valentine leukocidin-producing Staphylococcus aureus in primary skin infections and pneumonia. Clinical Infectious Diseases. 1999;29:1128-32.

[226] Harmsen D, Claus H, Witte W, Rothganger J, Claus H, Turnwald D, et al. Typing of methicillin-resistant Staphylococcus aureus in a university hospital setting by using novel software for spa repeat determination and database management. Journal of Clinical Microbiology. 2003;41:5442-8.

[227] Golding GC, JL; Spreitzer ,DJ; Veyhl, J; Surynicz, K; Simor, A; Mulvey, MR; Canadian Nosocomial Infection Surveillance Program. A preliminary guideline for the assignment of methicillin-resistant Staphylococcus aureus to a Canadian pulsed-field gel electrophoresis epidemic type using spa typing. Can J Infect Dis Med Microbiol. 2008;19:273-81.

[228] Lévesque S. Surveillance des souches de Staphylococcus aureus résistantes à la méthicilline isolées des bactériémies dans la province de Québec, rapport 2011-2012. INSPQ.

[229] Dallaire AM, Rioux D, Rachkov A, Patskovsky S, Meunier M. Laser-Generated Au-Ag Nanoparticles For Plasmonic Nucleic Acid Sensing. Journal of Physical Chemistry C. 2012;116:11370-7.

[230] Milheirico C, Oliveira DC, de Lencastre H. Update to the multiplex PCR strategy for assignment of mec element types in Staphylococcus aureus. Antimicrobial agents and chemotherapy. 2007;51:3374-7.

[231] Simor AE, Gilbert NL, Gravel D, Mulvey MR, Bryce E, Loeb M, et al. Methicillin-Resistant Staphylococcus aureus Colonization or Infection in Canada: National Surveillance and Changing Epidemiology, 1995-2007. Infection control and hospital epidemiology. 2010;31:348-56.

[232] Berger-Bachi B, Rohrer S. Factors influencing methicillin resistance in staphylococci. Archives of Microbiology. 2002;178:165-71.

[233] Jorgensen JH. Mechanisms of methicillin resistance in staphylococcus-aureus and methods for laboratory detection. Infection control and hospital epidemiology. 1991;12:14-9.

[234] Warren DK, Liao RS, Merz LR, Eveland M, Dunne WM. Detection of methicillin-resistant Staphylococcus aureus directly from nasal swab specimens by a real-time PCR assay. Journal of Clinical Microbiology. 2004;42:5578-81.

[235] Boehm DA, Gottlieb PA, Hua SZ. On-chip microfluidic biosensor for bacterial detection and identification. Sensors and Actuators B-Chemical. 2007;126:508-14.

[236] D'Souza SF. Microbial biosensors. Biosensors & Bioelectronics. 2001;16:337-53.

[237] Daniels JS, Pourmand N. Label-free impedance biosensors: Opportunities and challenges. Electroanalysis. 2007;19:1239-57.

[238] Ivnitski D, Abdel-Hamid I, Atanasov P, Wilkins E. Biosensors for detection of pathogenic bacteria. Biosensors & Bioelectronics. 1999;14:599-624.

[239] Lei Y, Chen W, Mulchandani A. Microbial biosensors. Analytica Chimica Acta. 2006;568:200-10.

[240] Sapsford KE, Bradburne C, Detehanty JB, Medintz IL. Sensors for detecting biological agents. Materials Today. 2008;11:38-49.

[241] Tawil N, Hatef A, Sacher E, Maisonneuve M, Gervais T, Mandeville R, et al. Surface Plasmon Resonance Determination of the Binding Mechanisms of L-Cysteine and Mercaptoundecanoic Acid on Gold. Journal of Physical Chemistry C. 2013.

[242] Tawil N, Mouawad F, Levesque S, Sacher E, Mandeville R, Meunier M. The Differential Detection of Methicillin-Resistant, Methicillin-Susceptible and Borderline Oxacillin-Resistant Staphylococcus aureus by Surface Plasmon Resonance. Biosens Bioelectron. 2013.

[243] Green RJ, Frazier RA, Shakesheff KM, Davies MC, Roberts CJ, Tendler SJB. Surface plasmon resonance analysis of dynamic biological interactions with biomaterials. Biomaterials. 2000;21:1823-35.

[244] Terakawa M, Takeda S, Tanaka Y, Obara G, Miyanishi T, Sakai T, et al. Enhanced localized near field and scattered far field for surface nanophotonics applications. Progress in Quantum Electronics. 2012;36:194-271.

[245] Fu JX, Park B, Zhao YP. Limitation of a localized surface plasmon resonance sensor for Salmonella detection. Sensors and Actuators B-Chemical. 2009;141:276-83.

[246] Cao BR, Xu H, Mao CB. Transmission Electron Microscopy as a Tool to Image Bioinorganic Nanohybrids: The Case of Phage-Gold Nanocomposites. Microscopy Research and Technique. 2011;74:627-35.

[247] Rouxhet PG, Genet MJ. XPS analysis of bio-organic systems. Surface and Interface Analysis. 2011;43:1453-70.

[248] Tessier PY, Chevolleau T, Cardinaud C, Grolleau B. An XPS study of the SF6 reactive ion beam etching of silicon at low temperatures. Nuclear Instruments & Methods in Physics Research Section B-Beam Interactions with Materials and Atoms. 1999;155:280-8.

[249] Gao J, Yan DH, Ni HG, Wang L, Yang YH, Wang XP. Protein-resistance performance enhanced by formation of highly-ordered perfluorinated alkyls on fluorinated polymer surfaces. Journal of colloid and Interface Science. 2013;393:361-8.

[250] Li XM, Luan SF, Shi HC, Yang HW, Song LJ, Jin J, et al. Improved biocompatibility of poly (styrene-b-(ethylene-co-butylene)-b-styrene) elastomer by a surface graft polymerization of hyaluronic acid. Colloids and Surfaces B-Biointerfaces. 2013;102:210-7.

[251] Pilolli R, Ditaranto N, Cioffi N, Sabbatini L. Non-destructive depth profile reconstruction of bio-engineered surfaces by parallel-angle-resolved X-ray photoelectron spectroscopy. Analytical and Bioanalytical Chemistry. 2013;405:713-24.

[252] Zhang C, Jin J, Zhao J, Jiang W, Yin JH. Functionalized polypropylene non-woven fabric membrane with bovine serum albumin and its hemocompatibility enhancement. Colloids and Surfaces B-Biointerfaces. 2013;102:45-52.

[253] Fischer S, Papageorgiou AC, Marschall M, Reichert J, Diller K, Klappenberger F, et al. L-Cysteine on Ag(111): A Combined STM and X-ray Spectroscopy Study of Anchorage and Deprotonation. Journal of Physical Chemistry C. 2012;116:20356-62.

[254] Gouget-Laemmel AC, Yang J, Lodhi MA, Siriwardena A, Aureau D, Boukherroub R, et al. Functionalization of Azide-Terminated Silicon Surfaces with Glycans Using Click Chemistry: XPS and FTIR Study. Journal of Physical Chemistry C. 2013;117:368-75.

[255] Dobrzanska DA, Cooper AL, Dowson CG, Evans SD, Fox DJ, Johnson BR, et al. Oxidation of Tertiary Amine-Derivatized Surfaces To Control Protein Adhesion. Langmuir. 2013;29:2961-70.

[256] Awsiuk K, Budkowski A, Petrou P, Bernasik A, Marzec MM, Kakabakos S, et al. Model immunoassay on silicon surfaces: Vertical and lateral nanostructure vs. protein coverage. Colloids and Surfaces B-Biointerfaces. 2013;103:253-60.

[257] Schmitt SK, Murphy WL, Gopalan P. Crosslinked PEG mats for peptide immobilization and stem cell adhesion. Journal of Materials Chemistry B. 2013;1:1349-60.

[258] Helgstrand C, Munshi S, Johnson JE, Liljas L. The refined structure of Nudaurelia capensis omega Virus reveals control elements for a T=4 capsid maturation. Virology. 2004;318:192-203.

[259] Sylvestre JP, Poulin S, Kabashin AV, Sacher E, Meunier M, Luong JHT. Surface chemistry of gold nanoparticles produced by laser ablation in aqueous media. Journal of Physical Chemistry B. 2004;108:16864-9.

[260] CytodiagnosticsInc. http://www.cytodiagnostics.com/store/pc/60nm-Carboxyl-carboxyl-PEG3000-SH-Gold-Nanoparticles-0-5ml-166p1234.htm. 2013.

[261] Leff DV, Brandt L, Heath JR. Synthesis and characterization of hydrophobic, organically-soluble gold nanocrystals functionalized with primary amines. Langmuir. 1996;12:4723-30.

[262] Kumar A, Mandal S, Selvakannan PR, Pasricha R, Mandale AB, Sastry M. Investigation into the interaction between surface-bound alkylamines and gold nanoparticles. Langmuir. 2003;19:6277-82.

[263] Garcia-Gil S, Arnau A, Garcia-Lekue A. Exploring large O 1s and N 1s core level shifts due to intermolecular hydrogen bond formation in organic molecules. Surface Science. 2013.

[264] Boulais E, Lachaine R, Meunier M. Plasma Mediated off-Resonance Plasmonic Enhanced Ultrafast Laser-Induced Nanocavitation. Nano Letters. 2012;12:4763-9.

[265] Johnson PB, Christy RW. Optical constants of the noble metals. Physical Review B. 1972;6:4370-9.

[266] Luong JHT, Male KB, Glennon JD. Biosensor technology: Technology push versus market pull. Biotechnology advances. 2008;26:492-500.